UNIVERSIDADE FEDERAL DO PARANÁ

TIAGO CASSEB BARBOSA

PETROGÊNESE DAS ROCHAS VULCÂNICAS ÁCIDAS E INTERMEDIÁRIAS DA BACIA DO GUARATUBINHA – PR

CURITIBA

2018

TIAGO CASSEB BARBOSA

PETROGÊNESE DAS ROCHAS VULCÂNICAS ÁCIDAS E INTERMEDIÁRIAS DA BACIA DO GUARATUBINHA – PR

Dissertação de Mestrado apresentada ao Programa de Pós-Graduação em Geologia, Setor de Ciências da Terra da Universidade Federal do Paraná, como pré-requisito para obtenção do título de Mestre em Geologia.

Orientadora: Prof.ª Dr.ª Eleonora Maria Gouvea Vasconcellos

Coorientadora: Prof.ª Dr.ª Barbara Trzaskos

Coorientador: Prof. Dr. Oswaldo Siga Junior

CURITIBA

2018

FICHA CATALOGRÁFICA ELABORADA PELO SISTEMA DE BIBLIOTECAS/UFPR
BIBLIOTECA DE CIÊNCIA E TECNOLOGIA

B238p Barbosa, Tiago Casseb
Petrogênese das rochas vulcânicas ácidas e intermediárias da Bacia do Guaratubinha – Pr / Tiago Casseb Barbosa. – Curitiba, 2018.
94 p. : il. color. ; 30 cm.

Dissertação - Universidade Federal do Paraná, Setor de Ciências da Terra, Programa de Pós-Graduação em Geologia, 2018.

Orientador: Eleonora Maria Gouvea Vasconcellos.
Coorientadores: Barbara Trzaskos, Oswaldo Siga Junior.

1. Geoquímica. 2. Vulcanismo. 3. Magma mingling. I. Universidade Federal do Paraná. II. Vasconcellos, Eleonora Maria Gouvea III. Trzaskos, Barbara. IV. Siga Junior, Oswaldo. V. Título.

CDD: 551.9

Bibliotecária: Romilda Santos - CRB-9/1214

MINISTÉRIO DA EDUCAÇÃO
SETOR CIÊNCIAS DA TERRA
UNIVERSIDADE FEDERAL DO PARANÁ
PRÓ-REITORIA DE PESQUISA E PÓS-GRADUAÇÃO
PROGRAMA DE PÓS-GRADUAÇÃO GEOLOGIA

TERMO DE APROVAÇÃO

Os membros da Banca Examinadora designada pelo Colegiado do Programa de Pós-Graduação em GEOLOGIA da Universidade Federal do Paraná foram convocados para realizar a arguição da Dissertação de Mestrado de **TIAGO CASSEB BARBOSA** intitulada: **PETROGÊNESE DAS ROCHAS VULCÂNICAS ÁCIDAS E INTERMEDIÁRIAS DA BACIA DO GUARATUBINHA - PR**, após terem inquirido o aluno e realizado a avaliação do trabalho, são de parecer pela sua Aprovação no rito de defesa.

A outorga do título de mestre está sujeita à homologação pelo colegiado, ao atendimento de todas as indicações e correções solicitadas pela banca e ao pleno atendimento das demandas regimentais do Programa de Pós-Graduação.

CURITIBA, 10 de Abril de 2018.

ELEONORA MARIA GOUVÊA VASCONCELLOS
Presidente da Banca Examinadora (UFPR)

OSSAMA MOHAMED MILAD HARARA
Avaliador Externo (UFPR)

CARLOS AUGUSTO SOMMER
Avaliador Externo (UFRGS)

Dedico este trabalho aos meus pais, por todo o amor, apoio e dedicação ao longo dos oito anos da minha vida universitária, e que sem os quais seria improvável chegar aonde cheguei. Aos meus irmãos, pelos momentos de carinho e conforto, que estejamos sempre juntos. À Mônica, pelo amor, pela paciência e por me acompanhar a cada passo desta jornada, crescendo juntos a cada dia. Aos meus amigos, novos e antigos, que me ajudaram de forma direta ou indireta nessa aventura. Minha sincera gratidão e agradecimento.

AGRADECIMENTOS

À minha orientadora, Prof.ª Dr.ª Eleonora Maria Gouvea Vasconcellos, à minha coorientadora, Prof.ª Dr.ª Barbara Trzaskos, e ao meu coorientador Prof. Dr. Oswaldo Siga Jr., pela dedicação constante ao projeto, pela orientação, pelas sugestões e pela paciência.

Aos doutorandos Leonardo Mairink Barão e Renata Ribas Zanella, colegas de projeto, pelo enriquecimento de conteúdo deste trabalho e pela ajuda nos trabalhos de campo.

Aos Profs. Drs. Miguel Angelo Stipp Basei e Kei Sato, do Centro de Pesquisas Geocronológica – CPGeo da Universidade de São Paulo – USP, pelo apoio fundamental à realização do estudo geocronológico.

Aos coordenadores Profs. Drs. Eleonora Maria Gouvea Vasconcellos, Leonardo Fadel Cury, Anelize Bahniuk Rumbelsperger, Ossama Moahamed Milad Harara e Miguel Angelo Stipp Basei por permitirem o uso das instalações do Laboratório de Análise de Minerais e Rochas – LAMIR, do Laboratório de Pesquisa em Microscopia – LAPEM, da UFPR, e do Laboratório de Preparação de Amostras do CPGeo, da USP.

A toda equipe técnica do LAMIR, na UFPR, e do CPGeo, na USP, em especial aos técnicos Franciele de Oliveira Czerzinski, Ivan Arthur Bindo e Vasco A. P. Loios pela orientação, dedicação e companheirismo.

Ao CNPq pelo suporte financeiro ao projeto.

A minha família e amigos por todo o apoio e carinho.

Invictus

Out of night that cover me,
Black as the Pit from pole to pole,
I thank whatever gods may be
For my unconquerable soul.

In the fell clutch of circumstance
I have not winced nor cried aloud.
Under the bludgeoning of chance
My head is bloody, but unbowed.

Beyond this place of wrath and tears
Looms but the Horror of the shade,
And yet the menace of the years
Finds, and shall find me, unafraid.

It matter not how strait the gate,
How charge with punishments the scroll,
I am the master of my fate:
I am the captain of my soul.

William Ernest Henley

RESUMO

Na porção meridional da Província Mantiqueira, assentada sobre rochas do Domínio Luis Alves, situa-se a Bacia do Guaratubinha, que abriga o grupo, de idade neoproterozoica, homônimo. Este é composto de rochas vulcanossedimentar, majoritariamente por rochas vulcânicas, de composição intermediária (andesitos) ou ácida (riolitos). Dada a importância dessas rochas para a melhor compreensão da evolução da bacia, este estudo, de cunho petrogenético, tem como objetivo definir o provável mecanismo gerador das rochas vulcânicas. Portanto, considerando sua idade e os processos relacionados ao surgimento dessas rochas. Para o desenvolvimento deste estudo foram realizadas análises petrográficas, litogeoquímicas, de geoquímica isotópica e geocronológicas. A partir de observações de campo e das análises geoquímicas, interpreta-se que as rochas não são cogenéticas, possuindo um número maior de diferenças do que semelhanças petrogenéticas entre si. As diferenças são observadas em diversas escalas, da macroscópica à microscópica, variando em aspectos estruturais, texturais e composicionais. Diferenças em aspectos microscópicos são controladas principalmente pela variação composicional nas assembleias minerais. As rochas estudadas possuem um caráter sub-alcalino, sendo que as rochas intermediárias se enquadram em uma tendência toleítica, enquanto que as rochas ácidas estão de acordo com uma tendência cálcio-alcalina. Observando o comportamento da dispersão das amostras em diagramas de variação, nota-se que os *trends* evolutivos somente são observados quando se individualizam os grupos. De modo geral, observam-se processos de depleção (óxidos) e enriquecimento (elementos traços) em direção aos membros mais evoluídos. Outra importante feição observada é a ocorrência de estruturas de *magma mingling*, onde material andesítico e riolítico se misturaram sem que houvesse a formação de um material híbrido, consumindo as partes envolvidas. Este fato se dá pela imiscibilidade de um magma em relação ao outro, corroborando a ausência de correlação entre eles. A análise de dados isotópicos também aponta diferenças evolutivas entre os magmas. Ambos os conjuntos teriam sua origem em nível crustal a partir de protólitos paleoproterozoicos, no entanto, os magmas intermediários evoluíram de acordo com um modelo de estágio simples, enquanto que as rochas ácidas seguem um modelo de estágio duplo. A datação U/Pb em zircão permitiu identificar três conjuntos de cristais nas rochas intermediárias. O primeiro conjunto é composto de cristais vulcânicos, que estabelecem a principal época de cristalização dessas rochas entre 593 e 580 Ma. Os demais conjuntos foram identificados como sendo cristais herdados das unidades basais à bacia. A caracterização dos magmas estudados como não cogenéticos é um forte argumento para eliminação da hipótese de fusão parcial de mesma fonte. O fato desta incompatibilidade ser definida também a partir dos dados isotópicos contrapõe a hipótese de contaminação. Portanto, a hipótese genética mais adequada para a formação de rochas intermediárias e ácidas é a fusão e evolução a partir de fontes distintas.

Palavras-chave: Geoquímica. Vulcanismo. *Magma Mingling*.

ABSTRACT

In the southern portion of Mantiqueira Province, overlaying rocks of Luis Alves Domain, it is found the Guaratubinha Basin, which holds the homonymous Neoproterozoic group. That group is composed by volcanic-sedimentary, majorly by volcanic rocks of intermediate (andesites) and acid (rhyolite) compositions. Giving the importance of those rocks to better understanding of the basin evolution, this research's main goal, with a petrogenesis insight, is to indicate the most probable formation mechanism of volcanic rocks. Thus, comprehending the time and the processes related to those rocks origin. In order to promote such study, it was performed petrographic, lithogeochemical, isotopic geochemical and geochronological analyses. From field observation and geochemical analyses, it could be interpreted that the both magmas are not cogenetic, presenting a greater number of differences over petrogenetic similarities. The differences occur in vary scales, from macroscopic to microscopic, and varying in structural, fabric and compositional aspects. Microscopic differences are controlled by the compositional variations in the mineral assemblage of volcanic rocks. It was interpreted that the studied rocks can be classified as sub-alkaline, with the intermediate ones following a tholeiitic trend, whereas acid ones follow a calcic-alkaline trend. Observing the plot pattern on bivariate diagrams, it was noticed that evolutionary trends are only distinguishable when the magmas are individualized. In general, they present a process of depletion (oxides) and enrichment (trace elements) towards the most evolved terms. Another important observed feature was the occurrence of magma mingling structures, when the andesitic and rhyolitic magmas mix up without consuming one of the involved parts and forming a hybrid material. That result is given by the immiscibility of one magma comparing to the other, corroborating their incompatibility. The isotopic analysis also reveals more evolutionary differences between the studied rocks. Both rock sets originated at crustal depth evolving independently from each other. The intermediate set evolves according to a simple-stage model while the acid set evolves as a double-stage model from parental rocks that originated during Paleoproterozoic. Geochronological data reveals that the intermediate rocks bear three types of zircon crystals. First type is volcanic ones, which indicate the main volcanism period between 593 and 580 Ma. The second and third are xenocrystals inherited from Guaratubinha basin bed rocks, the Rio-Pien Suite, from Neoproterozoic, and Luis Alves Domain, from Paleoproterozoic. The characterization of studied magma as non-cogenetic is a strong evidence to discard the partial melting of single source hypothesis. In addition, the fact that this same incompatibility is defined by isotopic data as well, contradicts the contamination hypothesis. Therefore, the most suitable petrogenetic hypothesis is that those magmas were generated and evolve from different sources.

Key-words: Geochemistry. Volcanism. Magma Mingling.

LISTA DE FIGURAS DA DISSERTAÇÃO

LISTA DE FIGURAS DO ARTIGO

LISTA DE TABELAS DA DISSERTAÇÃO

LISTA DE TABELAS DO ARTIGO

LISTA DE SIGLAS

BIFs – Banded Iron Formation (Formações Ferríferas Bandadas)

CPGeo – Centro de Pesquisas Geocronológicas

DEM – Digital Elevation Model (Modelo Digital de Elevação – MDE)

Ga – Bilhões de anos (Billion years)

HFSE – High Field Strength Elements (Elementos de Grande Carga Iônica)

ICP-MS – Inductively Coupled Plasma Mass Spectrometry (Espectrometria de Massa por Indução de Plasma Acoplado)

K_D – Partition Coefficient (Coeficiente de Partição)

LABAP – Laboratório de Análises de Bacias Paleozóicas

LA-ICP-MS – Laser Ablation Inductively Coupled Plasma Mass Spectrometry (Ablação a Laser Acoplado ao Espectrômetro De Massa – ICP-MS-LA)

LAMIR – Laboratório de Análise de Minerais e Rochas

LAPEM – Laboratório de Pesquisa em Microscopia

LILE – Large Ion Lithophile Elements (Elementos de Grande Raio Iônico)

LOI – Loss on Ignition (Perda ao Fogo)

Ma – Milhões de anos (Million Years)

MEV – Microscópio Eletrônico de Varredura

MINEROPAR – Serviço Geológico do Paraná

NAP – Núcleo de Apoio à Pesquisa

r^2 – Coefficient of Correlation (Coeficiente de Correlação)

REEs – Rare Earth Elements (Elementos Terras Raras – ETRs)

SHRIMP – Sensitive High Resolution Ion Microprobe (Microssonda Iônica de Alta Resolução e de Alta Sensibilidade)

T_{DM} – Time of Mantle Depletion (Tempo de Depletação do Manto)

TAS – Total alkali vs. Silica Diagram (Diagrama de Álcalis Totais vs. Sílica)

UFPR – Universidade Federal do Paraná

UnB – Universidade de Brasília

USP – Universidade de São Paulo

XRF – X Ray Fluorescence (Fluorescência de Raios X – XRF)

WR – Whole Rock (Rocha Total – RT)

LISTA DE ABREVIAÇÕES

Amp – Amphibole (Anfibólio)

Chl – Chlorite (Clorita)

Ep – Epidote (Epidoto)

Pl – Plagioclase (Plagioclásio)

Qtz – Quartz (Quartzo)

SUMÁRIO

CAPÍTULO I

1 INTRODUÇÃO

Estudada desde 1967 por Fuck e diversos outros autores em trabalhos da Comissão da Carta Geológica do Paraná, a Bacia do Guaratubinha é um importante objeto de estudo, com possíveis pesquisas em diversas áreas do conhecimento geológico. Desde os trabalhos pioneiros, diversos outros pesquisadores trabalharam na bacia: Daitx & Carvalho (1980) com trabalhos geoquímicos; Licht (1988) em estudos regionais realizados pela MINEROPAR (Serviço Geológico do Paraná); Castro (1993) realizando a reavaliação tectonoestratigráfica da bacia; Siga Jr. (1995) em trabalhos geocronológicos; trabalhos petrográficos de detalhe das rochas vulcanoclásticas de Reis Neto *et al.* (2000) e Barão (2016) que obteve resultados sobre a análise tectonoestrutural do arcabouço da bacia.

Geograficamente, a Bacia do Guaratubinha está localizada no município de São José dos Pinhais, entre os municípios de Morretes e Tijucas do Sul, aproximadamente a 30 km a sudeste de Curitiba. Seus acessos principais se dão por meio das rodovias federais BR-277 e BR-376, assim como por estradas municipais (Figura 1). A bacia apresenta um formato romboédrico com eixo maior alinhado a NE. Possui largura e comprimento, aproximados, de 10 e 32 km.

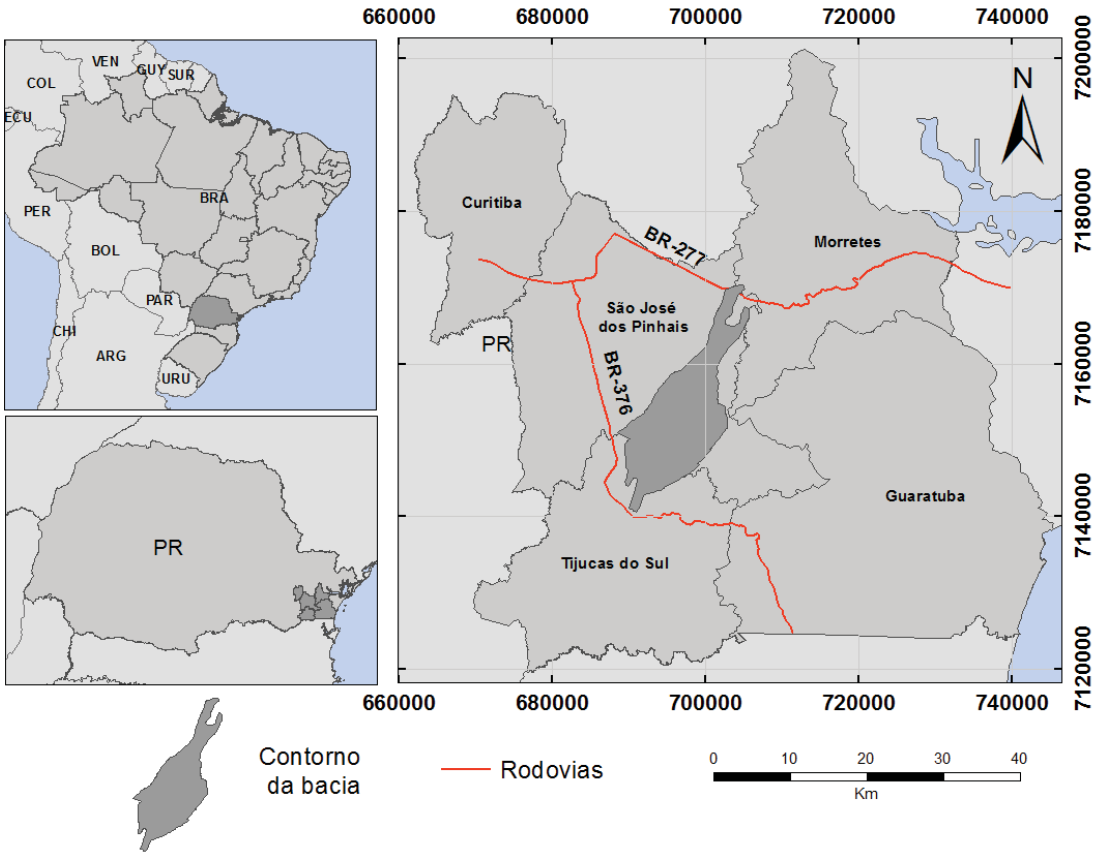

Figura 1 – Mapa de localização geográfica da Bacia do Guaratubinha.

2 JUSTIFICATIVA

De modo geral, os trabalhos realizados na Bacia do Guaratubinha tiveram como objetivo entender os principais aspectos petrográficos, estratigráficos e estruturais das rochas que preenchem a bacia. Feições indicativas de mistura de magma, identificadas por Barbosa (2015) mostraram a necessidade de estudo específico, com objetivos petrogenéticos das rochas vulcânicas e vulcanoclásticas associadas. Este estudo, iniciado por Barbosa (2015), justifica-se pela necessidade de se compreender a evolução do vulcanismo da Bacia do Guaratubinha.

3 HIPÓTESE

Barbosa (2015) concluiu que os derrames andesíticos e riolíticos formam dois conjuntos que se distinguem pela assinatura geoquímica e *trends* evolutivos, sendo que os dois magmas não são cogenéticos. Portanto, a partir desta conclusão, propõem-se três possíveis hipóteses a respeito da gênese

dos derrames. A primeira hipótese seria a geração de rochas intermediárias a partir de um magma primitivo e intermediário, com a geração de rochas ácidas pela contaminação deste magma primitivo por rochas encaixantes. A segunda hipótese está relacionada a diferentes taxas de fusão parcial a partir de uma mesma fonte, gerando dois magmas distintos. Por fim, a terceira hipótese é de que os magmas seriam provenientes de fontes distintas.

4 OBJETIVOS

O objetivo principal deste trabalho é propor um modelo petrogenético para as rochas vulcânicas intermediárias e ácidas da Bacia do Guaratubinha. O modelo se prestará a compreender a origem e relação genética das rochas vulcânicas indicando qual, dentre as três hipóteses, é a mais provável. Para tanto, são estabelecidos dois objetivos específicos. O primeiro é a caracterização petrográfica e geoquímica das rochas vulcânicas, compreendendo a relação genética e os eventos geológicos formadores dos derrames. O segundo é o estabelecimento da idade de geração destas rochas. Esta separação é feita considerando que, para atingir o primeiro objetivo específico, serão necessárias análises litogeoquímicas e de geoquímica isotópica, ao passo que para completar o segundo, é necessária a análise geocronológica.

5 GEOLOGIA REGIONAL

As rochas que compõem o embasamento da Bacia do Guaratubinha estão inclusas no contexto tectonogeológico da porção sudeste da Província Mantiqueira. Na região do Primeiro Planalto Paranaense encontra-se a porção de interesse deste trabalho, incluindo cinco unidades geológicas pré-cambrianas principais: Terreno Luis Alves, Terreno Curitiba, Suíte Granítica Cálcio-alcalina Rio-Pien, Suíte Granítica Alcalina Serra da Graciosa e a Bacia do Guaratubinha (Figura 2).

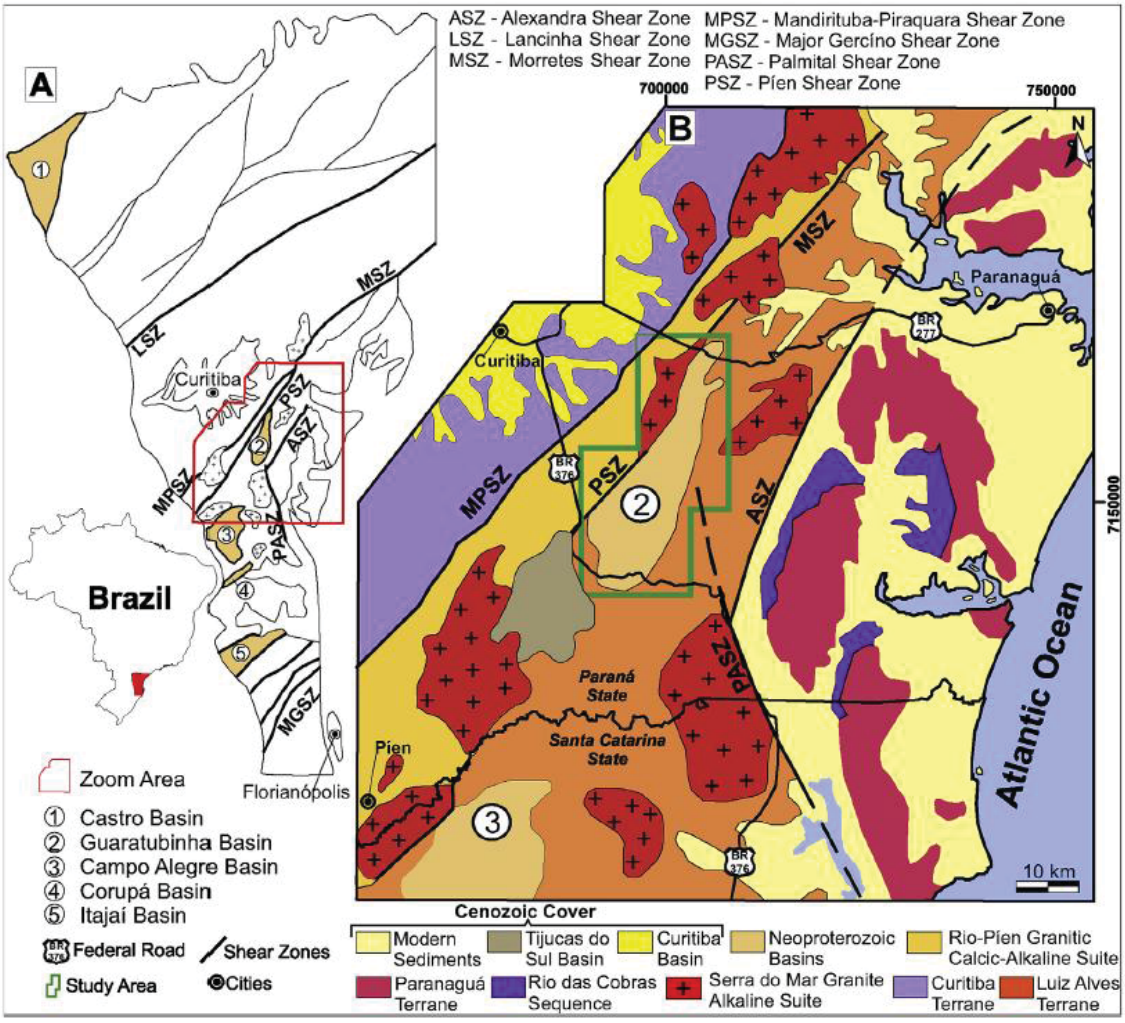

Figura 2 – Mapa geológico da Bacia do Guaratubinha e regiões adjacentes. A área da bacia está destacada pelo polígono verde. Fonte: Barão *et al.*, 2017.

5.1 TERRENO LUIS ALVES

O Terreno Luis Alves é formado por gnaisses granolíticos com estrutura maciça ou bandada, alternando níveis milimétricos a centimétricos, quartzo-feldspáticos e de minerais máficos. De tonalidades cinza-esverdeadas, as rochas variam entre leuco e mesocráticas, e entre granulometria fina a média. Além dos gnaisses, também são encontradas rochas graníticas e migmatíticas. De maneira subordinada também há rochas ultramáficas, quartzitos, BIFs, gnaisses cálcio-alcalinos e kinzigitos (granulitos ricos em Al e Mg) e quartzitos (Siga Jr, 1995; Siga Jr. *et al.*, 1993; Siga Jr. *et al.*, 1995; Basei *et al.*, 1992; Basei *et al.*, 1998a; Harara *et al.*, 2002; Harara *et al.*, 2003). Dados geocronológicos apontam que o Terreno Luis Alves apresenta idades de formação arqueana, entre 2800 e 2600 Ma, e durante o Paleoproterozoico,

entre 2200 e 1900 Ma (Basei, 1985; Siga Jr., 1995). A razão inicial de Sr ($^{87}Sr/^{86}Sr$) obtida pelos pesquisadores, está entre 0,701 a 0,704 e indica que o protólito provém ou do manto ou da crosta inferior. Os dados isotópicos de Sm-Nd indicam que o magma teve evolução em estágio duplo. O primeiro estágio ocorreu entre 2800 a 2700 Ma e o segundo estágio, entre 3100 e 3000 Ma, indicando longo período de residência crustal.

5.2 TERRENO CURITIBA

Esta unidade geológica pode ser dividida em duas porções. Na primeira são inclusos gnaisses bandados, migmatíticos, com leucossoma tonalítico-granodiorítico e mesossoma composto de biotita-anfibólio-gnaisses. De modo geral, os gnaisses bandados são leucocráticos com partes mesocráticas, granulometria média e texturas variáveis. Além destas rochas, há ocorrência de corpos anfibolíticos, gnaisses granolíticos e xistos magnesianos (Siga *et al.*, 1995; Silva *et al.*, 1998; Reis Neto *et al.*, 1998). A segunda porção é formada por granitos cálcio-alcalinos, deformados. Esta, formalmente denominada Suíte Granítica Cálcio-alcalina Rio-Pien, é interpretada como resultado de um arco magmático neoproterozoico (Machiavelli *et al.*, 1993). O conjunto de dados geocronológicos apresentados por Siga Jr. *et al.* (1993) indica dois grupos de idades. As análises realizadas incluem U-Pb e Rb-Sr em rocha total e Rb-Sr e Sm-Nd em minerais diversos. As idades mais novas são relativas a processos de migmatização, que ocorreram entre 620 e 550 Ma durante a Orogenia Brasiliana. As idades mais velhas são medidas a partir da porção mesocrática dos migmatitos, com idades entre 2150 e 1800 Ma, concordantes com o Ciclo Transamazônico.

5.3 SUÍTE CÁLCIO-ALCALINA RIO-PIEN

Esta unidade geológica, inclusa no Terreno Curitiba, compõe a porção sudeste deste terreno, sendo a porção que faz contato com o Luis Alves. Segundo Machiavelli *et al.* (1993) esta suíte pode ser dividida em dois corpos graníticos principais, o granitoide noroeste (GNO) e o granitoide sudeste (GSE). As litologias que compõem o GNO incluem biotita-hornblenda quartzo-monzonito e biotita monzogranito com granada e titanita. O GSE é composto de hornblenda quartzo-monzodiorito, biotita monzogranito, quartzo-monzonito e

granodiorito com magnetita e titanita. Os dados geocronológicos obtidos pelos autores indicam idade de colocação de 715 ± 30 Ma ($U\text{-}Pb_{(zircão)}$), evento metamórfico em 610 ± 40 Ma ($Rb\text{-}Sr_{(RT)}$) e processo de resfriamento regional entre 592 ± 30 Ma e 561 ± 15 Ma ($K\text{-}Ar_{(biotita)}$). Além de dados estruturais, as razões iniciais de Sr ($^{87}Sr/^{86}Sr$) de 0,707 para o GNO e 0,704 para o GSE, indicam que estes granitoides foram formados em contexto de arco vulcânico. Harara (2001) indica essa unidade como sendo um arco magmático com idades pré-colisionais entre 620 e 610 Ma, bem como idades tardi colisionais entre 605 e 595 Ma.

5.4 SUÍTE GRANÍTICA ALCALINA SERRA DA GRACIOSA

Kaul & Cordani (2000) descrevem esta suíte como sendo composta por 13 maciços graníticos. Os autores classificam esses maciços dentro de duas associações, nomeadas de 1 e 2. A associação 1 inclui sienogranitos, monzogranitos e álcali-feldspato granitos. A associação 2 inclui sienitos, quartzo sienitos e álcali-feldspato granitos. Essa granitogênese, de composição alcalina-peralcalina, é inclusa na Província Graciosa. Analisando dados geocronológicos de $U\text{-}Pb_{(zircão)}$, $K\text{-}Ar_{(biotita)}$, $K\text{-}Ar_{(anfibólio)}$, $Rb\text{-}Sr_{(RT)}$ e $Sm\text{-}Nd_{(RT)}$, Kaul (1997) conclui que os maciços graníticos dessa suíte foram formados aproximadamente a 580 Ma, com uma provável segunda fase de formação entre 560 e 540 Ma. O autor aponta que esta segunda fase está relacionada à formação de bacias vulcanossedimentares adjacentes, como as Bacias do Guaratubinha, Campo Alegre e Corupá. Siga Jr. (1995) propõem que a colocação desses maciços parece estar associada a regimes tectônicos predominantemente distensivos. Assim, relacionados a processos de adelgaçamento crustal ocorrido no âmbito dos terrenos gnáissico-migmatíticos do Complexo Atuba (Siga Jr *et al.*, 1995), envolvendo parte do Terreno Luis Alves. A Bacia do Guaratubinha encontra-se entre cinco maciços, conhecidos como Anhangava, Marumbi, Agudos, Morro Redondo e Serra da Igreja.

5.5 BACIA DO GUARATUBINHA

Em trabalhos pioneiros, Fuck *et al.* (1967) apontam o caráter vulcanossedimentar das rochas que preenchem a bacia. Castro (1993) foi o primeiro a ressaltar o fato das rochas vulcânicas e vulcanoclásticas

representarem quase a totalidade do preenchimento da bacia. O autor organizou as unidades em sequência estratigráfica com rochas sedimentares na base, sobrepostas por rochas vulcânicas intermediárias na porção mediana e por fim, no topo, a associação de rochas vulcânicas ácidas com rochas vulcanoclásticas. Barão (2016) considera estas unidades como três formações que compõem o Grupo Guaratubinha. Da base para o topo, estas formações se organizam da seguinte forma: Formação Miringuava, composta de sequência sedimentar com porções conglomeráticas até argilosas; Formação Vossoroca, composta por extenso derrame andesítico; Formação Serra do Salto, dividida em membros Osso da Anta, Castelhanos e Escutador. Tanto o Membro Osso da Anta quanto o Membro Castelhanos são formados por rochas vulcanoclásticas (ignimbritos, tufos e rochas epiclásticas). O Membro Escutador é composto de derrames de riolitos com dacitos subordinados. Siga Jr. *et al.* (1999) obtêm dados geocronológicos de $U\text{-}Pb_{(zircão)}$ e $Rb\text{-}Sr_{(RT)}$ que indicam janela de geração entre 600 e 570 Ma, medida em riolitos das bacias do Guaratubinha e Campo Alegre, bem como de granitos da Serra da Graciosa. A razão inicial de Sr ($^{87}Sr/^{86}Sr$) é considerada pelos autores como alta, acima de 0,707. A idade de depleção do manto (T_{DM}) foi calculada entre 2200 e 1850 Ma.

6 MATERIAIS E MÉTODOS

Os métodos foram divididos em trabalhos de campo, laboratório e escritório. Foi coletado um total de 31 amostras para realização de análises petrográficas, litogeoquímicas, de geoquímicas isotópica e geocronológicas. Em etapa de campo realizada em 2016, foram obtidas novas amostras. Somadas às amostras coletadas por Barbosa (2015), foram analisadas 14 amostras de andesitos, 13 de riolitos e 4 de tufos. Também foram descritas feições macroscópicas e estruturais dos derrames, bem como possíveis estruturas de misturas, facilitando o reconhecimento de litofácies.

6.1 PREPARAÇÃO DE AMOSTRAS

As amostras coletadas foram preparadas para quatro tipos de análises diferentes (petrográficas, litogeoquímicas, de geoquímica isotópica e geocronológicas), seguindo métodos de preparação de acordo com cada equipamento a ser utilizado. Para as análises petrográficas foram

confeccionadas 8 novas lâminas delgadas (3 de andesitos, 3 de riolitos e 2 de tufos), além das anteriormente apresentadas por Barbosa 2015. A laminação foi feita pela equipe técnica do Laboratório de Análises de Minerais e Rochas - LAMIR, da Universidade Federal do Paraná – UFPR, com participação do mestrando.

Tanto para a análise litogeoquímica quanto para a geoquímica isotópica, a preparação das amostras foi realizada no LAMIR. Inicialmente as amostras foram britadas utilizando britador de mandíbula da marca Renard e modelo BMA 85x120. Por vezes foi necessária a redução da amostra manualmente com uso de ferramentas. Em seguida foi realizada, para as amostras de andesito, a separação manual dos fragmentos britados utilizando lupa de mesa da marca Zeiss, modelo SteREO Discovery V.8. A separação é feita com o intuito de retirar fragmentos que possam mascarar o resultado das análises geoquímicas, como porções intemperizadas, amígdalas, veios de quartzo e percolações de óxidos/hidróxidos de ferro em fraturas. As amostras britadas foram então quarteadas em duas porções de aproximadamente 100 gramas cada. O processo é feito com quarteador metálico da marca Marconi e modelo MA 006/18x15.87. O quarteamento permite a separação de parte da amostra que represente o todo. Por fim, o material quarteado foi pulverizado em pulverizador de panela da marca AMEF, modelo AMP1-5. Cerca de 30g da amostra quarteada são despejados em uma panela, com interior de carbeto de tungstênio, com anel e peso central também de carbeto de tungstênio. A panela é levada ao moinho por aproximadamente 30 segundos para que o material possa atingir diâmetro menor que 180 mesh. O pó de rocha das duas porções separadas durante o quarteamento foi utilizado para as etapas analíticas de litogeoquímica e geoquímica isotópica.

A preparação das amostras para a geocronologia foi realizada no Laboratório de Preparação do Centro de Pesquisas Geocronológicas – CPGeo da Universidade de São Paulo – USP, de acordo com os procedimentos apresentados por Sato *et al.* (2014). As amostras foram submetidas à britagem, quarteamento e pulverização. No entanto, diferentemente da análise litogeoquímica, onde a pulverização foi feita em pulverizador de panela, neste caso ela foi feita em pulverizador de discos de aço. Este tipo de pulverizador

utiliza um par de discos de aço e rolamentos para reduzir as amostras diminuindo a fragmentação dos cristais que as compõem. Combinando a ação do pulverizador com uma bateria de peneiras obteve-se amostra com diâmetro menor que 250 mesh. As amostras pulverizadas passaram por processo de concentração e purificação de minerais. Neste processo o material pulverizado foi colocado em mesa vibratória, do tipo Wilfley, para a concentração de minerais pesados por via úmida. O concentrado de minerais foi então seco e sujeito ao efeito de um imã de mão para separação de minerais fortemente magnéticos como a magnetita. Em seguida o concentrado foi processado por separador magnético do tipo Frantz, com inclinação horizontal de aproximadamente 11° e corrente de 0,5 A, em média, para a separação de minerais magnéticos como magnetita, biotita, anfibólios e piroxênios. A porção concentrada de minerais não magnéticos foi tratada com bromofórmio e iodeto de metileno. O tratamento com bromofórmio (d = 2,87 g/cm^3) e com iodeto de metileno (d = 3,325 g/cm^3) ajudam a isolar os cristais de zircão (d $\cong$ 4,7 g/cm^3) pela diferença de densidade. O concentrado é separado em populações de diferentes morfologias e catados com ajuda de lupa de mesa. São levadas em consideração as variações de tamanho, cor, forma, arredondamento e metamictização. Os cristais são então fixados em placa de resina epóxi. A placa é lixada para expor a seção média dos cristais. É, em seguida, feito um imageamento em luz natural. Posteriormente aplica-se um revestimento de ouro com espessura entre 2 e 3 μm, para a catodoluminescência. Este processo é feito por meio de um microscópio eletrônico de varredura (MEV) do tipo FEI Quanta 250 e um detector XMAX CL. Por fim os cristais de zircão são submetidos ao método U/Pb (^{238}U/^{206}Pb e ^{235}U/^{207}Pb).

6.2 ANÁLISE PETROGRÁFICA

A análise de lâmina petrográfica tem como objetivo a observação da assembleia mineral, texturas, estruturas, fases de cristalização, relação de contato entre grãos, entre outras características. Aliado aos dados de campo, análise litogeoquímica e de geoquímica isotópica, é possível o agrupamento de litofácies com características petrográficas e estruturais, assim como assinaturas petrográficas e geoquímicas semelhantes. Por meio da descrição de lâminas petrográficas é possível identificar fases minerais que sejam

compatíveis com elementos traço, explicando anomalias geoquímicas apontadas em diagramas de variação e multielementares na litogeoquímica. A petrografia foi realizada no Laboratório de Pesquisas em Microscopia - LAPEM, da UFPR.

6.3 LITOGEOQUÍMICA

Inicialmente foi feita a revisão do estudo litogeoquímico realizado por Barbosa (2015). Neste estudo foram utilizadas as técnicas de fluorescência de raios X (FRX), para quantificar os óxidos em rocha total e a técnica de Espectrometria de Massa por Indução de Plasma Acoplado (ICP-MS) para quantificar os elementos traço, incluindo Terras Raras (ETRs), também em rocha total. Ambas as técnicas analisam gama variada e extensa de elementos, no entanto, são de interesse para o trabalho os óxidos SiO_2, TiO_2,Al_2O_3, $Fe_2O_{3(total)}$, MnO, MgO, CaO, Na_2O, K_2O, P_2O_5 e o LOI (*loss on ignition*); e elementos traço como Cs, Rb, Ba, Th, U, K, Ta, Nb, La, Ce, Sr, Nd, P, Hf, Zr, Sm, Ti, Tb, Y e ETRs. A FRX foi realizada no LAMIR em 31 amostras. Após a preparação, cada amostra foi transformada em pastilha fundida, composta por 0,9 g de pó da amostra misturado a 9 g de tetraborato de lítio, usado como fundente. Segundo Potts (1993) a FRX se inicia pelo bombardeamento com feixe de fótons de raios X em pastilha fundida. O bombardeamento ioniza os elétrons das camadas internas (em geral as camadas K e L) fazendo com que os elétrons migrem para camadas mais externas. Os elétrons, no entanto, se tornam instáveis e voltam ao seu nível energético natural, emitindo feixe de fótons fluorescentes. Essa fluorescência é captada por sensores previamente calibrados que reconhecem o padrão de onda característico de cada elemento. Os dados obtidos foram recalculados para base anidra a fim de eliminar a interferência de fases voláteis. Os dados tratados foram então projetados em diagramas de classificação, variação, multielementares e discriminantes. Diagramas bivariantes do tipo Harker, utilizando a sílica como óxido fracionante, foram utilizados para os óxidos. Para elementos traço foi utilizado o Rb como elemento fracionante. Estes diagramas foram utilizados a fim de que se pudesse avaliar *trends* evolutivos e reconhecer similaridades entre as amostras para a definição de fácies geoquímicas. Por fim, foram

confeccionados diagramas tectônicos discriminantes, a fim de apontar o provável ambiente de formação das rochas estudadas.

Junto aos dados previamente obtidos por Barbosa (2015) foi totalizado um banco de dados de elementos traço para as 31 amostras. Este banco contém dados de Elementos Terras Raras de 17 amostras, dessas, 9 são de rochas intermediárias e 8 são de rocha ácida. Após análise, os dados de elementos traço foram normalizados pelos valores mais adequados, condritos ou manto primordial e projetados em diagramas multielementares para definição da assinatura geoquímica. Foram confeccionados dois tipos de diagramas multielementares: o primeiro incluindo elementos traço em geral, contendo tanto elementos de grande raio iônico (LILE) quanto elementos de grande carga iônica (HFSE), normalizados pelo manto primordial de Wood *et al.* (1979); e diagramas para ETRs, normalizados pela média de condritos C1 de Boynton (1984).

6.4 GEOQUÍMICA ISOTÓPICA

As amostras foram preparadas e encaminhadas para análise no Laboratório de Geocronologia da Universidade de Brasília - UnB. Para esta finalidade as amostras foram solubilizadas e submetidas ao método $^{147}Sm/^{144}Nd$. A análise foi feita utilizando-se a técnica de ICP-MS. Segundo Potts (1993) a espectrometria de massa por indução de plasma acoplado se dá pela medição de íons segregados pela sua relação massa-carga. Inicialmente a amostra é solubilizada, nebulizada e misturada com gás argônio. Essa solução gasosa é ionizada por uma chama, convertendo-a em plasma com os íons dos elementos presentes na amostra. O plasma é direcionado por um orifício (*pinhole*) na ponta do cone de amostragem para a câmara de baixo vácuo. Em seguida, é direcionado por outro orifício num cone de *skimmer*, para a câmara de médio vácuo. Este conjunto de cones atua para manter o plasma concentrado, melhorando o desempenho do equipamento. O plasma é então direcionado para a câmara de alto vácuo onde se encontra o filtro de massa do espectrômetro. Esse filtro é composto de quatro tubos paralelos (*quadrupolo*) que geram um campo eletromagnético capaz de alterar a trajetória de deslocamento dos íons. Íons mais leves têm a trajetória mais alterada, ao

passo que íons mais pesados se mantêm mais imóveis. Os íons, separados pelo campo eletromagnético, atingem sensores previamente calibrados que os qualificam e quantificam.

Os dados provenientes desta análise foram tratados matematicamente, calculando a razão isotópica entre os elementos medidos nas rochas estudadas. Tendo a assinatura isotópica definida, pode-se deduzir importantes características petrogenéticas dessas rochas como a idade de derivação do manto (T_{DM}), bem como a profundidade de derivação dos magmas, crustal ou mantélica, a natureza de possíveis protólitos e o tempo de residência do crustal.

6.5 GEOCRONOLOGIA

Esta análise foi feita pelo método U/Pb em cristais de zircão provenientes de amostra de andesitos, no CPGeo da USP. A datação utilizou duas a técnicas: ICP-MS-LA e microssonda iônica. Geraldes (2010) descreve a técnica de ablação a laser acoplado ao espectrômetro de massa (ICP-MS-LA) como tendo sistemática semelhante à descrita anteriormente para o ICP-MS, com exceção do tratamento à amostra que é depositada no espectrômetro. Nesta técnica uma amostra sólida de mineral (cristal) é bombardeada por emissão a laser, volatilizando uma porção pontual do mineral. A parte volatilizada é misturada ao gás de argônio e segue os passos já descritos para o ICP-MS. O equipamento utilizado para está técnica, no CPGeo, foi o NEPTUNO – ICP-MS. Segundo Sato *et al.* (2012), este aparelho opera com configuração de taças de Faraday de IC_3 = ^{202}Hg, IC_4 = ^{204}(Hg+Pb), L_4 = ^{206}Pb, IC_6 = ^{207}Pb, L_3 = ^{208}Pb, H_2 = ^{232}Th e H_4 = ^{238}U. A configuração geral do equipamento é de potência de raio frequência = 1100W, taxa de gás refrigerador = 15 L/min (Ar), taxa de gás auxiliar = 0.7 L/min (Ar), taxa de gás amostral = 0.6 L/min. A configuração do laser: energia = 6mJ, taxa de repetição = 5 Hz, tamanho do spot = 25 - 38 μm, carga de gás hélio = 0.35 + 0.5 L/min. Ainda segundo os autores, a rotina de análise para U-Pb consiste em 2 medidas no vácuo, 2 NIST, 3 padrões externos, 13 amostras, 2 padrões externos e 2 medidas no vácuo. Cada rotina envolvem 40 ciclos com um ciclo por segundo. A interferência do ^{204}Hg no ^{204}Pb é corrigida por ^{202}Hg, onde a

razão $^{204}Hg/^{202}Hg$ é igual a 4.2. Para a razão de normalização de $^{207}Pb/^{206}Pb$ é utilizado uma combinação de NIST e padrões externos. No caso da razão de normalização de $^{206}Pb/^{238}U$ é usado um padrão externo. O padrão utilizado para análise de zircão é o GJ-red (600 Ma) de Elhlou *et al.* (2006).

A segunda técnica utilizada na datação dos cristais de zircão contou com o uso de um espectrômetro de massa de íons secundários acoplado com uma Microssonda Iônica de Alta Resolução e de Alta Sensibilidade (*Sensitive High Resolution Ion Microprobe* – SHRIMP IIe/MC). De acordo com Sato *et al.* (2014), o sistema de ablação é composto de um laser primário e um laser secundário. O primeiro é ajustado com as seguintes condições analíticas: abertura Kohler de 120 µm, tamanho do spot de 30 µm, e densidade de feixe de O^{-2} aproximadamente entre 2,5 e 7 ηA. O segundo é ajustado com as condições analíticas de: abertura da fonte de 80 µm e resolução de massa variando entre 5000 e 5500 (em 1%) para $^{196}(Zr_2O)$, ^{206}Pb, ^{207}Pb, ^{208}Pb, ^{238}U, $^{248}(ThO)$ e ^{254} (UO). Segundo os autores, o equipamento opera com uma rotina de tempo de rastreio entre 2 e 3 minutos com spot de 50 µm, além de 30 s de tempo de ablação fixado em um ponto central. A porção atingida pelo feixe de O^{-2}, é então direcionada para o sistema do espectrômetro de massa. O padrão utilizado para análise de zircão é o Temora 2.

Os resultados geocronológicos são tratados em *softwares* específicos, como o ISOPLOT para o cálculo das idades utilizando os pares radioativos e radiogênicos de $^{238}U/^{206}Pb$ e $^{235}U/^{207}Pb$. Em seguida os dados são projetados em diagrama de concórdia. O diagrama de concórdia indica a idade medida em relação à curva de evolução do U na crosta, bem como a evolução do sistema, se ele se manteve fechado ou aberto (ganho ou perda de Pb) (Geraldes, 2010). A definição das idades dos magmas é um importante fator de comparação entre eles, bem como auxilia a compreender quais eventos tectônicos eram atuantes na época da formação dos magmas.

7 RESULTADOS

Os resultados da pesquisa são apresentados no formato de artigo, no capítulo II deste volume. O artigo pretendido será submetido ao periódico científico *Precambrian Research*, portanto será apresentado em língua inglesa.

Após a fase analítica, os dados litogeoquímicos passam por tratamento matemático a partir do qual é gerado o banco de dados (Tabelas 1 a 8).

Tabela 1 – Tabela de dados litogeoquímicos de rochas intermediárias para óxidos (% peso), obtidos por fluorescência de raios X e recalculados em base anidra.

Amostra	GUA-78	GUA-59	GUA-138	GUA-77-2	GUA-07A	GUA-134	GUA-140	GUA-12	GUA-83	GUA-62-1	GUA-139	GUA-16	GUA-104	GUA-93
Litotipo	Andesito	Andesito	Andesito	Andesito	Andesito	Andesito	Andesito	Andesito	Andesito	Andesito	Andesito	Andesito	Andesito	Andesito
SiO_2	48,01	49,46	50,95	53,93	53,96	54,00	55,84	58,36	59,20	59,34	60,21	60,32	63,65	66,01
TiO_2	2,29	3,01	2,50	1,97	2,22	1,82	2,01	1,67	1,65	2,23	1,57	1,94	1,47	1,59
Al_2O_3	26,70	18,79	27,78	23,02	20,44	22,22	22,05	19,12	18,54	21,28	15,38	18,66	15,03	17,10
$Fe_2O_{3(total)}$	12,12	14,36	12,51	12,62	12,24	12,33	10,50	11,31	9,90	11,06	12,07	10,11	10,53	7,32
MnO	0,01	0,11	0,01	0,74	0,07	0,01	0,10	0,10	0,09	0,08	0,33	0,10	0,17	0,02
MgO	1,90	3,31	0,54	1,49	2,10	1,63	1,08	1,17	1,15	1,31	1,38	1,15	1,84	1,29
CaO	0,03	2,45	0,03	0,13	0,64	1,05	0,16	2,08	1,19	0,05	1,32	0,39	1,68	0,55
Na_2O	0,05	1,18	0,24	0,07	5,37	0,71	3,04	4,31	4,52	0,01	3,90	2,74	3,50	0,42
K_2O	8,72	4,83	5,27	5,08	2,26	4,14	4,44	1,46	3,15	3,60	3,03	3,74	1,71	5,13
P_2O_5	0,17	2,51	0,16	0,95	0,69	2,09	0,77	0,43	0,60	1,06	0,80	0,85	0,43	0,57
Total	100,00	100,00	100,00	100,00	100,00	100,00	100,00	100,00	100,00	100,00	100,00	100,00	100,00	100,00
LOI	5,19	6,98	6,62	8,62	5,57	7,57	6,23	4,96	3,08	10,81	3,92	6,52	4,12	4,22
Álcalis Totais	8,77	6,00	5,51	5,15	7,63	4,85	7,48	5,77	7,66	3,61	6,93	6,48	5,21	5,55

Tabela 2 – Tabela de dados litogeoquímicos de rochas ácidas para óxidos (% peso), obtidos por fluorescência de raios X e recalculados em base anidra.

Amostra	GUA-89	GUA-72-1	GUA-136	GUA-52-3	GUA-14	GUA-21	GUA-73-1	GUA-87	GUA-132	GUA-100	GUA-10	GUA-56-1	GUA-137	GUA-135	GUA-76	RIO-1	GUA-07R
Litotipo	Riolito	Tufo	Riolito	Riolito	Riolito	Riolito	Tufo	Riolito	Riolito	Tufo	Riolito	Riolito	Riolito	Riolito	Riolito	Tufo	Riolito
SiO_2	70,81	72,99	73,89	75,18	75,67	75,83	76,01	76,46	76,56	76,73	77,52	77,56	77,64	77,85	78,15	78,69	80,34
TiO_2	0,41	0,50	0,16	0,08	0,10	0,09	0,27	0,35	0,09	0,56	0,08	0,20	0,08	0,09	0,21	0,23	0,12
Al_2O_3	14,09	13,33	13,51	11,64	12,88	12,83	12,32	14,32	12,91	15,26	13,49	11,95	12,10	13,84	12,93	10,81	13,26
$Fe_2O_{3(total)}$	5,18	4,21	1,91	1,75	1,96	1,73	3,37	1,24	1,34	2,50	1,03	2,64	1,55	1,26	2,98	3,19	1,80
MnO	0,09	0,07	0,03	0,07	0,05	0,06	0,10	0,01	0,01	0,09	0,01	0,04	0,05	0,01	0,02	0,08	0,01
MgO	0,07	0,94	0,94	0,20	0,05	0,03	0,51	0,38	0,03	1,09	0,04	0,31	0,07	0,04	1,11	0,47	0,10
CaO	0,22	1,17	0,95	4,65	0,52	0,57	0,75	0,45	0,37	0,03	0,06	1,17	0,37	0,04	0,03	3,72	0,03
Na_2O	4,31	3,64	1,42	3,57	4,11	4,22	3,60	4,70	3,38	0,01	1,40	3,54	3,76	1,23	0,07	1,30	0,44
K_2O	4,77	2,99	7,16	2,84	4,65	4,62	2,98	1,95	5,31	3,58	6,35	2,57	4,37	5,64	4,48	1,48	3,89
P_2O_5	0,05	0,14	0,02	0,01	0,01	0,01	0,09	0,14	0,01	0,15	0,01	0,02	0,01	0,01	0,02	0,03	0,01
Total	100,00	100,00	100,00	100,00	100,00	100,00	100,00	100,00	100,00	100,00	100,00	100,00	100,00	100,00	100,00	100,00	100,00
LOI	1,94	1,62	3,96	0,82	0,84	1,85	0,90	1,89	0,98	0,59	2,54	2,51	3,56	1,33	1,10	5,32	1,46
Álcalis Totais	9,08	8,58	6,41	8,76	8,84	6,65	8,69	7,75	6,11	8,13	6,86	4,55	4,33	6,64	6,57	3,59	2,78

Tabela 3 – Tabela de dados litogeoquímicos para elementos traço (µg/g), obtidos por ICP-MS para rochas intermediárias.

Amostra	GUA-78	GUA-59	GUA-138	GUA-77-2	GUA-07A	GUA-134	GUA-140	GUA-12	GUA-83	GUA-62-1	GUA-139	GUA-16	GUA-104	GUA-93
Litotipo	Andesito	Andesito	Andesito	Andesito	Andesito	Andesito	Andesito	Andesito	Andesito	Andesito	Andesito	Andesito	Andesito	Andesito
Cs			1,74	11,10	1,70			1,00	4,00	1,30	-	1,20	2,30	1,40
Rb	273,00	84,00	77,90	142,50	163,00	139,00	91,00	36,80	108,40	76,70	78,00	87,60	37,80	147,30
Ba	4050,00	2933,00	4683,00	2942,00	472,00	2510,00	2554,00	715,00	855,00	1219,00	1632,00	2006,00	992,00	2004,00
Th			2,44	4,10	3,30			7,60	4,80	6,80		5,80	6,30	6,40
U			0,21	0,80	2,00			1,30	0,90	0,90		1,00	1,00	1,10
K2O (%)	8,72	4,83	5,27	5,08	2,26	4,14	4,44	1,46	3,15	3,60	3,03	3,74	1,71	5,13
Ta				1,80	0,80			1,00	0,80	1,30		1,30	1,10	1,10
Nb	49,00	31,00	14,30	32,60	16,60	44,00	42,00	19,70	15,90	27,90	29,00	24,40	16,70	17,60
La			19,20	110,10	128,20			60,50	52,60	104,40		95,30	57,50	63,80
Ce			38,80	212,40	173,50			120,60	97,20	217,60		192,70	109,50	112,00
Sr	285,00	165,00	126,00	269,20	287,30	98,00	315,00	303,00	275,50	47,50	159,00	216,50	453,00	56,30
Nd			16,30	118,90	116,10			53,70	49,50	104,50		92,70	51,90	60,80
P2O5 (%)	0,17	2,51	0,16	0,95	0,69	2,09	0,77	0,43	0,60	1,06	0,80	0,85	0,43	0,57
Hf			6,26	9,50	7,50			8,80	7,70	14,80		13,50	8,40	9,20
Zr	344,00	501,00	257,00	376,60	300,70	367,00	726,00	366,80	416,10	643,80	577,00	585,50	322,80	380,70
Sm			3,49	21,19	21,53			9,65	9,45	18,30		17,54	9,50	10,60
TiO2 (%)	2,29	3,01	2,50	1,97	2,22	1,82	2,01	1,67	1,65	2,23	1,57	1,94	1,47	1,59
Tb			0,74	2,52	3,05			1,23	1,32	2,32		2,16	1,17	1,33
Y	43,00	69,00	26,20	59,90	104,00	34,00	77,00	30,50	43,30	60,80	80,00	69,10	35,50	37,20

Tabela 4 – Tabela de dados litogeoquímicos para elementos traço (µg/g), obtidos por ICP-MS para rochas ácidas.

Amostra	GUA-89	GUA-72-1	GUA-136	GUA-52-3	GUA-14	GUA-21	GUA-73-1	GUA-87	GUA-132	GUA-100	GUA-10	GUA-56-1	GUA-137	GUA-135	GUA-76	RIO-1	GUA-07R
Litotipo	Riolito	Tufo	Riolito	Riolito	Riolito	Riolito	Tufo	Riolito	Riolito	Tufo	Riolito	Riolito	Riolito	Riolito	Riolito	Tufo	Riolito
Cs	0,30	3,81			1,60	1,43				6,80		2,90				1,40	0,81
Rb	88,10	97,40	307,00	128,00	202,80	210,00	83,00	63,00	234,00	221,60	302,00	183,60	200,00	305,00	216,00	59,80	151,00
Ba	115,00	934,00	987,00	384,00	7,00	11,20	1175,00	3489,00	11,00	343,00	252,00	134,00	66,00	52,00	836,00	222,00	327,00
Th	11,80	14,80			15,20	16,50				12,40		22,20				17,10	21,10
U	1,90	2,29			2,80	2,59				2,30		3,90				4,90	7,45
K2O (%)	4,77	2,99	7,16	2,84	4,65	4,62	2,98	1,95	5,31	3,58	6,35	2,57	4,37	5,64	4,48	1,48	3,89
Ta	1,50				2,60					1,20		3,00				1,60	
Nb	26,20	14,50	71,00	39,00	41,90	23,80	26,00	20,00	49,00	23,30	50,00	49,80	41,00	53,00	53,00	34,60	38,30
La	133,90	80,90			63,00	67,50				196,00		77,10				129,80	45,40
Ce	263,00	151,00			132,50	138,00				228,60		163,90				206,00	19,40
Sr	90,50	431,00	113,00	253,00	17,10	8,06	337,00	368,00	19,00	111,80	69,00	333,30	62,00	28,00	15,00	437,80	49,20
Nd	93,20	59,20			55,70	60,00				165,90		72,30				131,00	43,50
P2O5 (%)	0,05	0,14	0,02	0,01	0,01	0,01	0,09	0,14	0,01	0,15	0,01	0,02	0,01	0,01	0,02	0,03	0,01
Hf	15,30	6,95			12,70	11,50				10,40		25,20				21,30	11,10
Zr	721,60	262,00	418,00	258,00	288,30	267,00	774,00	304,00	303,00	400,40	230,00	831,60	234,00	237,00	734,00	958,70	293,00
Sm	13,80	10,60			13,38	14,50				31,90		16,54				23,81	10,30
TiO2 (%)	0,41	0,50	0,16	0,08	0,10	0,09	0,27	0,35	0,09	0,56	0,08	0,20	0,08	0,09	0,21	0,23	0,12
Tb	1,51	1,32			2,41	2,42				4,08		3,13				3,36	1,95
Y	41,20	41,30	94,00	76,00	83,20	89,20	75,00	55,00	91,00	101,60	33,00	119,10	83,00	46,00	67,00	35,50	79,70

Tabela 5 – Tabela de dados litogeoquímicos para elementos traço (µg/g) para rochas intermediárias normalizados pelo manto primordial de Wood *et al.* (1979). Valor de normalização para o Ti de acordo com Wood *et al.* (1981).

Amostra	GUA-78	GUA-59	GUA-138	GUA-77-2	GUA-07A	GUA-134	GUA-140	GUA-12	GUA-83	GUA-62-1	GUA-139	GUA-16	GUA-104	GUA-93
Litotipo	Andesito	Andesito	Andesito	Andesito	Andesito	Andesito	Andesito	Andesito	Andesito	Andesito	Andesito	Andesito	Andesito	Andesito
Cs			91,58	584,21	89,47			52,63	210,53	68,42		63,16	121,05	73,68
Rb	317,44	97,67	90,58	165,70	189,53	161,63	105,81	42,79	126,05	89,19	90,70	101,86	43,95	171,28
Ba	535,71	387,96	619,44	389,15	62,43	332,01	337,83	94,58	113,10	161,24	215,87	265,34	131,22	265,08
Th			25,42	42,71	34,38			79,17	50,00	70,83		60,42	65,63	66,67
U			7,78	29,63	74,07			48,15	33,33	33,33		37,04	37,04	40,74
K	345,87	191,56	209,06	201,67	89,82	164,25	176,05	58,09	124,82	142,67	120,34	148,34	67,82	203,52
Ta				41,86	18,60			23,26	18,60	30,23		30,23	25,58	25,58
Nb	79,03	50,00	23,06	52,58	26,77	70,97	67,74	31,77	25,65	45,00	46,77	39,35	26,94	28,39
La			27,04	155,07	180,56			85,21	74,08	147,04		134,23	80,99	89,86
Ce			20,42	111,79	91,32			63,47	51,16	114,53		101,42	57,63	58,95
Sr	12,39	7,17	5,48	11,70	12,49	4,26	13,70	13,17	11,98	2,07	6,91	9,41	19,70	2,45
Nd			12,64	92,17	90,00			41,63	38,37	81,01		71,86	40,23	47,13
P	18,77	277,24	17,99	104,88	76,41	231,34	85,35	48,11	66,60	117,19	88,76	94,41	47,85	63,04
Hf			17,89	27,14	21,43			25,14	22,00	42,29		38,57	24,00	26,29
Zr	31,27	45,55	23,36	34,24	27,34	33,36	66,00	33,35	37,83	58,53	52,45	53,23	29,35	34,61
Sm			9,06	55,04	55,92			25,06	24,55	47,53		45,56	24,68	27,53
Ti	19,09	25,06	20,87	16,44	18,51	15,16	16,79	13,88	13,75	18,60	13,11	16,21	12,22	13,28
Tb			7,47	25,45	30,81			12,42	13,33	23,43		21,82	11,82	13,43
Y	8,83	14,17	5,38	12,30	21,36	6,98	15,81	6,26	8,89	12,48	16,43	14,19	7,29	7,64

Tabela 6 – Tabela de dados litogeoquímicos para elementos traço (µg/g) para rochas ácidas normalizados pelo manto primordial de Wood *et al.* (1979). Valor de normalização para o Ti de acordo com Wood *et al.* (1981).

Amostra	GUA-89	GUA-72-1	GUA-136	GUA-52-3	GUA-14	GUA-21	GUA-73-1	GUA-87	GUA-132	GUA-100	GUA-10	GUA-56-1	GUA-137	GUA-135	GUA-76	RIO-1	GUA-07R
Litotipo	Riolito	Tufo	Riolito	Riolito	Riolito	Riolito	Tufo	Riolito	Riolito	Tufo	Riolito	Riolito	Riolito	Riolito	Riolito	Tufo	Riolito
Cs	15,79	200,53			84,21	75,26				357,89		152,63				73,68	42,63
Rb	102,44	113,26	356,98	148,84	235,81	244,19	96,51	73,26	272,09	257,67	351,16	213,49	232,56	354,65	251,16	69,53	175,58
Ba	15,21	123,54	130,56	50,79	0,93	1,48	155,42	461,51	1,46	45,37	33,33	17,72	8,73	6,88	110,58	29,37	43,25
Th	122,92	154,17			158,33	171,88				129,17		231,25				178,13	219,79
U	70,37	84,81			103,70	95,93				85,19		144,44				181,48	275,93
K	189,26	118,76	284,31	112,88	184,57	183,32	118,09	77,56	210,85	142,07	251,88	101,95	173,42	223,64	177,84	58,82	154,31
Ta	34,88				60,47					27,91		69,77				37,21	
Nb	42,26	23,39	114,52	62,90	67,58	38,39	41,94	32,26	79,03	37,58	80,65	80,32	66,13	85,48	85,48	55,81	61,77
La	188,59	113,94			88,73	95,07				276,06		108,59				182,82	63,94
Ce	138,42	79,47			69,74	72,63				120,32		86,26				108,42	10,21
Sr	3,93	18,74	4,91	11,00	0,74	0,35	14,65	16,00	0,83	4,86	3,00	14,49	2,70	1,22	0,65	19,03	2,14
Nd	72,25	45,89			43,18	46,51				128,60		56,05				101,55	33,72
P	5,67	15,76	2,26	1,16	1,01	1,12	10,11	15,85	1,12	16,50	1,13	2,26	1,11	1,14	2,27	3,42	1,15
Hf	43,71	19,86			36,29	32,86				29,71		72,00				60,86	31,71
Zr	65,60	23,82	38,00	23,45	26,21	24,27	70,36	27,64	27,55	36,40	20,91	75,60	21,27	21,55	66,73	87,15	26,64
Sm	35,84	27,53			34,75	37,66				82,86		42,96				61,84	26,75
Ti	3,42	4,16	1,36	0,70	0,85	0,76	2,29	2,90	0,76	4,71	0,68	1,70	0,67	0,77	1,71	1,89	1,04
Tb	15,25	13,33			24,34	24,44				41,21		31,62				33,94	19,70
Y	8,46	8,48	19,30	15,61	17,08	18,32	15,40	11,29	18,69	20,86	6,78	24,46	17,04	9,45	13,76	7,29	16,37

Tabela 7 – Tabela geral de dados litogeoquímicos para elementos Terras Raras (µg/g), para rochas ácidas e intermediárias.

Amostra	GUA-138	GUA-77-2	GUA-07A	GUA-12	GUA-83	GUA-62-1	GUA-16	GUA-104	GUA-93	GUA-72-1	GUA-14	GUA-21	GUA-100	GUA-07R	GUA-89	GUA-56-1	RIO-1
Litotipo	Andesito	Andesito	Andesito	Andesito	Andesito	Andesito	Andesito	Andesito	Andesito	Tufo	Riolito	Riolito	Tufo	Riolito	Riolito	Riolito	Tufo
La	19,20	110,10	128,20	60,50	52,60	104,40	95,30	57,50	63,80	80,90	63,00	67,50	196,00	45,40	133,90	77,10	129,80
Ce	38,80	212,40	173,50	120,60	97,20	217,60	192,70	109,50	112,00	151,00	132,50	138,00	228,60	19,40	263,00	163,90	206,00
Pr	4,54	28,56	30,93	14,41	12,76	26,75	23,85	13,63	15,82	17,00	15,74	16,80	47,08	11,60	28,41	20,02	34,21
Nd	16,30	118,90	116,10	53,70	49,50	104,50	92,70	51,90	60,80	59,20	55,70	60,00	165,90	43,50	93,20	72,30	131,00
Sm	3,49	21,19	21,53	9,65	9,45	18,30	17,54	9,50	10,60	10,60	13,38	14,50	31,90	10,30	13,80	16,54	23,81
Eu	1,67	5,03	3,85	2,20	2,23	4,81	4,51	2,21	3,58	1,44	0,14	0,16	2,22	0,36	0,72	0,33	1,21
Gd	4,00	20,10	20,16	7,87	8,48	16,22	15,51	7,91	9,06	9,51	13,19	13,60	26,22	11,10	10,63	17,54	21,81
Tb	0,74	2,52	3,05	1,23	1,32	2,32	2,16	1,17	1,33	1,32	2,41	2,42	4,08	1,95	1,51	3,13	3,36
Dy	4,78	13,05	16,61	7,10	7,83	13,23	12,24	6,71	7,16	7,61	14,90	14,70	22,14	12,40	8,46	20,02	19,91
Ho	1,10	2,25	3,16	1,32	1,59	2,45	2,55	1,34	1,45	1,52	3,09	3,13	3,84	2,82	1,72	4,40	3,96
Er	3,10	5,46	8,48	3,59	4,64	6,68	7,25	3,76	3,93	4,13	9,29	8,84	9,77	8,12	5,05	13,71	10,91
Tm	0,48	0,69	1,16	0,54	0,65	0,98	1,01	0,56	0,60	0,59	1,35	1,34	1,33	1,27	0,79	2,03	1,61
Yb	3,12	4,27	6,67	3,63	4,18	6,33	6,45	3,91	3,54	3,61	8,72	8,74	7,56	8,51	5,06	12,55	10,12
Lu	0,48	0,59	0,95	0,51	0,66	0,95	1,01	0,58	0,55	0,53	1,28	1,25	1,01	1,30	0,87	1,88	1,59

Tabela 8 – Tabela geral de dados litogeoquímicos para elementos Terras Raras (µg/g) normalizados pela média de condritos C1 de Boynton (1984).

Amostra	GUA-138	GUA-77-2	GUA-07A	GUA-12	GUA-83	GUA-62-1	GUA-16	GUA-104	GUA-93	GUA-72-1	GUA-14	GUA-21	GUA-100	GUA-07R	GUA-89	GUA-56-1	RIO-1
Litotipo	Andesito	Andesito	Andesito	Andesito	Andesito	Andesito	Andesito	Andesito	Andesito	Tufo	Riolito	Riolito	Tufo	Riolito	Riolito	Riolito	Tufo
La	61,94	355,16	413,55	195,16	169,68	336,77	307,42	185,48	205,81	260,97	203,23	217,74	632,26	146,45	431,94	248,71	418,71
Ce	48,02	262,87	214,73	149,26	120,30	269,31	238,49	135,52	138,61	186,88	163,99	170,79	282,92	24,01	325,50	202,85	254,95
Pr	37,21	234,10	253,52	118,11	104,59	219,26	195,49	111,72	129,67	139,34	129,02	137,70	385,90	95,08	232,87	164,10	280,41
Nd	27,17	198,17	193,50	89,50	82,50	174,17	154,50	86,50	101,33	98,67	92,83	100,00	276,50	72,50	155,33	120,50	218,33
Sm	17,90	108,67	110,41	49,49	48,46	93,85	89,95	48,72	54,36	54,36	68,62	74,36	163,59	52,82	70,77	84,82	122,10
Eu	22,72	68,44	52,38	29,93	30,34	65,44	61,36	30,07	48,71	19,59	1,90	2,18	30,20	4,90	9,80	4,49	16,46
Gd	15,44	77,61	77,84	30,39	32,74	62,63	59,88	30,54	34,98	36,72	50,93	52,51	101,24	42,86	41,04	67,72	84,21
Tb	15,61	53,16	64,35	25,95	27,85	48,95	45,57	24,68	28,06	27,85	50,84	51,05	86,08	41,14	31,86	66,03	70,89
Dy	14,84	40,53	51,58	22,05	24,32	41,09	38,01	20,84	22,24	23,63	46,27	45,65	68,76	38,51	26,27	62,17	61,83
Ho	15,32	31,34	44,01	18,38	22,14	34,12	35,52	18,66	20,19	21,17	43,04	43,59	53,48	39,28	23,96	61,28	55,15
Er	14,76	26,00	40,38	17,10	22,10	31,81	34,52	17,90	18,71	19,67	44,24	42,10	46,52	38,67	24,05	65,29	51,95
Tm	14,81	21,30	35,80	16,67	20,06	30,25	31,17	17,28	18,52	18,21	41,67	41,36	41,05	39,20	24,38	62,65	49,69
Yb	14,93	20,43	31,91	17,37	20,00	30,29	30,86	18,71	16,94	17,27	41,72	41,82	36,17	40,72	24,21	60,05	48,42
Lu	14,91	18,32	29,50	15,84	20,50	29,50	31,37	18,01	17,08	16,46	39,75	38,82	31,37	40,37	27,02	58,39	49,38

CAPÍTULO II – ARTIGO

PETROGENESIS OF VOLCANIC ROCKS IN A NEOPROTEROZOIC STRIKE-SLIP BASIN – SOUTHESTERN, BRAZIL

Tiago Casseb Barbosa[1], Eleonora Maria Gouvea Vasconcellos[2], Barbara Trzaskos[3], Oswaldo Siga Junior[4], Kei Sato[4], Leonardo Mairink Barão[1].

[1]Programa de Pós-Graduação em Geologia, Universidade Federal do Paraná; [2]Laboratóriro de Análise de Minerais e Rochas - LAMIR – Departamento de Geologia, Universidade Federal do Paraná; [3] Laboratório de Análise de Bacias Paleozoicas - LABAP – Departamento de Geologia, Universidade Federal do Paraná; [4]Instituto de Geociências, Universidade de São Paulo.

ABSTRACT

In the southern portion of Brazil, the Guaratubinha basin is found overlaying archean and paleoproterozoic rocks. This geological unit can be framed within the strike-slip basin style. Along with others it forms a group of Neoproterozoic basins filled up by volcanic-sedimentary rocks. The basin filling is composed majorly by volcanic rocks, divided into two groups: intermediate (andesites) and acid (rhyolite). Giving the importance of those rocks to better understanding of the basin evolution a petrogenesis approaches into volcanic and the associated volcaniclastics rocks was done. The main goal of this research is to indicate the most probable formation mechanism of volcanic rocks. From field observation and geochemical analyses, it could be interpreted that the both magmas are not correlate or cogenetic, presenting a greater number of differences over similarities. The differences occur in different scales, from macroscopic to microscopic, and varying in structural, fabric and compositional aspects. On macroscopic scale, the intermediate rocks are marked by a well develop flux structure. On other hand, the acid ones are delimited by columnar jointing. Different microscopic aspects are controlled by the compositional variations in the mineral assemblage of volcanic rocks. More specifically, the differences are given by the type of feldspar. The studied rocks can be classified as sub-alkaline, with the intermediate ones following a tholeiitic trend, whereas acid ones follow a calcic-alkaline trend. Observing the plot pattern on bivariate diagrams, it was noticed that evolutionary trends are only distinguishable when the magmas are individualized. In general, they present a process of depletion (oxides) and enrichment (trace elements) towards the most evolved terms. Another important observed feature was the occurrence of magma mingling, when the andesitic and rhyolitic magmas mix up without consuming one of the involved parts and forming a hybrid material. That result is given by the immiscibility of a magma to the other, corroborating their incompatibility. The isotopic analysis also reveals more evolutionary differences between the studied rocks. Both rock sets originated at crust and evolve independently from each other. The intermediate set evolves according to a simple-stage model

while the acid set evolves as a double-stage model from paleoproterozoic parental rocks. Geochronological data reveals that the intermediate rocks bear volcanic zircon crystals with main volcanism period between 580 and 593 Ma. It was also found xenocrystals, inherited from neoproterozoic and paleoproterozoic bedrocks. The characterization of studied magma as non-cogenetic is a strong evidence to discard the partial melting of single source hypothesis. In addition, the fact that this same incompatibility is observed on isotopic data as well, contradicts the contamination hypothesis. Therefore, the most suitable petrogenetic hypothesis is that those magmas were generated and evolve from different sources.

Key-words: Geochemistry. Volcanism. Magma Mingling.

1 INTRODUCTION

The Guaratubinha Basin is found in the southern part of Mantiqueira Province (Figure 1), along with a group of late to post-collisional basins which were filled up with an association of sedimentary, volcanic and volcaniclastic rocks. This group also includes Campo Alegre and Corupá (Almeida *et al.*, 1981; Waichel *et al.*, 2000; Teixeira *et al.*, 2004). Additionally, the basin is fit into a strike-slip style (Barão *et al.*, 2017). Bimodal volcanism is reported to occur in pull-apart basin, in worldwide examples, with similar conditions observed in Guaratubinha basin (e.g. Dostal *et al.*, 2017; Gutmanis, 1989; Ibañes *et al.*, 2017; Tatar *et al.*, 2007). This paper main goal is to characterize the volcanic rocks geochemically and isotopically, while dating the andesitic rocks, in order to create a petrogenetic model that satisfactorily explains the circumstances on which those rocks were forms.

2 GEOLOGICAL CONTEXT

The Guaratubinha Basin has been studied since 1967, by many geologists such as Reinhardt Fuck (Fuck *et al.*, 1967), when it's first describe its rocks. Since then, many other researchers have been studying the Guaratubinha Basin from different geological aspects. Daitx & Carvalho (1980) performance the first geochemistry research, Licht (1988) follow their steps, expanding it to an economic insight. Castro (1993) was the first to describe the rocks that fill the basin as being composed mainly by volcanic and volcaniclastic sets. Siga Jr. (1995) worked with geochronology dating of rhyolites. Most recently, Barão (2016) compiles the main tectonic-stratigraphic ideas and

redesign the stratigraphic column and establish a tectonic-evolutionary model for the basin. The bedrocks of Guaratubinha Basin include several units of archean and paleoproterozoic metamorphic rocks (Almeida *et al.*, 1981). From those, the relevant for this paper are: Luis Alves Terrane, Curitiba Terrane, Rio-Pien Granitic Calcium-Alkali Suite, Serra da Graciosa Granitic Alkali Suite and the Guaratubinha Basin (Figure 1).

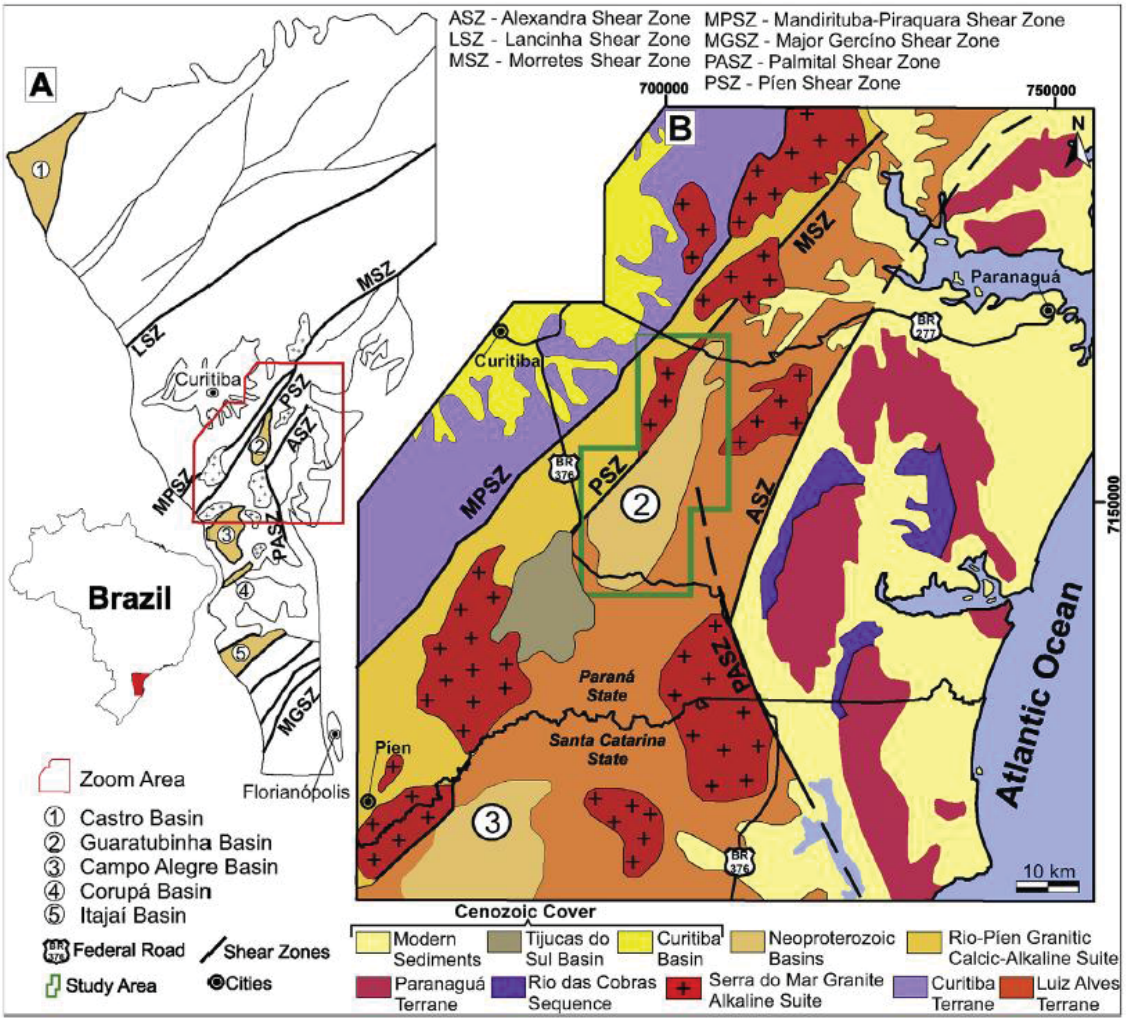

Figure 1 – Regional geological setting of Guaratubinha Basin. Basin area is contoured with green polygon. Source: Barão *et al.*, 2017.

Since Fuck *et al.* (1967), Guaratubinha Basin is known to be fills with volcano-sedimentary rocks. Barão (2016) consider those rocks as a Group, formed by three formations, with one of them being divided into three Members. From the bottom to the top, the sequence begins with Miringuava Formation, a sedimentary pack with conglomerates, sandstones and mudstones. Next is the Vossoroca Formation, an extensive andesitic lava flow. Finally overlaying those

last formations is the Serra do Salto Formation, divided into three members: Osso da Anta, Castelhanos and Escutador. Both Osso da Anta and Castelhanos Members are formed by volcaniclastic rocks, as Osso da Anta being formed by ignimbrites where as Castelhanos by tuffs, ignimbrites and epiclastic rocks. Escutador Member is formed by rhyolitic lava flow (Figure 2). Siga Jr. *et al.* (1999) show that $U\text{-}Pb_{(zircon)}$ and $Rb\text{-}Sr_{(wr)}$ data indicates a generation window between 600 – 570 Ma for the rhyolites from Guaratubinha and Campo Alegre basins, as well as for the Serra da Graciosa granites. The Sr initial rate ($^{87}Sr/^{86}Sr$) is considered high, above 0.707. A mantle differentiation age (T_{DM}) was calculated between 2200 – 1850 Ma. Barbosa (2015) analyzed the lithogeochemical characteristics of andesites and rhyolites, concluding that those magmas are not cogenetic. Their differences of evolutionary trends and geochemical signatures indicate that genesis may be related to: different partial melting taxes; or different source material; or contamination.

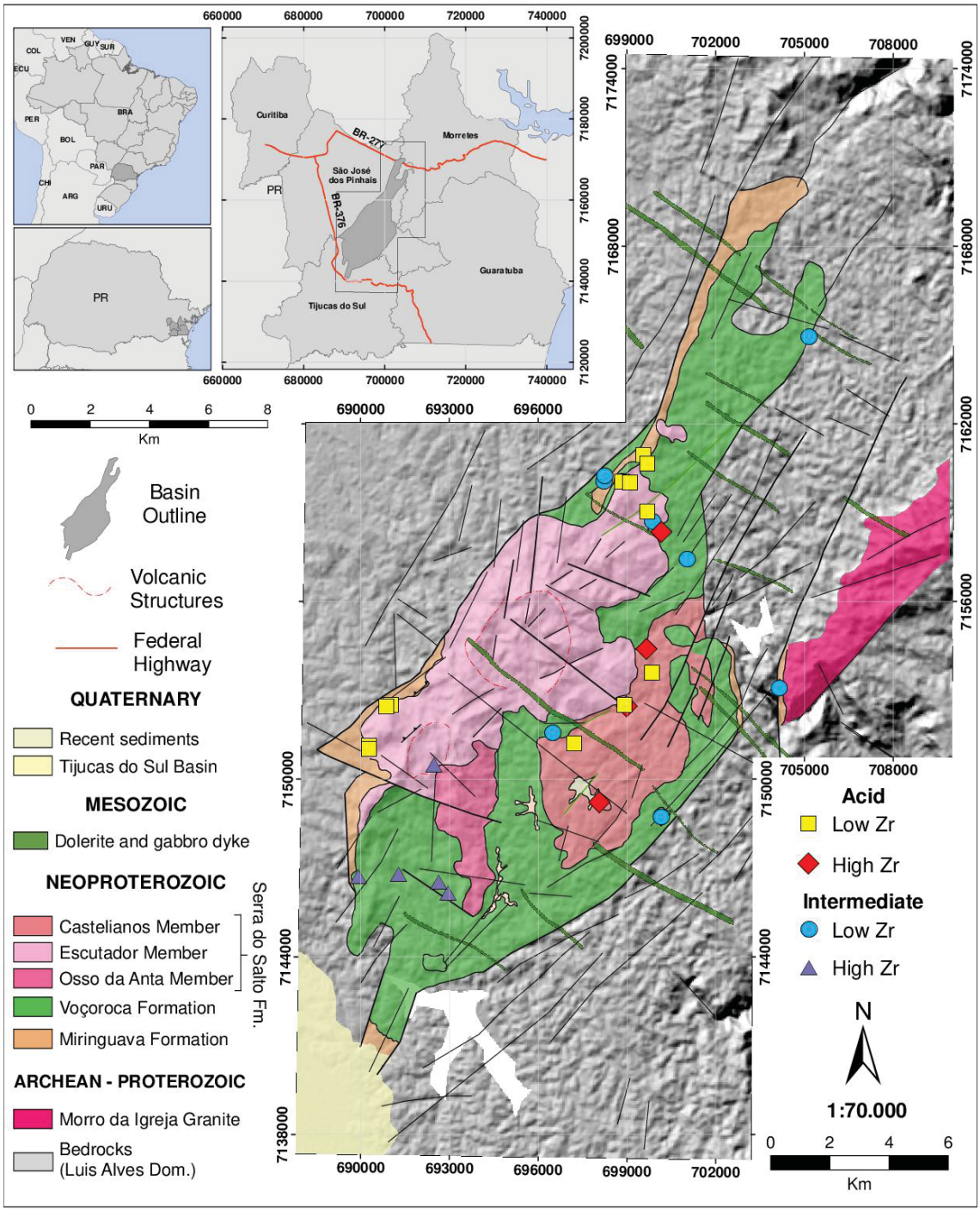

Figure 2 – Geological map of Guaratubinha Group. Source: Barão *et al.* 2017.

3 MATERIALS AND METHODS

In order to accomplish a complete geochemical and isotopic characterization of the volcanic rocks, it is necessary to analyze the samples from four main aspects: petrographic, lithogeochemical, isotopic geochemical and geochronological. The full set of samples analyzed in this paper includes 14

andesites, 13 rhyolites and 4 tuffs. There were made a total of 8 thin sections (3 andesites, 3 rhyolites and 2 tuffs) for the petrographic analysis. The geochemical database used for this paper contains the full data of all 31 samples regarding the oxides. Trace elements data was partially obtained for the all samples. From that data, 17 samples also contain full data for REEs. 3 samples were analyzed for isotopic geochemistry. 2 samples were analyzed for geochronology.

The petrography was conducted at Microscopy Research Laboratory (LAPEM) in Federal University of Paraná (UFPR). The lithogeochemistry was carried out in two to research centers. Initially the analysis was conducted at Mineral and Rock Analyses Laboratory (LAMIR) in UFPR. Later it was carried out at Laboratory of Chemistry and ICP in NAP Geoanalytical-USP. The isotopic geochemistry was performed at Geochronology Laboratory in University of Brasília (UnB). Finally, the geochronology was done at Geochronological Research Center (CPGeo) in University of São Paulo (USP). The petrographic analysis is mainly responsible to individualize lithofacies within the volcanic flows. In addition, the petrography it's the most important tool to understand geochemical anomalies that were pointed out during others phases of this study. The lithogeochemistry analysis is use to classify geochemically the rocks by identifying their evolutionary trends and geochemical signatures. The first one can be obtained by using an X-Ray Fluorescence (XRF) to analyze oxides: SiO_2, TiO_2, Al_2O_3, $Fe_2O_{3(total)}$, MnO, MgO, CaO, Na_2O, K_2O, P_2O_5 and LOI (loss on ignition). The latter one is obtained by using Inductively Coupled Plasma Mass Spectrometry (ICP-MS) to analyze trace elements: Cs, Rb, Ba, Th, U, K, Ta, Nb, Sr, P, Hf, Zr, Ti, Tb, Y and Rare Earth Elements (REEs). REEs are classified as trace elements and despite some were used on a general multi-elementary diagram, the whole REEs series is also analyzed on separate diagrams, due to their petrogenetic importance. Those procedures also help on defining lithofacies by indicating similarities and differences in the rock groups. The lithogeochemistry also includes the analysis of discrimination diagrams. Those are used with the purpose of pin point the possible tectonic environment which the magma could evolve. The isotopic geochemistry analysis concerns about the ratio between pairs of isotopes to define the isotopic signatures of the

studied rocks, which help us to understand some of their petrogenetic features. The isotope pair used in this paper was $^{147}Sm/^{143}Nd$, analyzed through ICP-MS. It was possible to estimate the depth level of a magma formation. In addition it could be estimated when the magma depleted from the mantle (T_{DM}) reservoir, the crustal residential time of magma and other petrogenetic parameters. Geochronology also uses pairs of isotopes, although it is used for dating purpose only. In this paper it was use the U-Pb series, which includes $^{238}U/^{206}Pb$ and $^{235}U/^{207}Pb$. The analysis was done by using two techniques, first was ICP-MS with laser ablation (LA-ICP-MS) and the second ionic microprobe (SHRIMP). The results were used to calculate the age of crystallization for intermediate lava flows.

4 CALCULATIONS

Most of the methods applied on this research need some calculation in order to achieve the necessary parameter. Whereas some methods use simple mathematics, other required more complex equations. The isotopic geochemistry analysis takes into consideration relations between isotopes that can be express by the following equations (Rutherford & Soddy, 1903; DePaolo, 1988; Geraldes, 2010).

$$\varepsilon_{Nd(T)} = \left\{ \frac{\left(^{143}Nd/^{144}Nd\right)(T)_{sample}}{\left(^{143}Nd/^{144}Nd\right)(T)_{CHUR}} - 1 \right\} 10000 \quad (1)$$

$$f_{(Sm/Nd)} = \frac{\left(^{147}Sm/^{144}Nd\right)_{sample} - \left(^{147}Sm/^{144}Nd\right)_{CHUR}}{\left(^{147}Sm/^{144}Nd\right)_{CHUR}} \quad (2)$$

Through those parameter it possible to distinguish between simple-stage or double-stage evolution model, which need different equations in order to calculated the T_{DM} (Sato, 1998; Sato & Siga Jr., 2001). Those equations are the following, used for simple an double models, respectively

$$T_{DM} = \frac{1}{\lambda_{Sm}} \times ln\left(1 + \frac{\left(^{143}Nd/^{144}Nd\right)_{DM} - \left(^{143}Nd/^{144}Nd\right)_{sample}}{\left(^{147}Sm/^{144}Nd\right)_{DM} - \left(^{147}Sm/^{144}Nd\right)_{sample}}\right) \quad (3)$$

$$T_{DM} = \frac{1}{\lambda} \times ln\left(1 + \frac{\left\{\left(^{143}Nd/^{144}Nd\right)_{DM} - \left[\left(^{143}Nd/^{144}Nd\right)_{sample} + \left(^{147}Sm/^{144}Nd\right)_{T1} - \left(^{147}Sm/^{144}Nd\right)_{T2} \times \left(e^{\lambda T2} - 1\right)\right]\right\}}{\left(0.219 - \left(^{147}Sm/^{144}Nd\right)_{T1}\right)}\right) \quad (4)$$

5 RESULTS

This section of the paper includes not only the results for the four main petrogenetic analyses of petrography, lithogeochemistry, isotopic geochemistry and geochronology but also the lithological and structural information of intermediate and acid rocks, observed in the field trips.

5.1 FIELD INFORMATION

During the geological mapping, it was observed some characteristics of the volcanic flows. In the field, the intermediate rocks are recognizable as andesites, given by a quartz-feldspar phenocrystals and amygdales among an aphanitic mass. The andesites have a magmatic flow structure given by orientation of amygdales or plagioclase phenocrystals. They occur more frequently in the southern and northern portions of the basin, also appearing of the eastern part (Figure 2). Usually the andesitic lava flows are found overlaying by abrupt contact with rhyolitic lava flows (Figure 3). The acid rocks are recognizable in field as rhyolites given by their mineral composition are made of k-feldspar and quartz phenocrystals among an aphanitic mass. The rhyolites lava flows present columnar jointing structures (Figure 4), which indicated the cooling time of those lava flows was slow. Those rhyolitic lava flows occur in the middle-west portion of the basin. They seem to have flowed from circle like structures (Figure 2), observed on digital elevation model (DEM). Those structures could be interpreted as ancient volcanic cones.

Figure 3 – Abrupt contact between andesite and rhyolites. Lava flows contact (red dash line).

Figure 4 – Columnar jointing on rhyolitic lava flows.

Along the northern contact zone between andesitic and rhyolitic lava flows, their contact is given by magma mingling features, where it can be observed a complex intercalation of white and reddish-brown strips encompassing andesite blocks. The rich quartz content of the white strips indicated that they are rhyolites affected by weathering and kaolinization, while the reddish-brown strips, which contain fragments of amygdales and more

rarely plagioclase, are andesites also affected by weathering and argilization processes (Figure 5).

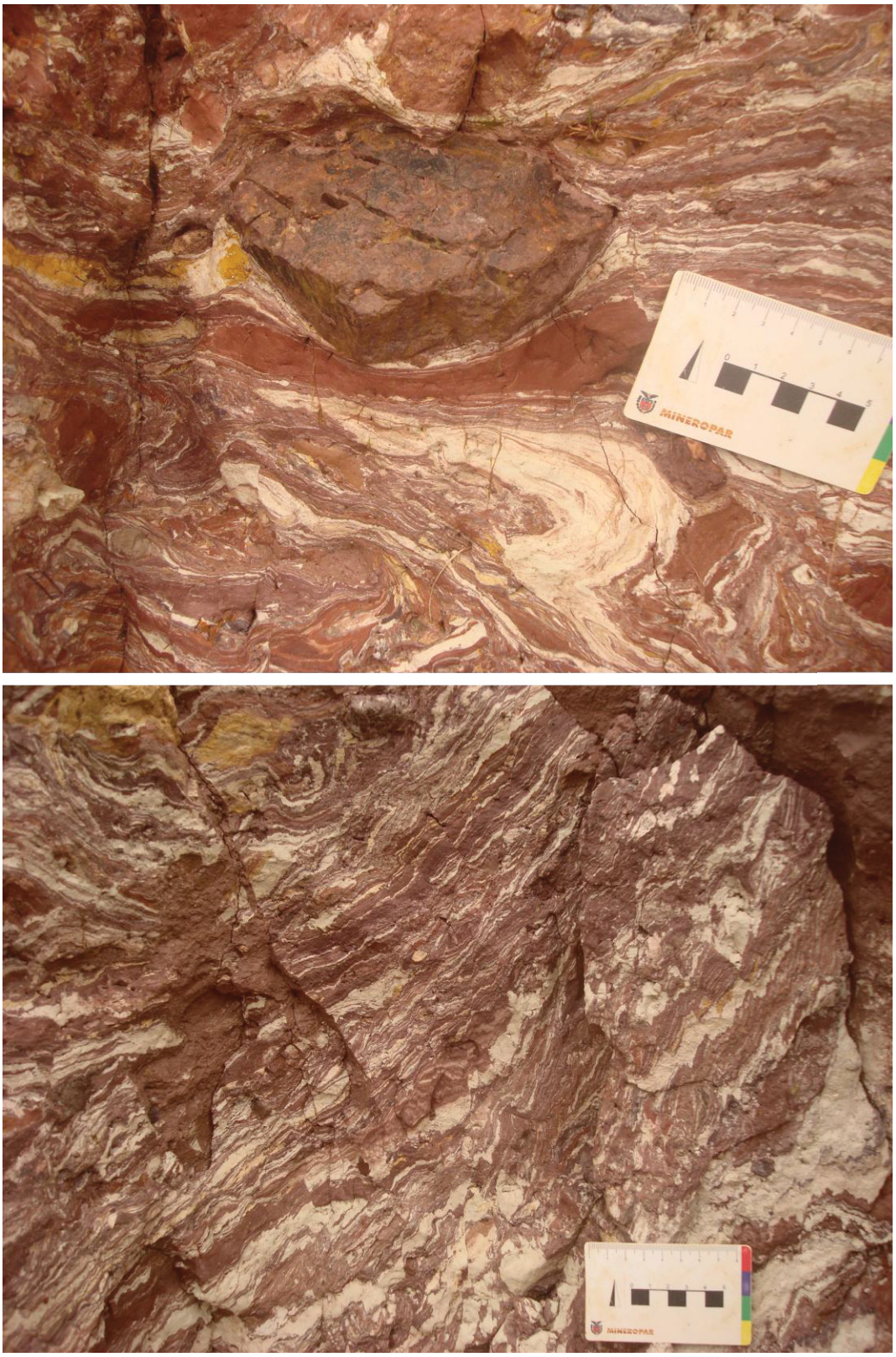

Figure 5 – Magma mingling features on contact zone of andesitic and rhyolitic lava flows.

5.2 PETROGRAPHIC ANALYSIS

The andesites thin sections (GUA-07-4, GUA-12 and GUA-16-2) show a porphyritic texture as the common fabric for those rocks. The mineral assemblage can be divided into phenocrystals and matrix minerals. The phenocrystal group is usually composed by andesine (30 – 35 mol % An), quartz and a non-distinguishable amphibole. The matrix seems to be composed by plagioclase, quartz, opaque minerals and volcanic glass (Figures 6A). Most of phenocrystals present undulose extinction. In most cases the andesine also presents Carlsbad twinning (Figure 6B) and more rarely polysynthetic twinning (Figure 6C). The feldspar phenocrystals have a tabular habit with the bigger axis align according to an incipient orientation, which may indicate a magmatic flow structure (Figure 6D). Some minerals as result of weathering or hydrothermal alterations can be found associate with the feldspars, amphiboles and opaque minerals, as well as filling up amygdales (Figure 6E). Chlorite and epidote are found nearby or covering feldspar crystals or substituting amphibole crystals. In the latter case it can be seen a zoning define by only chlorite crystals on the border whereas epidote and chlorite are combine in the center zone (Figure 6F). In addition to chlorite and epidote, amygdales are also filled by quartz. Those quartz crystals from the amygdales are smaller and clearer than the phenocrystals, indicating their genesis differs from one another.

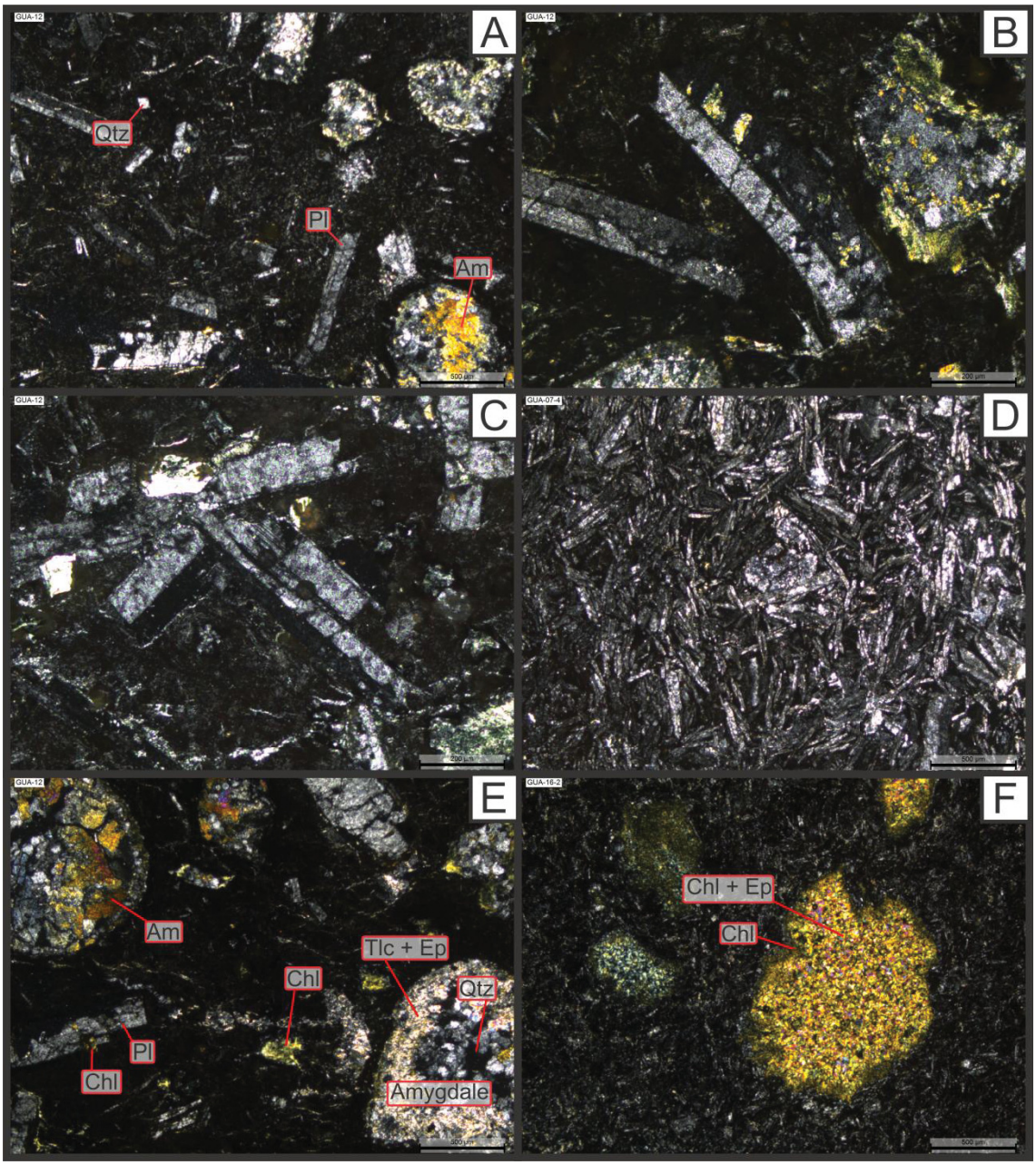

Figure 6 – Andesites micrographs on orthoscopic light. (A) General view of andesites' thin section showing quartz, plagioclase and amphibole phenocrystals. (B) Detail of Carlsbad twinning. (C) Detail of polysynthetic twinning. (D) Incipient orientation of plagioclase crystals showing magmatic flow structure. (E) General view of secondary minerals in andesites' thin sections. (F). Zoning pattern showing chlorite as external zone and chlorite plus epidote as internal zone filling amygdales.

The rhyolite thin sections (GUA-14-2, GUA-21-3, GUA-52-3) show a rock which fabric is define by porphyritic texture similar to the andesites. However, in this case there are phenocrysts of sanidine, microcline and quartz among a matrix formed by alkali feldspar, quartz and opaque minerals. Different

from the andesites, it wasn't observed undulose extinction on any of the rhyolites thin sections. Microcline crystals are recognizable by their distinct cross-hatched twinning while sanidine crystals present Carlsbad twinning with perthitic texture (Figures 7A and 7B). Another difference to be observed from rhyolite thin sections to andesite ones is that there are no indication of magmatic flow structure on rhyolites thin sections. The rhyolites are also affected by weathering or hydrothermal alterations, however on a lesser grade than the andesite. Chlorite and epidote are the main alteration product as well as talc, even though it is less common. Although they are usually related to alkali feldspar, from both phenocrystals and matrix crystals, they also occur associated with opaque minerals (Figure 7C).

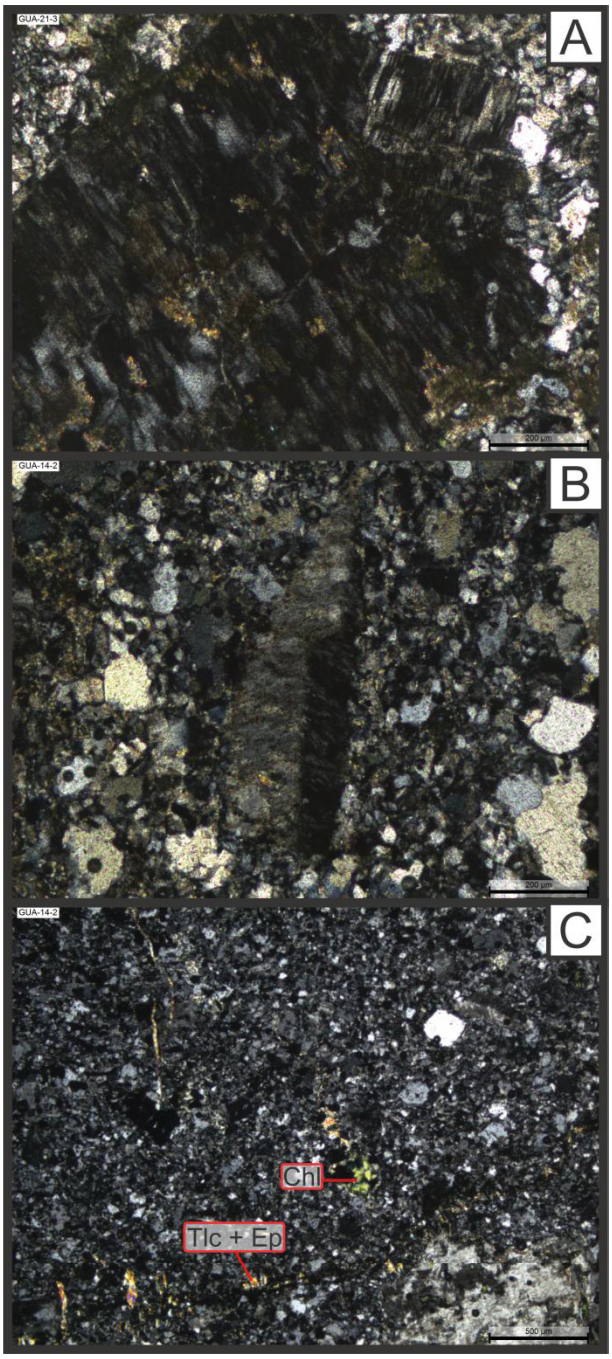

Figure 7 – Rhyolites micrographs on orthoscopic light. (A) Details of Cross-hatched twinning on microcline phenocrystals. (B) Details of Carlsbad twinning on sanidine phenocrysts. (C) General view of secondary minerals in rhyolites' thin sections.

The volcaniclastic rocks found in the Guaratubinha Basin are genetically related to the rhyolites (Barbosa, 2015). Therefore, some samples were included on the analyses in order to confirm that statement. They were classified according to the grain size classification establish by Fisher (1966). It can be observed on hand samples a layering of fine and very fine grains, or in

other words, silt-sized and clay-sized grains. Thus, those volcaniclastic rocks were considered to be composed mainly by ash, and could be classified as tuffs, according to used classification diagram.

Tuffs thin sections' (GUA-72-1 and GUA-73-1) mineral assemblage combine minerals observed in andesites and rhyolites, such as plagioclase, alkali feldspar, amphibole and quartz. This fact may occur because some andesites' outcrops could have been eroded during the eruption which formed those volcaniclastic rocks. The tuff main structure is sets of horizons, divided by their grain size (Figure 8A). The coarser horizon is composed by quartz, microcline with cross-hatched twinning (Figure 8A), plagioclase with polysynthetic twinning, sanidine and amphibole (Figure 8B). The thinner horizon is composed by crystals of quartz, feldspar and opaque mineral. As secondary minerals it can be observed chlorite and epidote in the intergranular pores (Figure 8B).

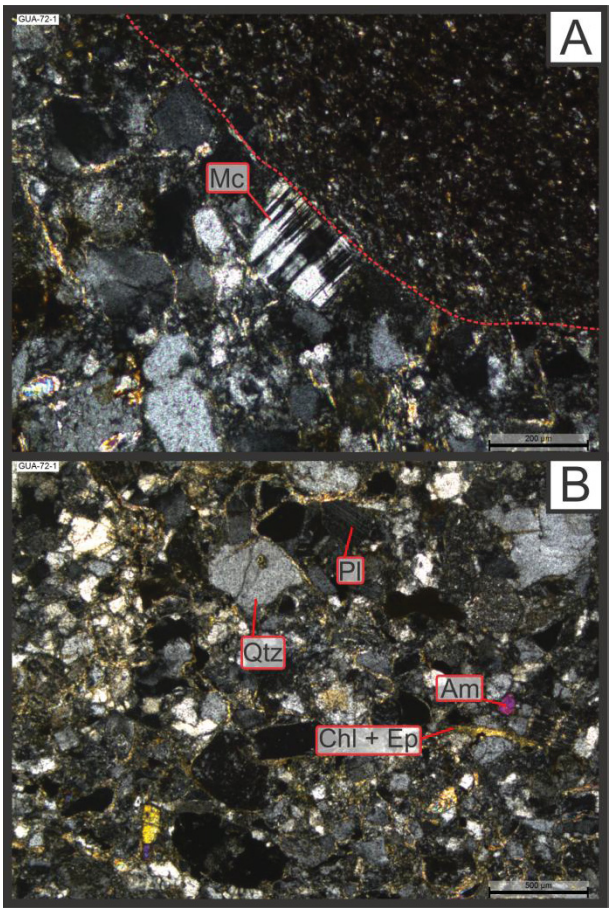

Figure 8 – Tuffs micrographs on orthoscopic light. (A) Limit of layering on tuff (red dash line). Detail of cross-hatched twinning on microcline clast. (B) General view of coarse layer clasts in tuff's thin sections, showing quartz, plagioclase, amphibole and secondary minerals.

5.3 LITHOGEOCHEMISTRY

Although volcaniclastic rocks are not the focus of this paper, some of tuff samples were included. It is considered that they were formed during the same volcanic event of rhyolites, since they have a similar geochemical signature (Barbosa, 2015). Hence the tuff samples are going to be analyzed and represented as rhyolite samples from now on.

This section of the paper concerns with using whole rock data to analyze geochemical classification, evolutionary trends and geochemical signature. The whole rock database shows two sets of rocks concerning their SiO_2 content, considering Le Maitre's classification (Le Maitre *et al.*, 1989). The first set has a range from 48.01 to 60.32 weight percentage (wt %), therefore being classified as intermediate rocks. The second set has a range from 63.65 to 80.34 wt %, thus this set of rocks is classified as acid. Two samples (GUA-93 and GUA-104) were initially classified as acid due to their silica content, 63.65 and 66.01 wt %, respectively, which is higher than 63 wt % (limits between intermediate and acid). However, their geochemical behavior was compatible with intermediate rocks. That happens because their silica content before anhydrous base recalculation was lower than 63 wt % but still very close to it (60.33 and 62.55). Therefore, those two samples will be included in the intermediate rock set, even though their silica content is above the limit between intermediate and acid fields.

The total alkali vs. silica (TAS) diagram (Le Maitre *et al.*, 1989) shows that the intermediate rocks group can be classified as phono-tephrite, trachy-basalt, basaltic andesite, basaltic trachy-andesite, trachy-andesite and andesite. The acid rocks group are classified as rhyolite (Figure 9). Two samples plotted on dacite field are the ones that are going to be included on the intermediate group.

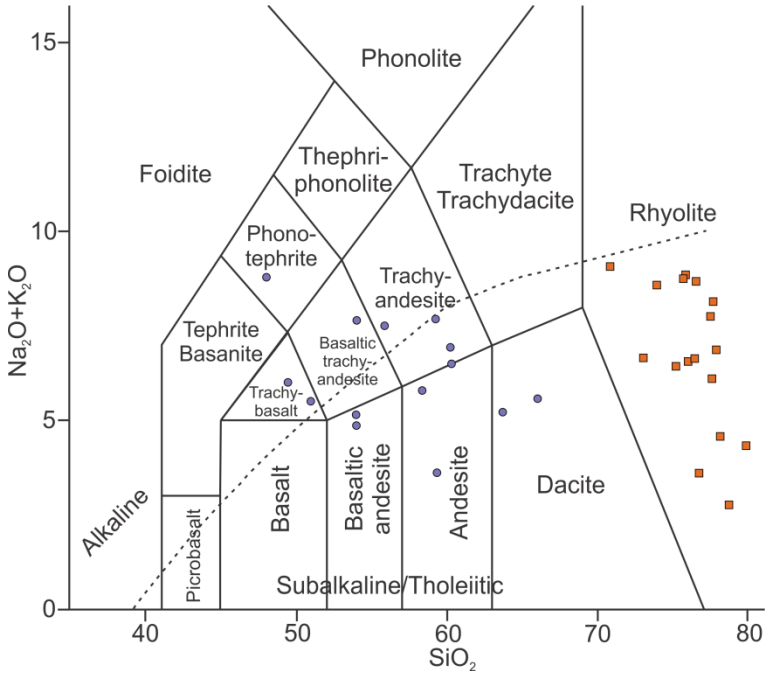

Figure 9 – Total alkalis vs. silica diagram ($(Na_2O+K_2O) – SiO_2$) from Le Maitre *et al*. (1989). Used to classify intermediate (purple circles) and acid rocks (orange squares) sets. Boundary (dashed line) between alkaline and subalkaline/tholeiitic zones (Irvine & Baragar, 1971).

The AFM diagram (Irvine & Baragar, 1971) shows that the studied rocks, previously classified as subalkaline on TAS, can be fit into two magmatic series. The intermediates ones plotted into tholeiitic series, groping close to the AF axis. The acids set starts plotting in a similar way to the intermediate set, with low MgO content, represented in the diagram as M value. Then it begins to turn toward the center of the diagram. Comparing to magmatic series proposed by the author, it can be assumed that the acid set has dominant calcic-alkaline character, with some samples tending to the alkaline series (Figure 10). The acid sample that plotted among the intermediate one was petrographic describe as a tuff. As mention before, the tuff mineral assemblage often incorporate andesite mineral, which is a feature observed during petrographic analysis. That fact may be responsible to why this sample presented a tholeiitic character.

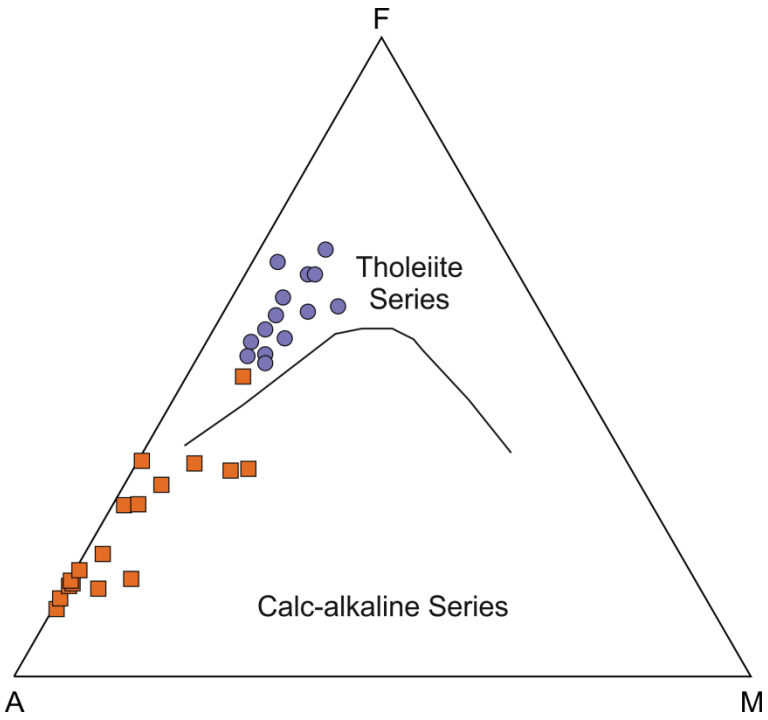

Figure 10 – AFM diagram of Irvine & Baragar (1971). Used to classify subalkaline intermediates (purple circle) and acids (orange squares) rocks sets.

For both sets, intermediate and acid rocks, the Harker diagrams using oxides show an alignment of the samples, indicating that they are plot according to a trend of evolution. For both sets those evolutionary trends are better represented by a polynomial functions (curves) rather than linear functions (straight lines). The coefficients of correlation (R^2) of polynomial functions are generally lower than 0.5, even though they are usually higher than those of linear function. At most cases those trends indicated a descent pattern (depletion) of elements percentages towards the most evolve samples. Considering the intermediate rocks this pattern is more evident on TiO_2, Al_2O_3, $Fe2O3_{(total)}$ and K_2O diagrams (Figure 11). For the acid rocks, that same depletion pattern can observed on $Fe_2O_{3(total)}$ diagram (Figure 12). It is important to notice that the diagrams which are possible to determine a pattern are the ones for oxides which are considered less mobiles, such as TiO_2 and Fe_2O_3. Although the depletion pattern can be observed for both intermediate and acid sets, the diagrams clearly show that those sets develop in different ways.

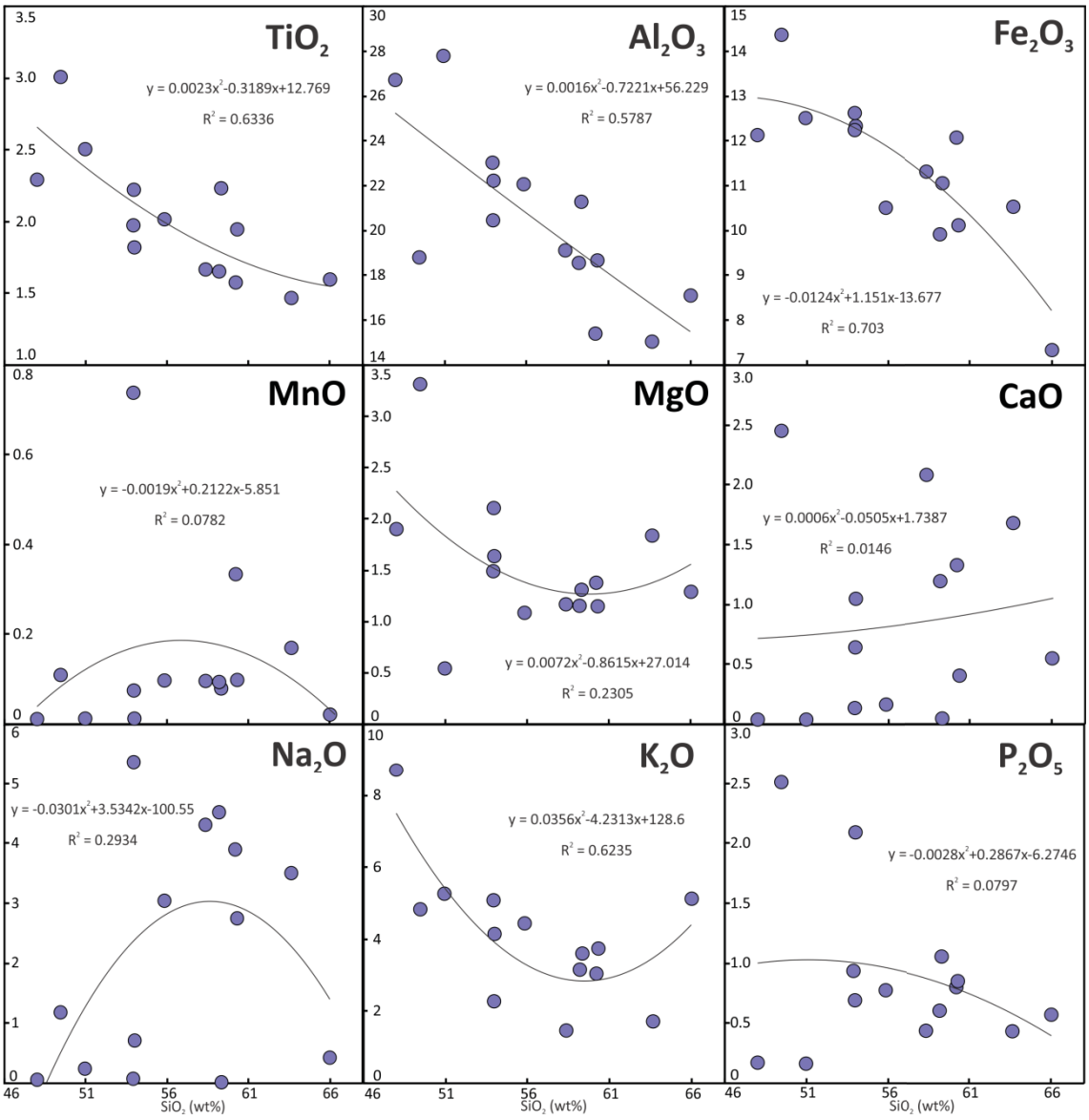

Figure 11 – Harker diagrams of intermediate (purple circles) rocks set with trend line (continuous black line).

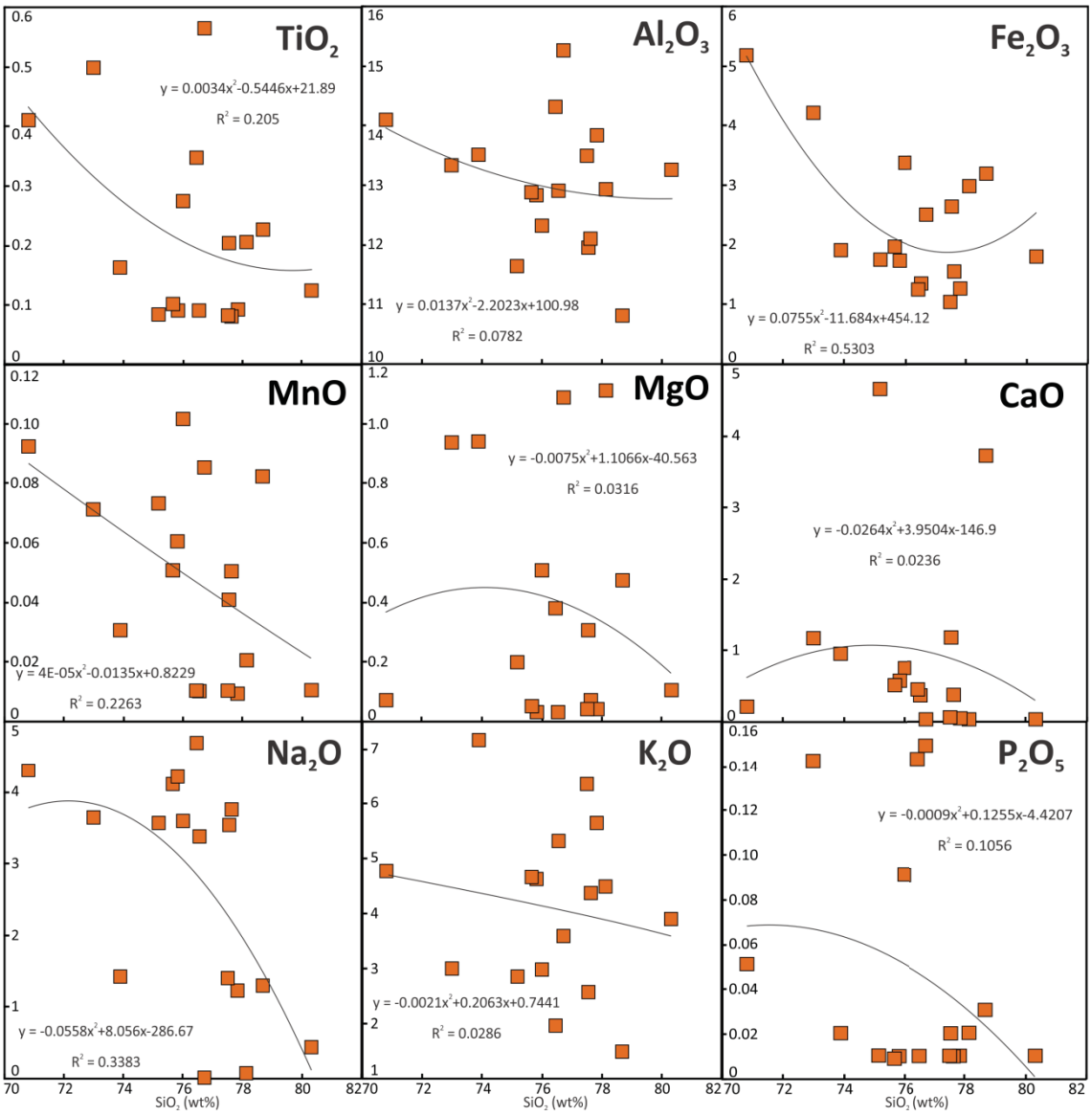

Figure 12 – Harker diagrams of acid (orange squares) rocks set with trend line (continuous black line).

The trace elements variation diagrams were usually plotting to scattered to be analyzed. The coefficients of correlation (R^2) were generally very low, meaning that no evident evolutionary trends were easily recognized. Therefore, it was conducted a statistic analysis of the whole rocks database. It seems that, besides silica itself, many trace elements as Rb, Sr, Y, Zr, Nb and Ba allow us to individualize more sets of rocks. According to statistics parameters presented on the table below (Table 1), it is possible to plot a more visual definition of those set using histograms.

Table 1 – Statistic parameters for intermediate and acid rock sets.

Rock set	Trace element	n	Mean	Std. deviation	Min.	25%	50%	75%	Max.
Intermediate	Rb	14	110.2	60.7	36.8	77.9	89.3	141.6	273
	Sr		218.3	114.8	47.5	134.6	242.9	286.7	453
	Y		55	22.9	26.2	35.9	51.6	69.1	104
	Zr		440.4	141.9	257	349.7	378.7	558	726
	Nb		27.2	11.4	14.3	16.9	26.2	32.2	49
	Ba		2111.9	1259.1	472	1048.8	2005	2838.3	4683
Acid	Rb	17	179.5	83.2	59.8	97.4	200	221.6	307
	Sr		161.3	159.1	8.1	28	90.5	333.3	437.8
	Y		71.2	25.4	33	46	76	89.2	119.1
	Zr		442	250.8	230	262	303	721.6	958.7
	Nb		38.5	14.9	14.5	26	39	49.8	71
	Ba		549.7	847.2	7	66	252	836	3489

The density ($h(x)$) histograms of those elements take into consideration the quotient of the absolute frequency by the number of elements times the range of values from each class as given in the following equation:

$$h(x) = \frac{f_i}{n(c_i - c_{(i-1)})} \tag{5}$$

The density histograms show that those elements usually divide the intermediate and acid rock sets into many populations (Figure 13). Zr seems to be the one the makes a most even division, with a roughly equal amount of classes per group. For the intermediate rocks, Zr values range from 200 to 900 µg/g. According to its density histogram, there are three clusters of samples. First one with values between 200 and 450 µg/g. Second, with values between 500 and 650 µg/g. Third one with values above 700 µg/g. The acid set show a similar behavior for Zr, with only two clusters of samples however. The first one ranges from 200 to 500 µg/g while the second ranges from 700 to 1000 µg/g. It seems logical then that the Zr allow individualizing two clusters of samples, the first being samples with low Zr, bellow 500 µg/g, and high Zr, above 500 µg/g.

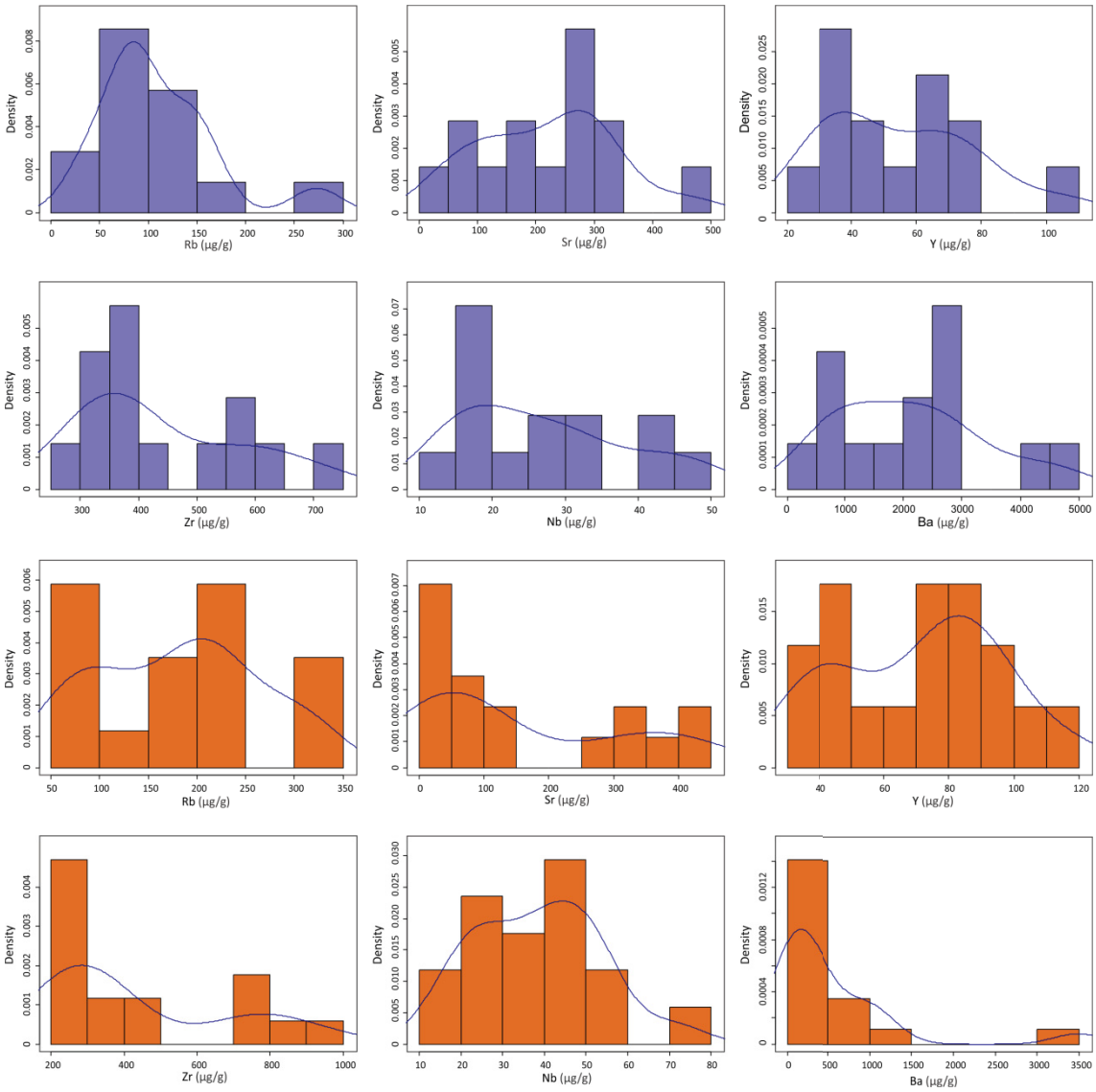

Figure 13 – Density histogram of Zr for intermediate (purple) and acid (orange) rock sets with distribution curve (blue line).

Considering the distribution of classes observed on the density histograms, the studied rocks can be divided into 4 sets considering Zr and SiO_2 behavior: low Zr intermediate set; high Zr intermediate set; low Zr acid set; high Zr acid set. Those sets are respectively composed by 9, 5, 12 and 5 samples. This division aids to better visualize evolutionary trends on the trace elements variation diagrams. After applying it to different bivariate plots, using the previously mention trace elements along the x-axis it seems that Rb is the most appropriate element to be used as fractional variant.

Well defined evolutionary trends can be observed on both low and high Zr groups from intermediate rocks set. For the low Zr, it is observed a general

ascendant pattern (enrichment) toward the most evolve samples (Figure 14). Nb and Ba diagrams can be point out as the best represents of that enrichment pattern. High Zr shows the best correlations so far. In this case, the diagrams also show an enrichment pattern toward the most evolve samples, similar to low Zr diagrams. Although the Zr diagram presents the highest r^2, the enrichment is better seen on Sr, Y, Nb and Ba, notably on the first one.

Similar to was observed on oxides Harker diagrams, the acid rock set also present a most scattered plot when comparing to intermediates. Therefore, evolutionary trends are not so distinguishable. It seems that the trends vary between enrichment and depletion, with the first been more common to low Zr set and the second more common to high Zr (Figure 15). Nb is the one which better define an enrichment trend for both low and high Zr sets. Depletion trends are better visualized on Sr and Ba diagrams from low Zr set.

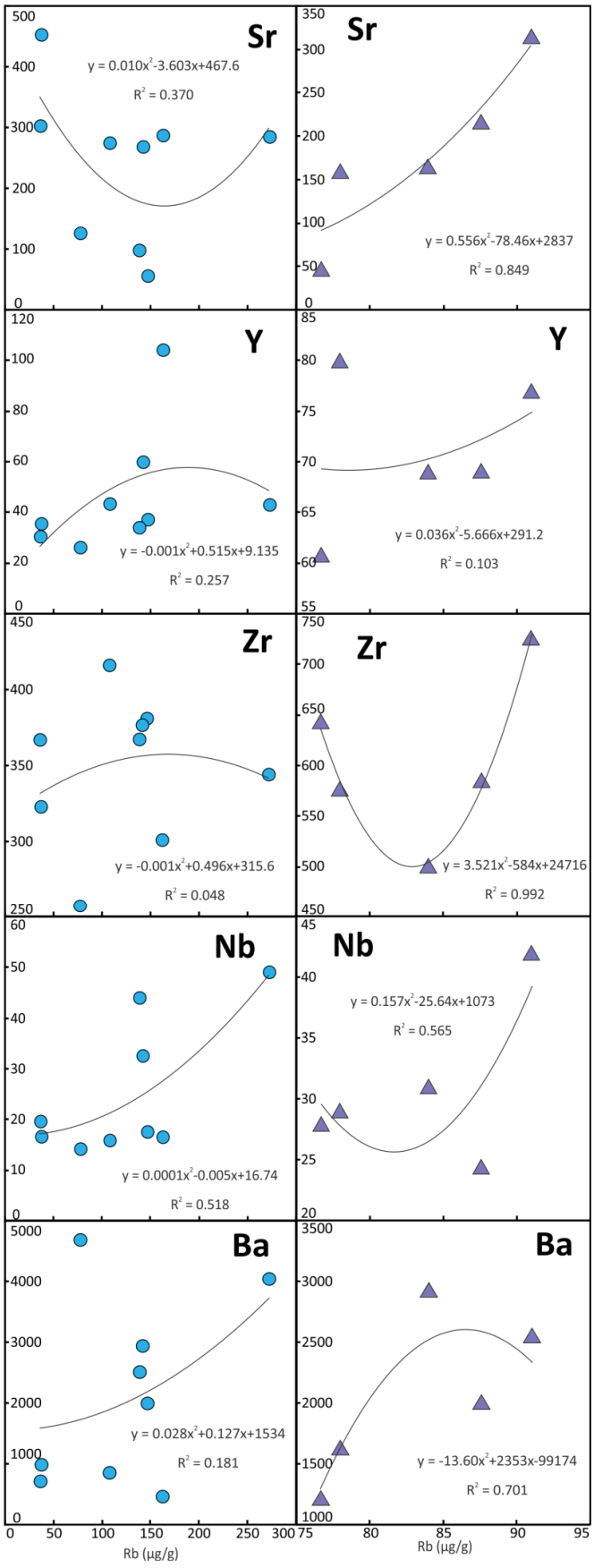

Figure 14 – Bivariate trace elements diagrams of intermediate rocks. Data from low Zr (blue circles) and high Zr (purple triangles) with trend line (continuous black line).

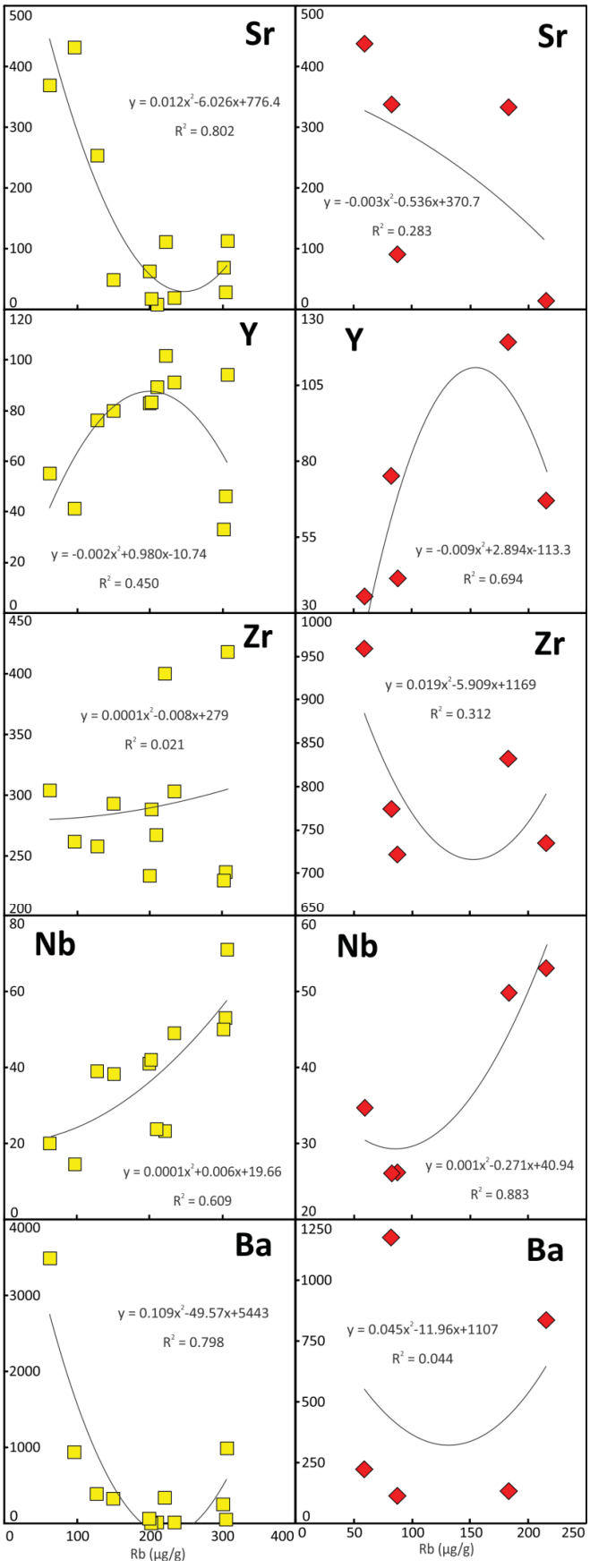

Figure 15 – Bivariate trace elements diagrams of acid rocks. Data from low Zr (yellow squares) and high Zr (red diamonds) with trend line (continuous black line).

The multi-elementary diagrams show two different geochemical signatures for the intermediate and acid rocks, even though they share a few similarities. According to Wood *et al.* (1979), the trace elements used are arranged in increasing order of bulk partition coefficient (K_D) between realistic upper mantle mineral assemblages and basaltic melts. Both signatures show a depletion pattern concordant to incompatibility increase. Positive anomalies of Ba, K, La and P are observed on intermediates sets diagram (Figure 16). From those positive anomalies only that of La seems to be observed on acids sets diagrams (Figure 17). An expressive Sr negative anomaly is present on both groups. The acid rocks set also present negative anomalies of Ba, P and Ti.

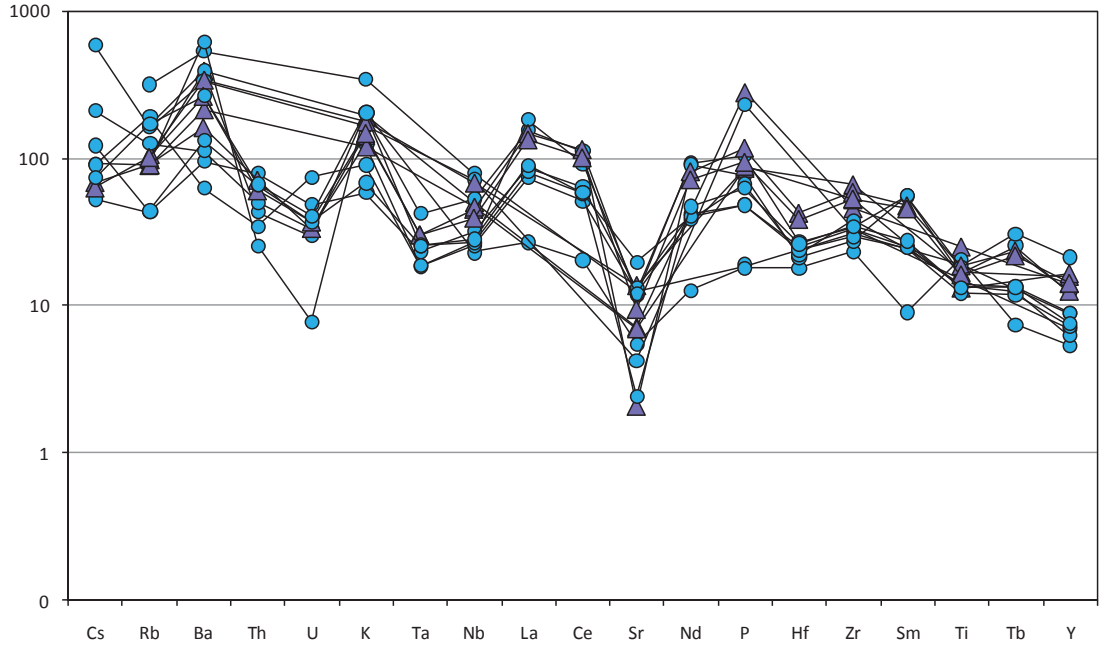

Figure 16 – Multi-element diagram for trace elements of intermediates sets. Data from low Zr intermediates (blue circles) and high Zr intermediates (purple circles) sets. Normalize by primordial mantle of Wood *et al.* (1979); Ti normalization value from Wood *et al*. (1981).

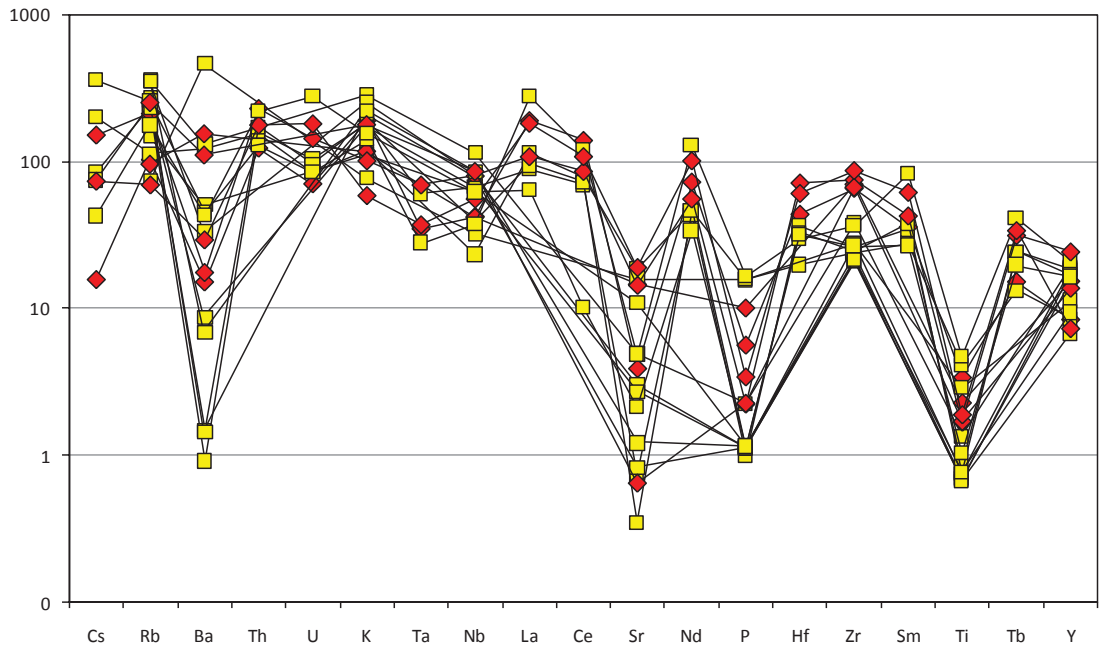

Figure 17 – Multi-element diagram for trace elements of acids sets. Data from low Zr acid (yellow squares) and high Zr acid (red diamonds) sets. Normalize by primordial mantle of Wood *et al.* (1979); Ti normalization value from Wood *et al*. (1981).

The REEs diagrams show a similar behavior of multi-elementary ones. Here the geochemical signature for both groups are different and yet show some similarities. Both are enrich on light REEs (La to Eu) and depleted on heavy ones (Gd to Lu). No significant positive anomalies can notice on diagrams for both groups aside from two low Zr intermediate samples which show Eu anomalies (Figure 18). The acid set shows a very expressive negative anomaly of Eu, which isn't observed on the intermediate set. Two of low Zr and one high Zr acid sets show a negative anomaly of Ce (Figure 19).

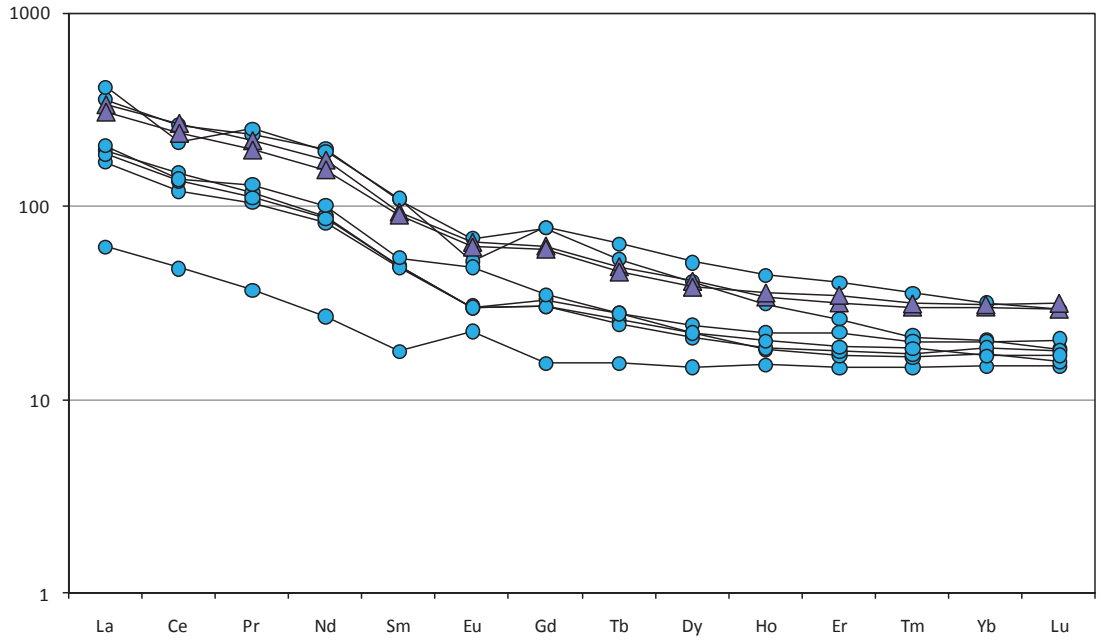

Figure 18 – Rare Earth Elements diagram of intermediates sets. Data from low Zr/Hf intermediates (blue circles) and high Zr/Hf intermediates (purple triangles) sets. Normalize by average of C1 chondrites of Boynton (1984).

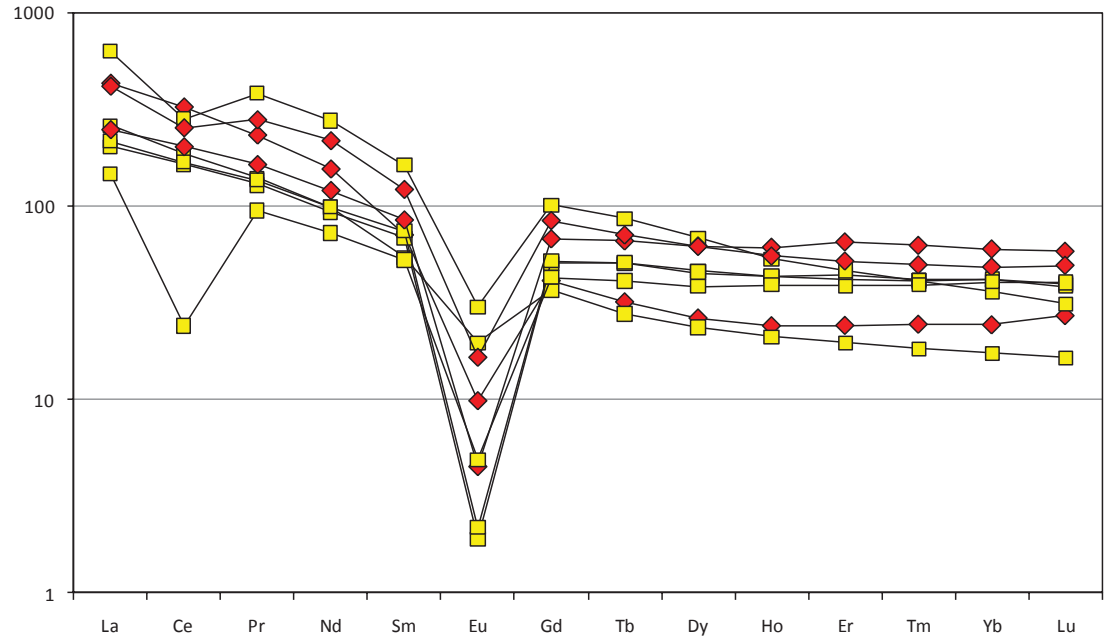

Figure 19 – Rare Earth Elements diagram of acids sets. Data from low Zr/Hf acid (orange squares) and high Zr/Hf acid (red diamonds) sets. Normalize by average of C1 chondrites of Boynton (1984).

Whole rock data can also be applied on discrimination diagrams. Ti vs. Zr diagram (Pearce, 1982) is used for intermediate rock whereas Rb-Y-Nb and

Rb-Yb-Ta variations plots (Pearce *et al.*, 1984) are used for the acid set. Both types of discrimination charts generally show a within-plate tectonic environment for both sets (Figures 20 and 21).

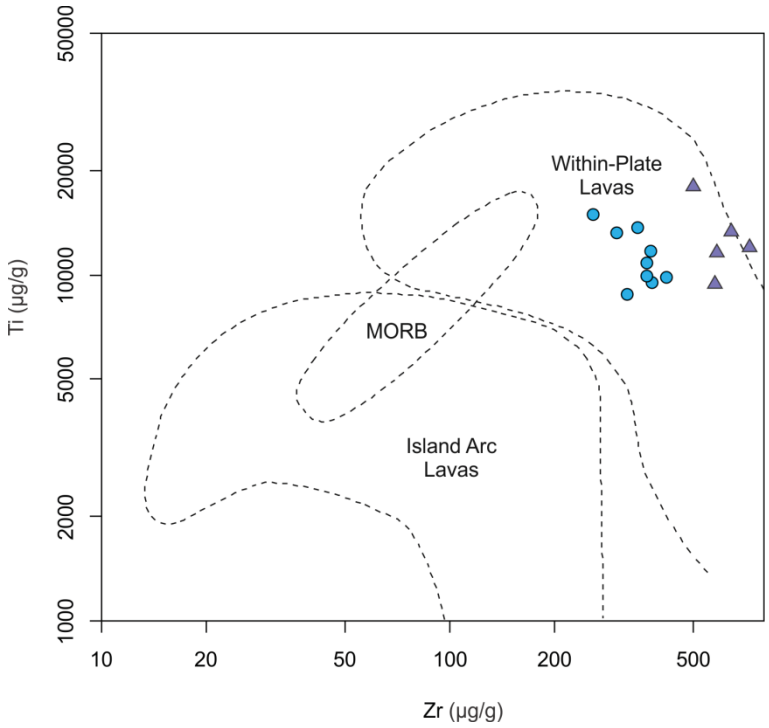

Figure 20 – Ti vs. Zr. discrimination diagram, from Pearce (1982), of intermediate rocks. Low Zr rocks (blue circle) and high Zr rocks (purple triangles).

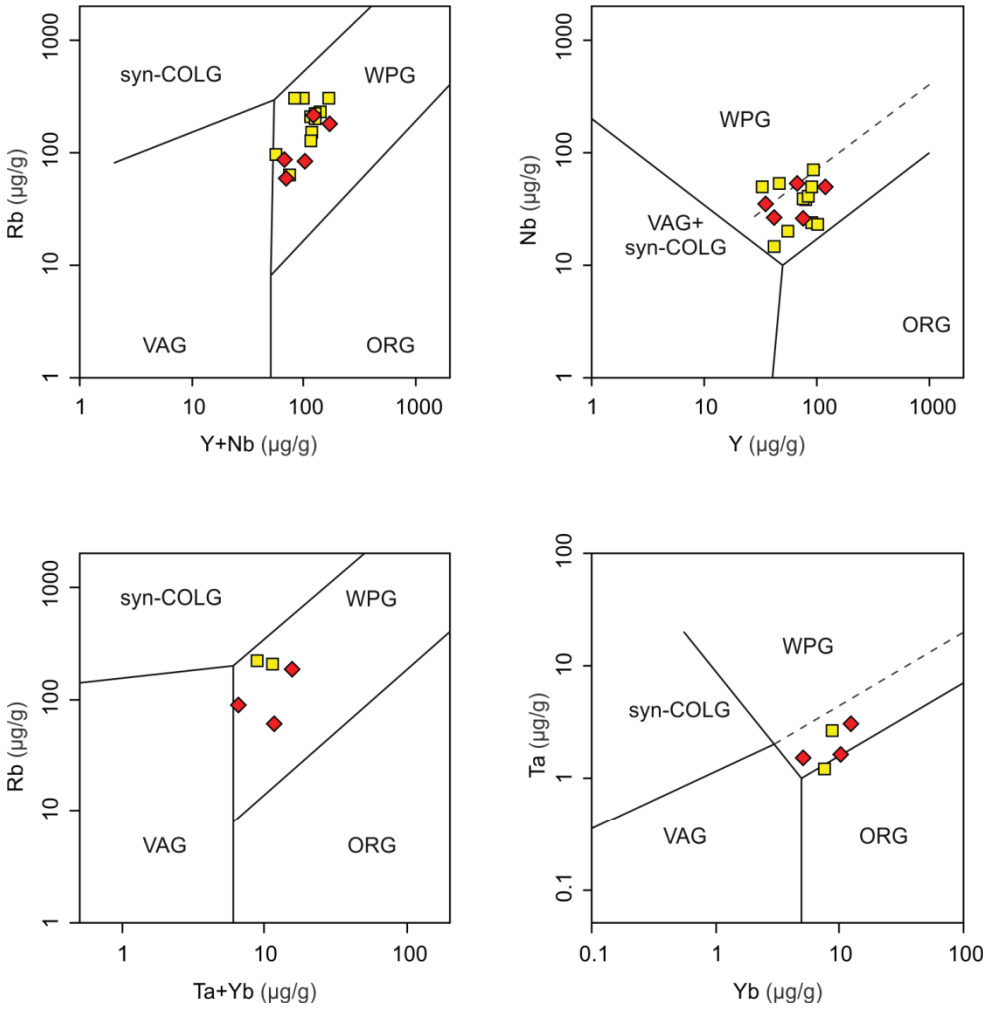

Figure 21 – Rb-Y-Nb and Rb-Yb-Ta variations plots (Pearce *et al.*, 1984) of acid rocks. Low Zr rocks (yellow squares) and high Zr rocks (red diamonds).

5.4 ISOTOPIC GEOCHEMISTRY

According to Geraldes (2010), the geological study of isotopes may be divided into two branches, concerning their applicability. The first one is the geochronology, a more classical field of study which aims to estimate an absolute age for studied rocks. The second is isotopic geochemistry, which uses newer applications for isotopic pairs in order to estimate petrogenetic features from target rocks. The $^{147}Sm/^{144}Nd$ isotopic data acquired from intermediate and acid rocks is presented on the table bellow (Table 2).

Table 2 – Isotopic data for $^{147}Sm/^{144}Nd$ from intermediate and acid rock sets.

Sample	GUA-12	GUA-83	GUA-56-1
Lithotype	Andesite	Andesite	Rhyolite
Sm (µg/g)	10.081	10.539	19.953
Nd (µg/g)	56.213	55.502	86.114
$^{147}Sm/^{144}Nd$	0.1084	0.1148	0.1401
$^{143}Nd/^{144}Nd$	0.511531 ± 3	0.511622 ± 2	0.511806 ± 4
$f_{Sm/Nd}$	-0.45	-0.42	-0.29
$\varepsilon_{(0)}$	-21.59	-19.82	-16.23
T_{DM} (Ma)	2194.5	2195.5	2150
$\varepsilon_{(TDM)}$	3.11	3.11	3.20
T_1 (Ma)	580	580	604
$\varepsilon_{(T1)}$	-15.06	-13.75	-11.87

The first parameter that can be point out is the fractionation factor ($f_{Sm/Nd}$). It was measured a value of -0.42 and -0.45 for intermediate samples. For the acid sample, the obtained value was -0.29. The $^{147}Sm/^{144}Nd$ data also reveals the currently ε_{Nd} values for the studied rocks additionally to the measured rate of $^{147}Sm/^{144}Nd$ and $^{143}Nd/^{144}Nd$. Through a number of calculations (equations 1, 2, 3 and 4) using those three parameters, it was obtained the time of mantle depletion (T_{DM}) for those rocks. They are about 2.150 and 2.2 Ga for acid and the intermediate rocks, respectively. Furthermore, it was obtain the ε_{Nd} relative to those T_{DM} values. Minding that the valid petrogenetic features come from crystallization time, it was calculated the ε_{Nd} values of andesites and rhyolites from that time. The crystallization age used for the first ones was 580 Ma, a data obtained for this paper. For the latter ones it was used a values of 604 Ma, given by Siga Jr. *et al.* (2000). Those parameters were then used to plot the T_{DM} diagram using the mantle evolutionary trend line proposed by DePaolo *et al.* (1991). The T_{DM} diagram shows the variations of ε_{Nd} values as a function of time (Ga) for the three samples (Figure 22). The acid rock presents a double-stage evolution with a close mantle derivation age (T_{DM}) the other samples. The intermediate rocks present a single-stage evolution, with good correlation between them, despite the variations of ε_{Nd} values.

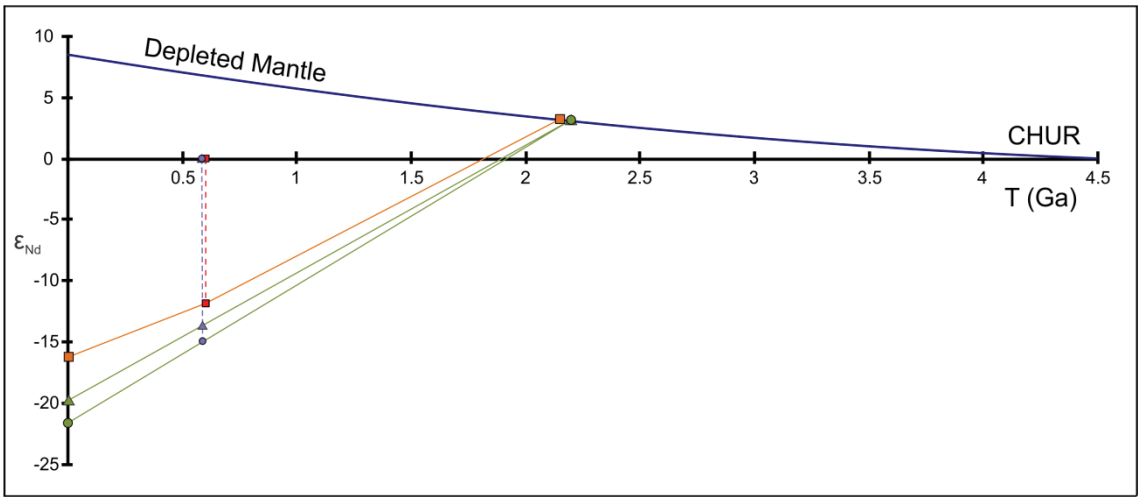

Figure 22 – T_{DM} diagram of intermediate (green) and acid (orange) rocks. Mantelic evolutionary trend line (blue line) proposed by DePaolo *et al.* (1991). Rhyolite crystallization (red dash line). Andesite crystallization (purple dash line). Samples: GUA-12 (green circle), GUA-83 (green triangle) and GUA-56-1 (orange square).

5.5 GEOCHRONOLOGY

The geochronology data reveals three populations of zircon crystals, found in intermediate rocks. The first population is composed by crystals that are fine-sized grains, slim, with prismatic habit and pyramid shape on both ends. When seen on natural light they are translucent and clear (Figure 23). When observed through cathodoluminescence, those crystals present well-defined growth lines and no pre-existing core nor diffusion or fractions on the core zone (Figures 24). Although this group of crystals appear to be more round on the GUA-07 sample, the still preserve the internal structure and characteristics. The dating of zircon crystals of both samples (GUA-07 and GUA-18) indicates a $^{238}U/^{206}Pb$ mean age between 580.5 ± 3.5 and 592.7 ± 3.9 Ma (Figure 25).

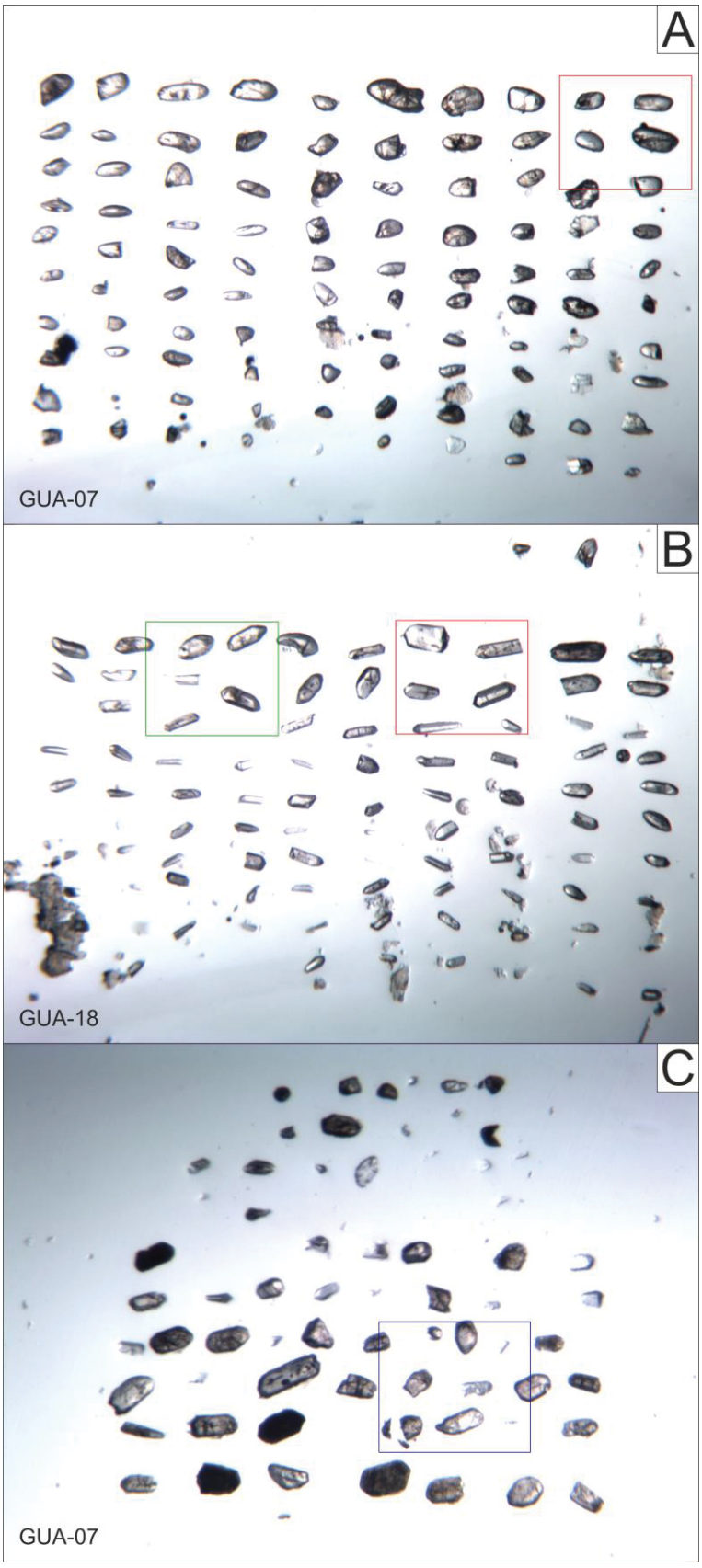

Figure 23 – General view of neoproterozoic and paleoproterozoic zircon crystals on natural light. Crystals display at figures 24 (red polygon), 26 (green polygon) and 28 (blue polygon).

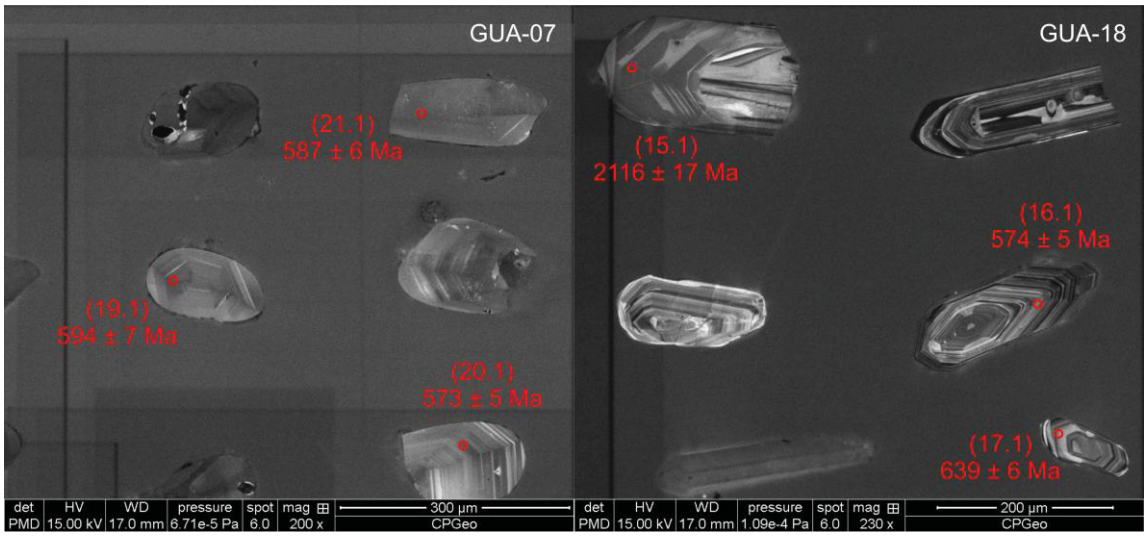

Figure 24 – Volcanic zircon crystals (≈ 580 Ma) on cathodoluminescence.

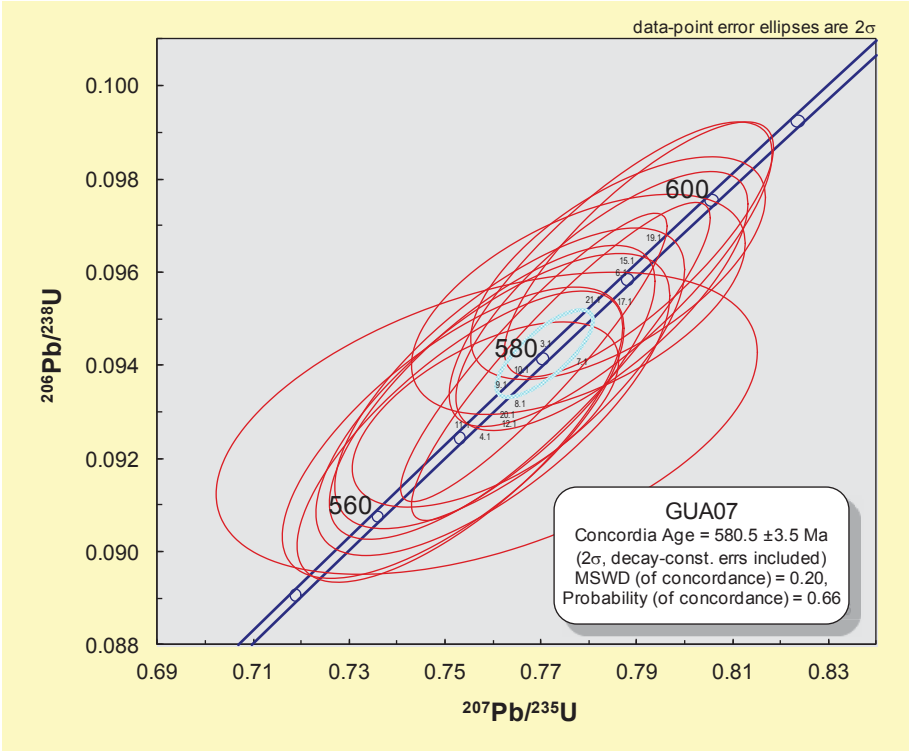

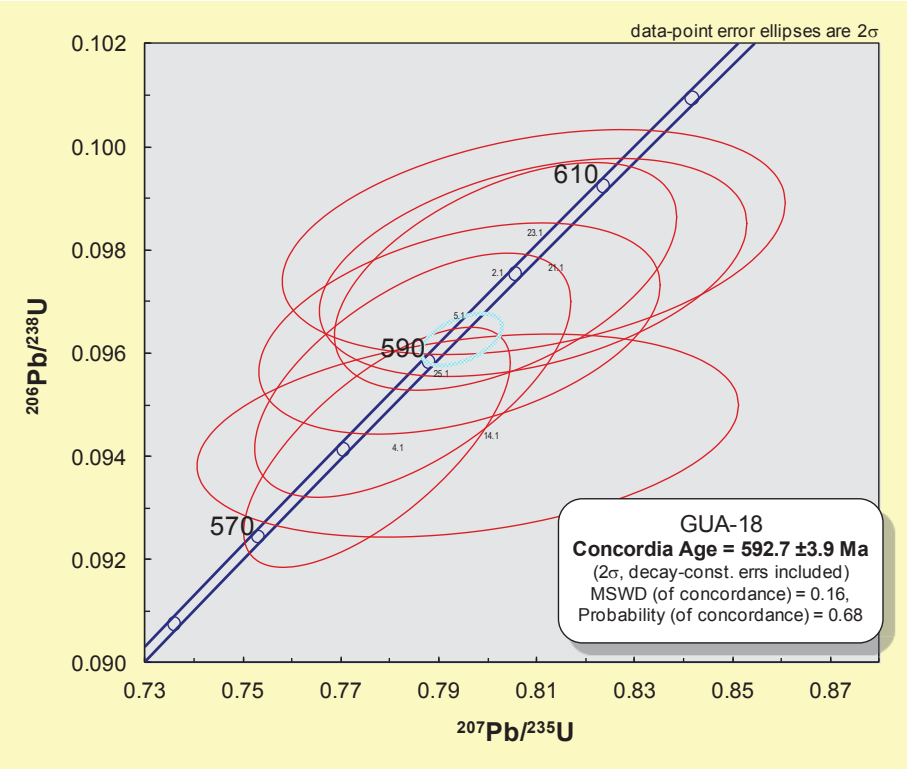

Figure 25 - Concordia diagram of volcanic zircon crystals from intermediate rocks.

The second population has an intermediate age range between the founded populations. This population is composed by fine-sized crystals, similar to the first ones. They present themselves as more thick and rounded crystals. It is observable a turbidity on natural light (Figure 23). On cathodoluminescence turbid aspect seems to be given by the presence of inclusions. It is also notice the presence of pre-existing core on most crystals (Figure 26). The calculated $^{238}U/^{206}Pb$ mean age of this population is 619.9 ± 5.1 Ma (Figure 27).

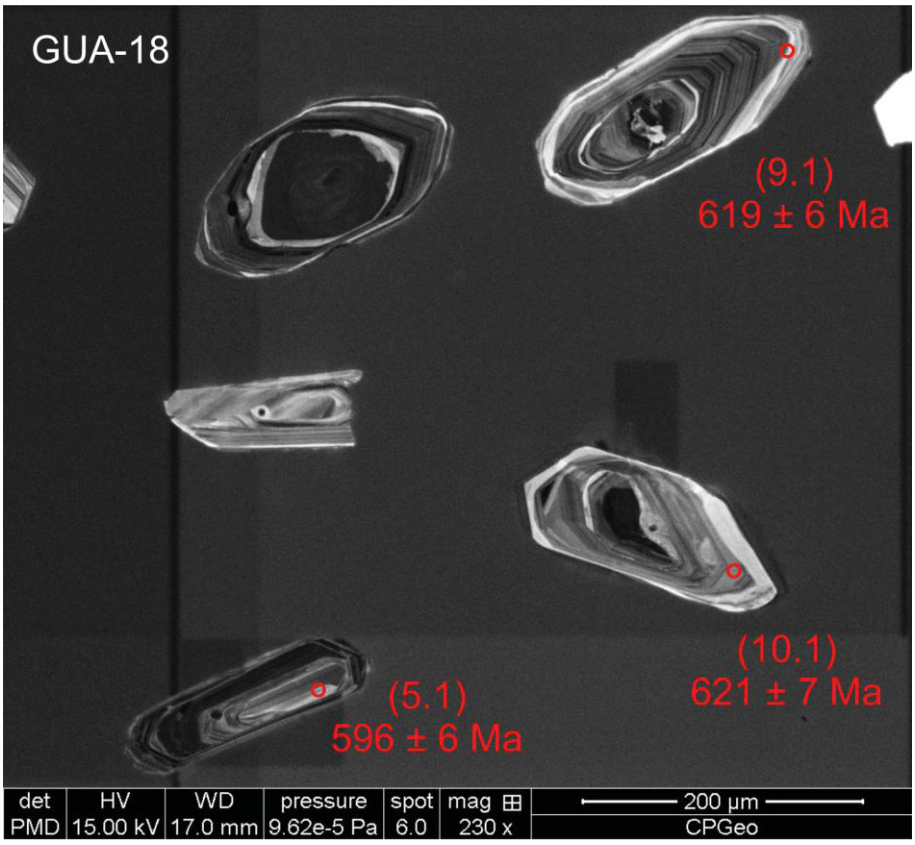

Figure 26 – Newer inherited zircon crystals (≈ 620 Ma) on cathodoluminescence.

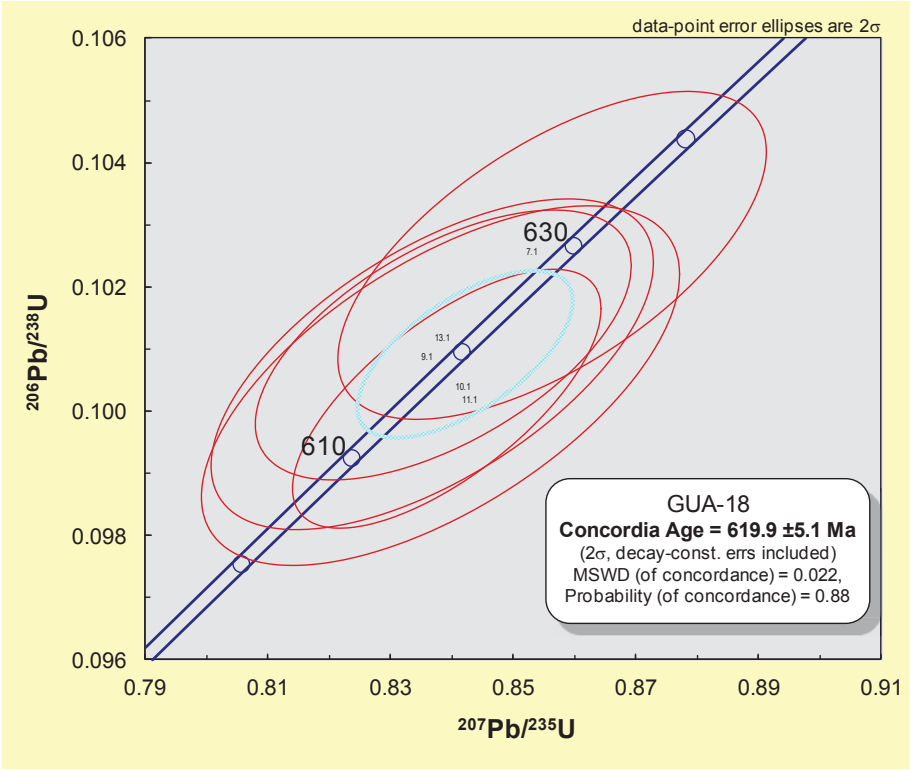

Figure 27 – Concordia diagram for newer inherited zircon crystals.

The third population is recognizable as the older one. Those zircon crystals are coarser than the volcanic ones, although they can still be classified as fine-sized grains. The crystals have a worn out prismatic habit, making them usually round and fracture. Observing on natural light they are turbid from inclusions and a black material impregnation. On cathodoluminescence it is observable a well-defined concentric radial mineral growth lines marked by black zones given by large amount of U on the mineral fabric (Figure 28). The dating of those crystals indicates a $^{238}U/^{206}Pb$ mean age of 2282 ± 16 Ma (Figure 29).

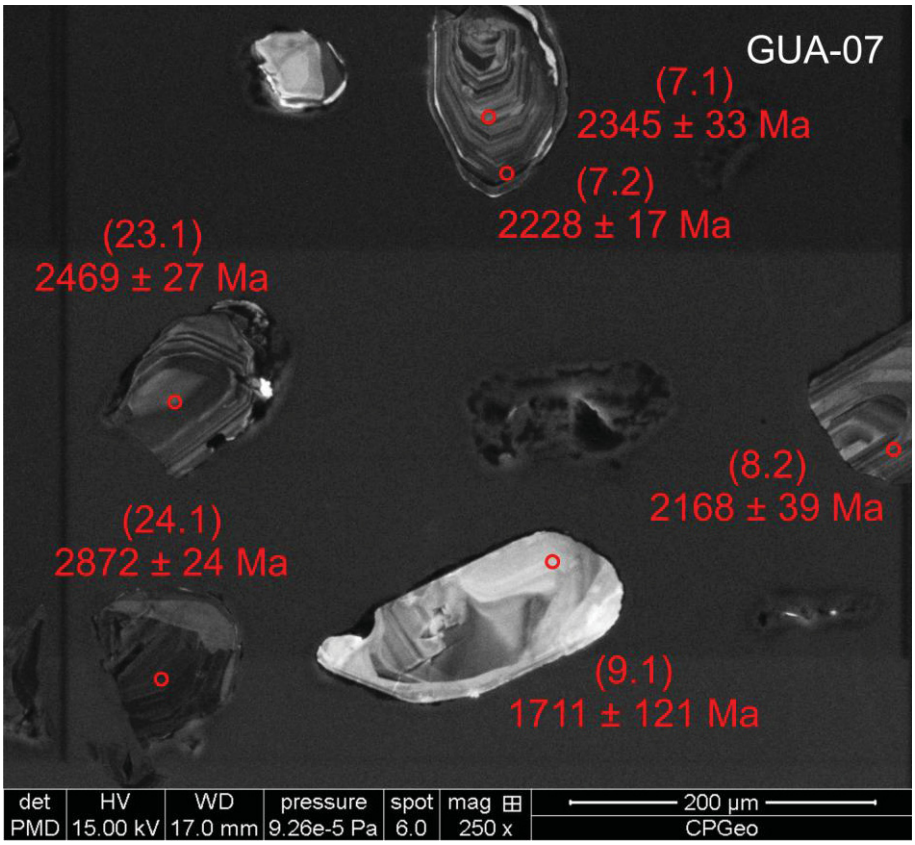

Figure 28 – Older inherited zircon crystals (≈ 2200 Ma) on cathodoluminescence.

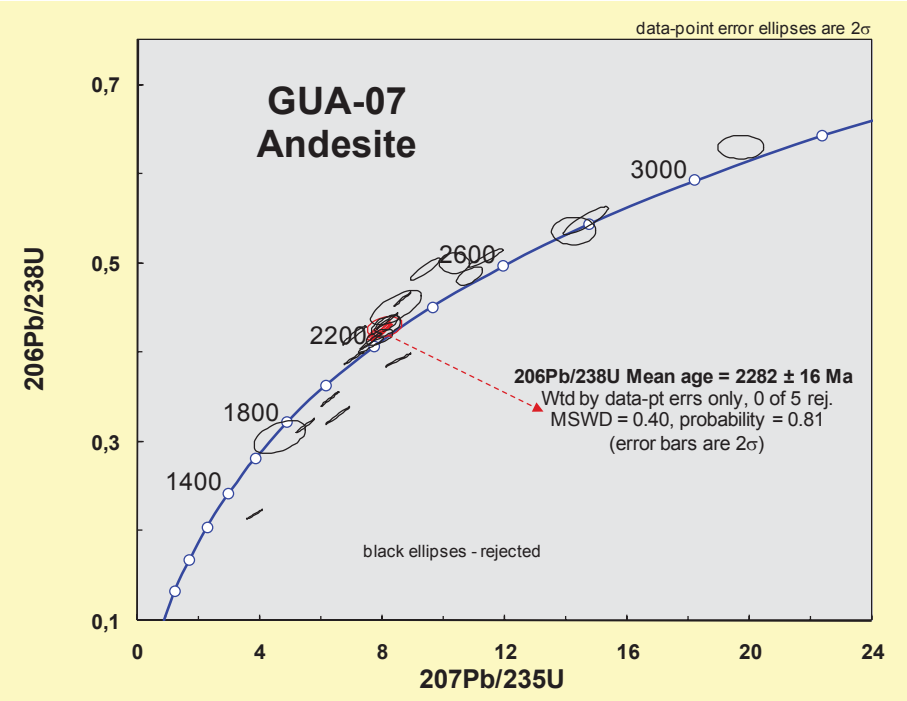

Figure 29 – Concordia diagram for older inherited zircon crystals.

6 DISCUSSION

Barbosa (2015) main conclusion was that the intermediate and acid magmas are not cogenetic, with their genetic process being related to three possible hypotheses: different partial melting taxes for a single source; different source materials; contamination of intermediate magma by host rocks. The fact that they are not cogenetic implies that those magmas will have more differences than similarities. This paper results show that those differences can be observed on many scales. Starting by macroscopic-scale observations, the intermediate lavas contains a well develop flow structures, whereas none has been identify on acid rocks. Indeed those structures, define by amygdaloidal and porphyritic zones, helps us to better understand the intermediate internal differentiation. According to Jerram & Petford (2014) inflation model for lava flow emplacement, the complete building of internal lava flow structure could take years to be formed. Therefore it can be assumed that lava flows structures, such as orientation of amygdales and phenocrystals give us a sense that the intermediate rocks had a long cooling time. In addition, the intermediates rocks rich in amygdales can be define as the flow crust, while the porphyritic ones can be identify as the flow core (Figure 30).

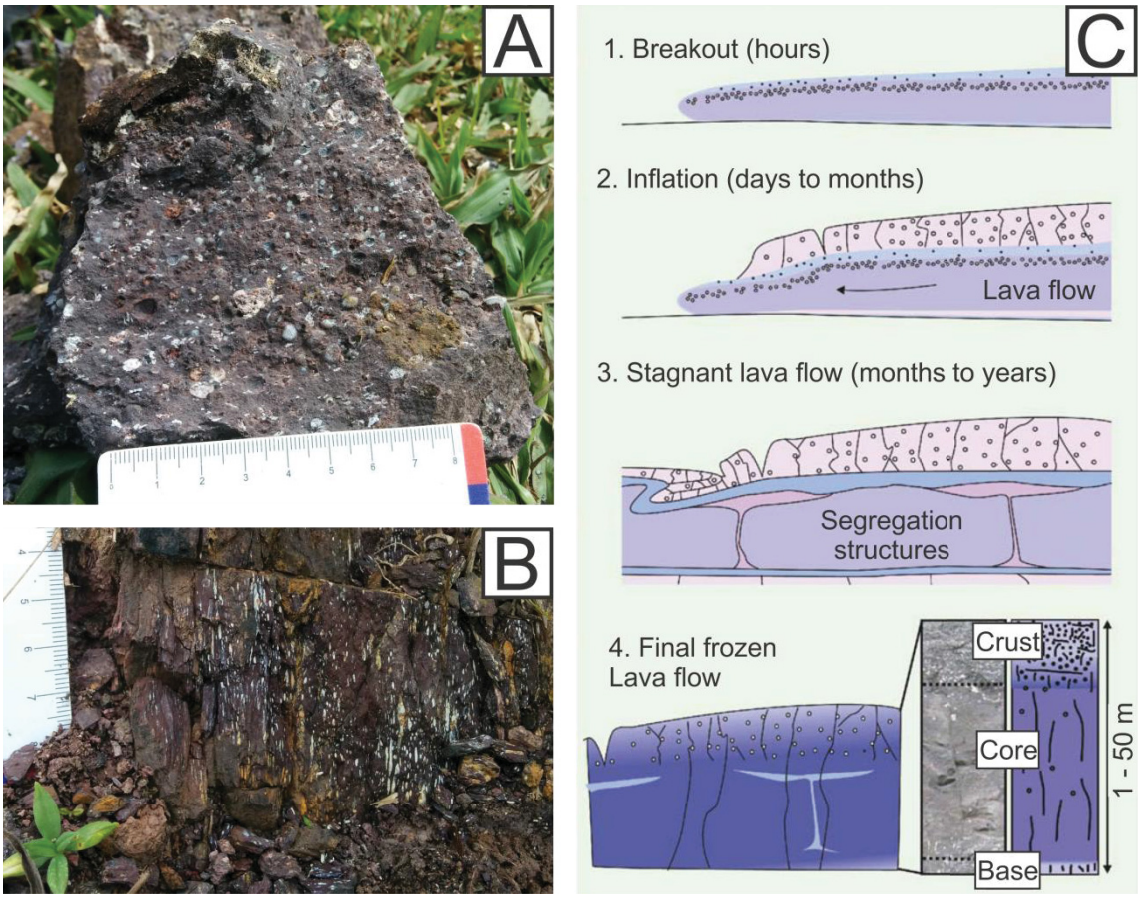

Figure 30 – Magmatic flow structure on andesites. A. Amygdale zone. B. Porphyritic zone. C. Inflation model for lava flow emplacement (Jerram & Petford, 2014).

More differences are observed considering the stratigraphy of the lava flows. The acids ones are usually found overlaying the intermediates ones, limited by abrupt contact. Therefore the intermediates lava flows can be considered either contemporary or older than the acids ones. Another important aspect of those rocks observed on field is magma mingling features. The magma mingling process happens when two or more magmas interact on their fluid state but still remain immiscible (Jerram & Petford, 2014). Given the existence of magma mingling features (Figure 5), it can be speculated that at some measure of time, those lava flows' extravasations period overlap each other. Meaning that, at some point, those lavas were erupting together or at least they were no totally crystallized, allowing the mingling structure to be to form. Campos *et al.* (2011) pointed out that the mingling features depend on the combined action of stretching and folding dynamics. During fluids mixing experiences Ottino (1989) achieve a complex pattern of mingled filaments (Figure 31), which are similar to what was observed in field.

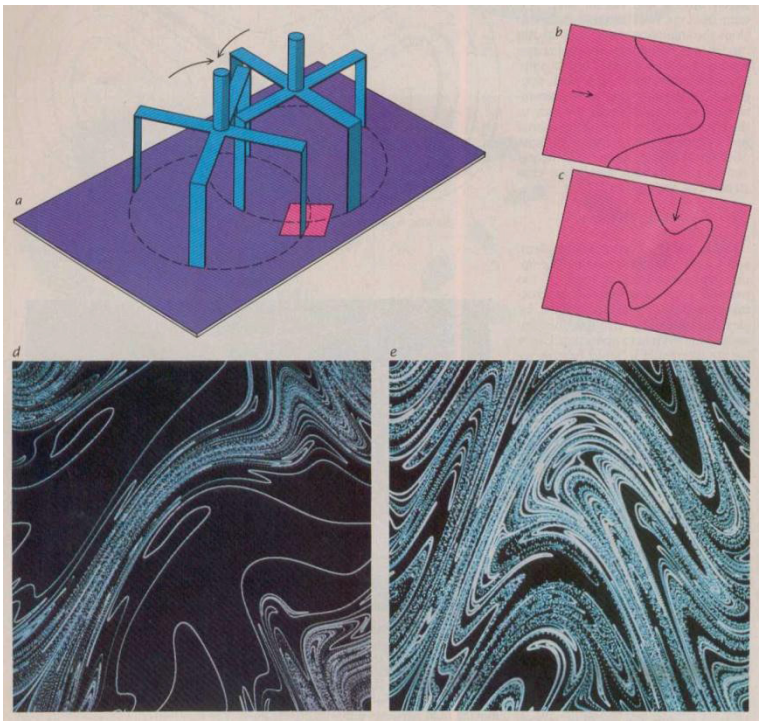

Figure 31 – Fluids mixing experiment. Source: Ottino (1989).

According to Jerram & Petford (2014), the immiscibility of a magma, necessary to mingling formation, is given by their rheological characteristics (Table 3). Minding the intermediate and acid magmas immiscibility and that no magma mixing feature has been identify on the basin, it can be point out that no possible hybrid of those magma was formed. That fact supports the idea, presented by Barbosa (2015) that there was not one fractional crystallization process including both magmas.

Table 3 - Relationship between composition, physical properties and intrusion temperatures of crystal-free melts. Source: Jerram & Petford (2014).

Lithotype	SiO_2 (wt%)	Density (kg/m^3)	Viscosity (Pa s)	Temperature (°C)
Basalt/ Gabbro	45-52	3.00-2.80	$1\text{-}10^3$	1000-1200
Andesite/ Granodiorite	52-65	2.80-2.60	$500\text{-}10^4$	800-1000
Rhyolite/ Granite	65-75	2.60-2.40	$104\text{-}10^9$	700-900

Those magmas differences are better seen on petrologic and geochemical aspects. It is true that both sets have a fabric of porphyritic texture, define by usually quartz-feldspathic phenocrystals among a quartz-feldspathic matrix. However, on intermediate rocks, it was found mainly andesine, quartz and amphibole, whereas on acid rocks, it was found sanidine, microcline and quartz as phenocrystals (Figures 6 and 7). The differences of mineral assemblage reflect on geochemical aspects. Classification diagrams showed those rocks mainly as subalkaline (Figure 9). According to AFM diagram (Figure 10), the $Fe_2O_{3(total)}$ seems to be a primarily parameter of differentiation for those magmas. The $Fe_2O_{3(total)}$ content goes from 1.03 to 5.18 wt% for acid rocks and from 7.32 to 14.36 wt% for intermediate rocks. That variation is what gives the separation of acid rocks as calc-alkaline series and intermediate rocks as tholeiitic series on AFM diagram.

The first perceptible aspect of oxides Harker diagrams is the fact that the evolutionary trends are better recognizable on diagrams of oxides that are considered immobile, such as TiO_2, Al_2O_3 and Fe_2O_3. Mobile oxides diagrams (MgO, CaO, Na_2O and K_2O) plotted in a scattered way, indicating that the high alteration degree of those rocks is disfiguring the charts. A similar behavior of mobile oxides diagrams was reported by Waichel (1998) and Citroni (1998) when analyzing volcanic rocks from Campo Alegre basin. In general, variation diagrams of oxides show a depletion trend towards the most evolve samples for both sets, individually (Figure 11 and 12). In addition, the intermediate and acid sets' trends of evolution present no relation to one another, since they are usually separated by a gap on both axes (Figure 32). That gap on x axis is about 4.8 wt% of silica and is given by their natural separation between intermediate and acid rocks. The gap on y axis varies from one element to another, but it is usually given by the higher content of oxides in intermediate rocks than acid ones. That incompatibility of evolutionary trends discards the petrogenetic hypothesis of different partial melting taxes of a single source. According to Rollinson (1993), the partial melting trend on variation diagram is controlled by the chemistry of the solid phases being added to the melt. In addition, Cox *et al.* (1979) states that the sudden change of direction of the liquid path (evolutionary trend) is characteristic of liquids evolving by fractional

crystallization or conversely by progressive partial fusion (partial melting). Considering that, if the studied intermediate and acid magmas were actually formed by partial melting from a single source, they would have plot according to a polynomial function (curve) on Harker diagrams that included all samples. Since that trend was not observed, it means that the two sets of rocks do not share a common source. Therefore, it is then more accurate to separate and analyze them individually.

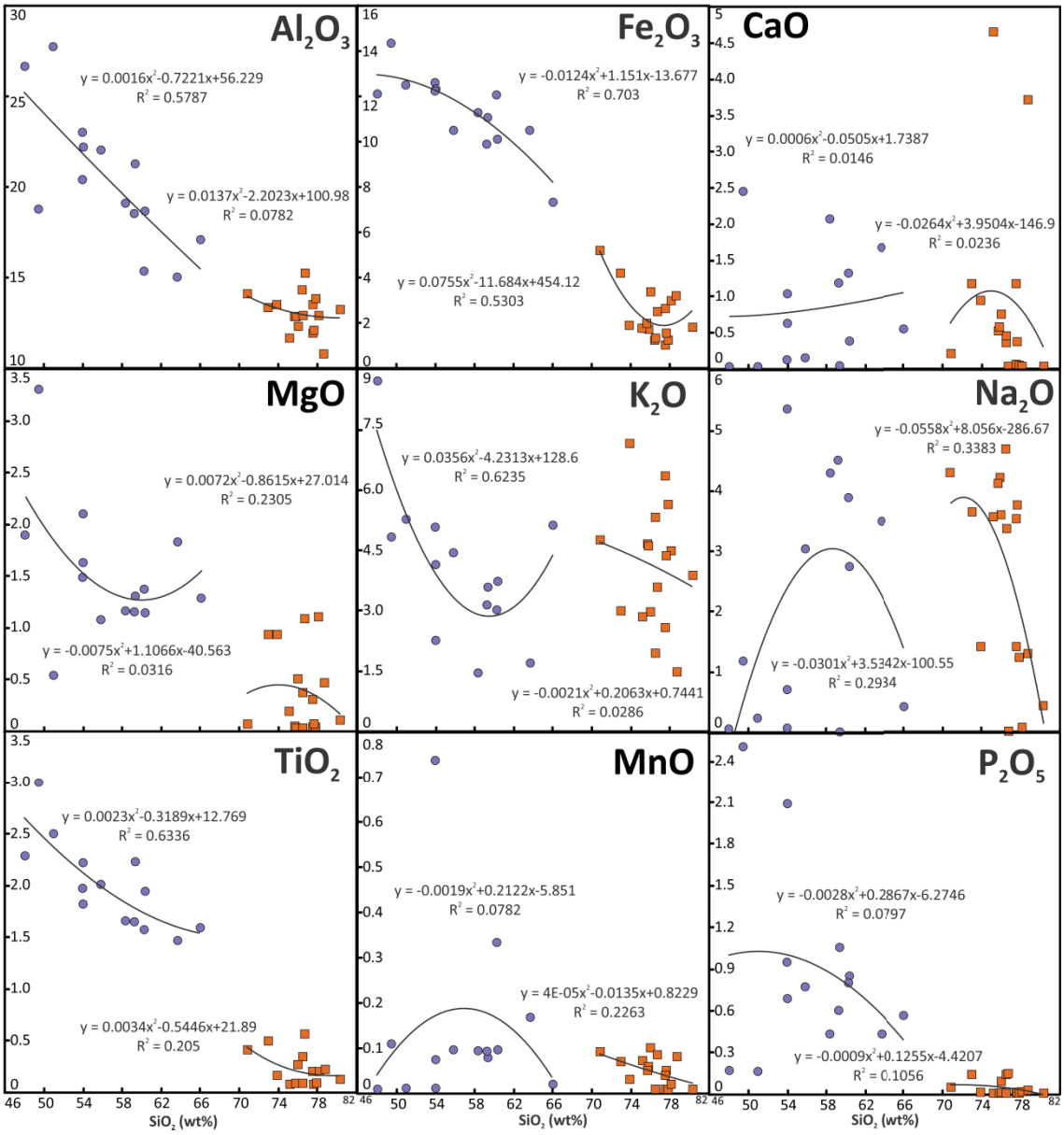

Figure 32 - Harker diagrams for oxides. Data from intermediate (purple circles) and acid (orange squares) rocks sets with trend line (continuous black line).

Harker diagrams of intermediate rocks show a depletion pattern toward the most evolved sample (Figures 11). According to Cox *et al.* (1979), the plotting behavior evident on immobile oxides can be interpreted as fractional crystallization or partial melting, since both processes produce similar curved trends. Fractional crystallization is represented by a 'liquid line of descent', which is the path taken by residual liquids as they evolve through the differential withdrawal of minerals from the magma (Bowen, 1928). A similar interpretation can be extended to the studied acid rocks. Their Harker diagrams also present scattered plots for mobile oxides, while immobile ones show a depletion trends (Figure 12). Rollinson (1993) argues that one of few ways to distinguish fractional crystallization from partial melting is the fact the first usually occur on shallow depths, as a crustal phenomenon, while the second occur at great depths, in the mantle. The isotopic data presented indicated an origin at mantelic depth for the studied rocks. However, their crystallization took place at crustal levels. All in all, the genetic process related to the evolutionary trend noticeable on the Harker diagrams is probably the fractional crystallization. Comparing to Campo Alegre basin, both Waichel (1998) and Citroni (1998) charted similar oxides Harker diagrams. Although, the pair of authors proposed that the volcanic rocks from Campo Alegre basin are genetic related, with most acid members been originated from differentiation process from the most basic ones.

The plot of trace elements bivariate diagrams seems to corroborate the oxides behavior, since there is still no observable relation between intermediate and acid sets. The subdivision of samples concerning their high and low Zr content refined their evolutionary trends aiding the patterns to be clearer. The intermediate rocks reveal an enrichment trend, for both low and high Zr, which plots according to a curve (Figure 14). A similar pattern can be observed on acid set diagrams (Figure 15). The difference in this latter case is the presence of both enrichment (low Zr) and depletion (high Zr). Likewise oxides diagrams, the curvilinear trend, noticeable for trace elements, can be interpreted as a fractional crystallization process. Concerning the geographic distribution of those rocks (Figure 2), the low Zr intermediate rocks cover the central and northern portions of the basin. Complementarily, the high Zr intermediate occur

on the southern part of the basin. That distribution might indicate that the intermediate lava flow was towards south. Minding that Zr is an incompatible element, it tends to remain in the liquid rather than be incorporated in crystals. Therefore, it is expect that the last portions of the lava to crystallize are the ones holding the higher content of Zr. The acid rocks do not present an easily noticeable limit. They might be separated into western and eastern occurrence for low and high Zr, respectively. The same interpretation used for used for intermediate rock can be applied here. Since the volcanic structures that probably feed the acid lava flows are found in the western part of the basin, the eastern part contain the lavas that crystallize last, so holding the higher content of Zr (Figure 2).

Multi-element and REEs diagrams show two important patterns. First is a depletion trend concordant to incompatibility increasing, concordant to what was observed on bivariate diagrams. Second is a progressive differentiation stages within each rock groups, which means, in other words, that each rock has a smaller content of a certain element (Figures 16 to 19). Fractional crystallization is the most likely differentiation process indicated by that pattern, since it was already point out by bivariate diagrams' analysis. According to partition coefficient values given by Rollinson (1993) some anomalies observed during multi-elementary geochemical analysis can be explain by the magmas mineral assemblages. For instance, the Ti is mainly fractionated by hornblende and magnetite. Both minerals are found in intermediate rocks composition and not on acid ones, which explains the positive anomaly for the first and negative anomaly for the second one (Figure 16 and 17). Hornblende was identified on petrography and a large amount of magnetite was observed during samples preparation for geochronology analysis. One sample of the intermediate set (GUA-138) showed a negative anomaly for U (Figure 16), which is an element usually fractionated by biotite or allanite (epidote) (Rollinson, 1993). Epidote was a common secondary mineral observe for both studied sets (Figure 6 and 7), so this specific case seems to be a local variation. The phosphorous negative anomaly on acid set (Figure 17) could be explained by the lack of apatite, even considering that it wasn't observed on any of the sets. Apatite also fractionated more Ce than La, which perhaps would explain why two of acid

samples are given a negative anomaly for Ce and positive for La (Figure 17). The lack of plagioclase of the acid rocks explains the negative anomaly for Sr and Eu (Figure 17 and 19). Also, its presence on intermediates rocks explain the high values and positive anomaly of Eu of that set (Figure 18). However, the intermediate set also have an expressive Sr anomaly (Figure 16) which incoherent with the plagioclase presence. The fact that those rocks are highly altered from weathering process, specially the intermediates, might have contributed to this negative anomaly. Analyzing $(La/Yb)_N$ vs. Ce_N diagrams (Alexander *et al.*, 2000), it is noticeable that, likewise multi-element and REEs charts, the intermediate and acid sets show a progressive fractional grade (Figure 33). The differentiation between low and high Zr are more distinguishable in intermediate's diagram, whilst acid rocks plot, those groups are overlaying each other. That same pattern is reflected on the geographic distribution of those rocks (Figure 2). Despite using different normalization standards, inhibiting a more detail comparison, Waichel (1998) and Citroni (1998) results of trace elements analysis show many similarities with the ones presented on this paper.

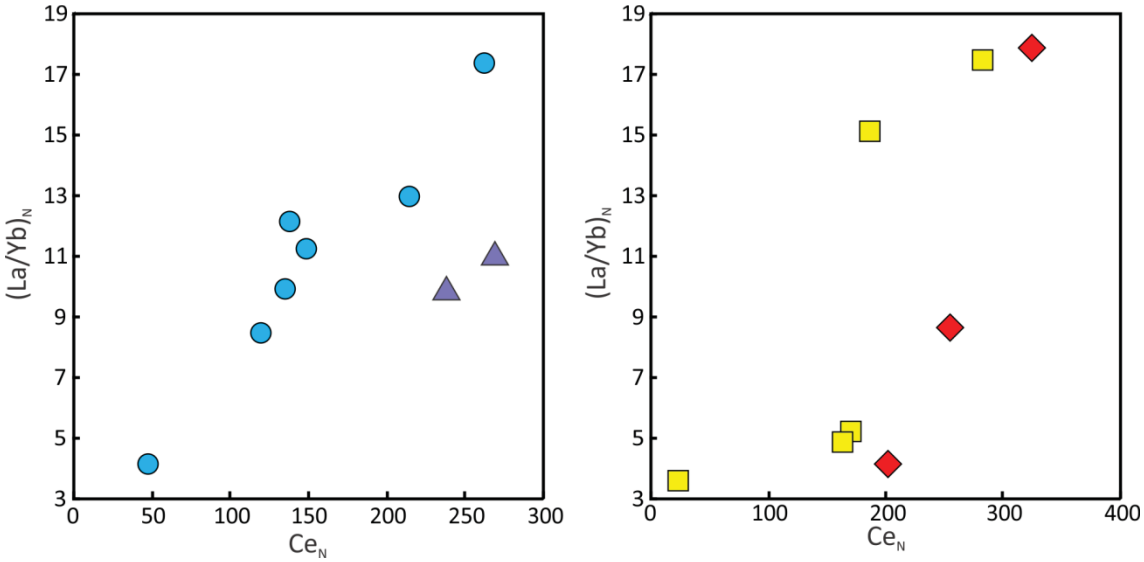

Figure 33 – $(La/Yb)_N$ vs. Ce_N diagram for intermediate (left) and acid (right) rocks. Samples subdivide into low Zr intermediate low (blue circles), high Zr intermediate (purple triangles), low Zr acid (yellow squares) and high Zr acid (red diamonds).

Discrimination diagrams must be used with caution. However, the ones presented in this paper (Figures 20 and 21) seem to fulfill the expectations and

corroborate the interpretations. Both intermediate and acid sets plot in within-plate tectonic environment. Citroni (1998) and Waichel (1998) also present similar results for volcanic rocks from Campo Alegre basin.

Regarding isotopic data, many important petrogenetic characteristics can be interpreted, despite a small number of samples having been analyzed. The information represented by the T_{DM} chart reveals that intermediate and acid rocks have similar, but not equal, petrogenetic features (Figure 22). The first parameter that must be analyzed is the $f_{Sm/Nd}$ (equation 2). This variable indicates the fractionation factor between the sample and the depleted mantle. If the calculated value differs from 0.45 ± 0.1, it means that some geological event fractionates the $^{147}Sm/^{144}Nd$ ratio and the development of that specific rock must be interpreted as a double-stage rather than a simple-stage evolution (Sato, 1998; Sato & Siga Jr., 2001). This is the case for the acid sample, whilst the intermediate samples fit into a simple-stage evolution. The T_{DM} for both cases can be obtained through equations 3 and 4. Considering this, it can be assumed that the parental magma of intermediate rocks derivate from the mantle around 2.2 Ga and remain in the crust until it went through partial melting process, originating the intermediate magma that crystallized into the rock that is studied today. The acid rocks shows a different evolution which can be interpreted as the parental magma derivate from mantle around 2.15 Ga and eventually going through some geological process able to fractionate the $^{147}Sm/^{144}Nd$ ratio. That process might be the partial melting which originate the acid magma that formed the rhyolites and associated volcaniclastic rocks that fills the basin today. Although, more study is needed in order to confirm that. Knowing that both, intermediate and acid magmas, parental rocks were formed during the Paleoproterozoic is a strong indication that the bed rocks of Guaratubinha basin, such as Luis Alves Domain, are the most probable candidates. The negative values of ε_{Nd} data from the crystallization age indicate that magma, which originated each rock, was formed at crustal depth (Geraldes, 2010). Comparing to Campo Alegre basin, Citroni (1998) presented the same type of results as the ones in this paper. The $\varepsilon_{Nd(crystallization)}$ values are negatives. In addition, the T_{DM} ages presented by the author are similar to the ones calculated for the Guaratubinha volcanic rocks.

The geochronology analyses reveal three populations of zircon crystals in the intermediate rocks. The first one is recognizable as being of volcanic origins, representing crystals formed during the crystallization of those rocks. The second and third populations are recognizable as two different groups of inherited crystals. They can be classified as such mainly because of their morphology and age comparison with literature's data. The first population is the only one which crystals do not present a pre-existing core (Figure 24). Additionally, the first population morphology also fit into what is expected for a volcanic crystal of andesites rocks (Wan *et al.*, 2012; Terentiev *et al.*, 2016; Anczkiewicz & Anczkiewicz, 2016; Siégel *et al.*, 2018; He *et al.*, 2018). The Concordia diagrams (Figure 25) show a concentration of ellipses around 580 on GUA-07 sample, and around 593 on GUA-18 sample. Those ages seems reasonable when compared to other geochronological studies (Siga Jr., 1995; Siga Jr. *et al.* 2000; Basei et al. 1998b), establishing the main crystallization period for intermediate volcanism period between 580 and 593 Ma.

The second population can be considered as xenocrystals (Figures 26), capture by the andesite during their ascent through crust, for two main reasons. First, they present an age range around 620 Ma (Figure 27), which is consistent with Rio-Pien Suit granites formation (Machiavelli *et al.*, 1993; Harara, 2001). Second, is that there is structural evidence that the intermediate magma use the GMF as uprising conduct, which kept them in direct contact with Rio-Pien Suit granites (Barão *et al.*, 2017). The third population of older inherited zircon crystals (Figure 28) may be a strong indication of the source material of intermediate rocks along with Sm-Nd data. The mean age of those inherited crystals (Figure 29), 2282 ± 16 Ma, is concordant to Paleoproterozoic ages calculated for Luis Alves Terrane (Siga Jr., 1995). The author indicated the presence of two populations of zircon crystals. The first population, a pinkish colored, has an age of 2247 ± 18 Ma. The second, brownish, presented an age of 2360 ± 100 Ma. The age proximity with the first population indicates the relation between the inherited crystals founded in intermediate rocks with them, even if they do not present physical resemblance. Field information indicated the intermediate rocks as being older than acid ones, hence, the crystallization age of those latter ones must be after 580 Ma. However, since a more accurate

data could not being obtained for this paper, on all calculations it was taken into consideration the literature data of 604 Ma (Siga Jr. *et al.*, 2000).

7 PETROGENESIS MODEL

The environmental characteristics of volcanism in strike-slip fault system describe by Tibaldi *et al.* (2009) are summarized in the following figure (Figure 34). Lithogeochemical, isotopic and geochronological data present on this paper are concordant with andesite and rhyolite formation at crustal depth, establish by the authors.

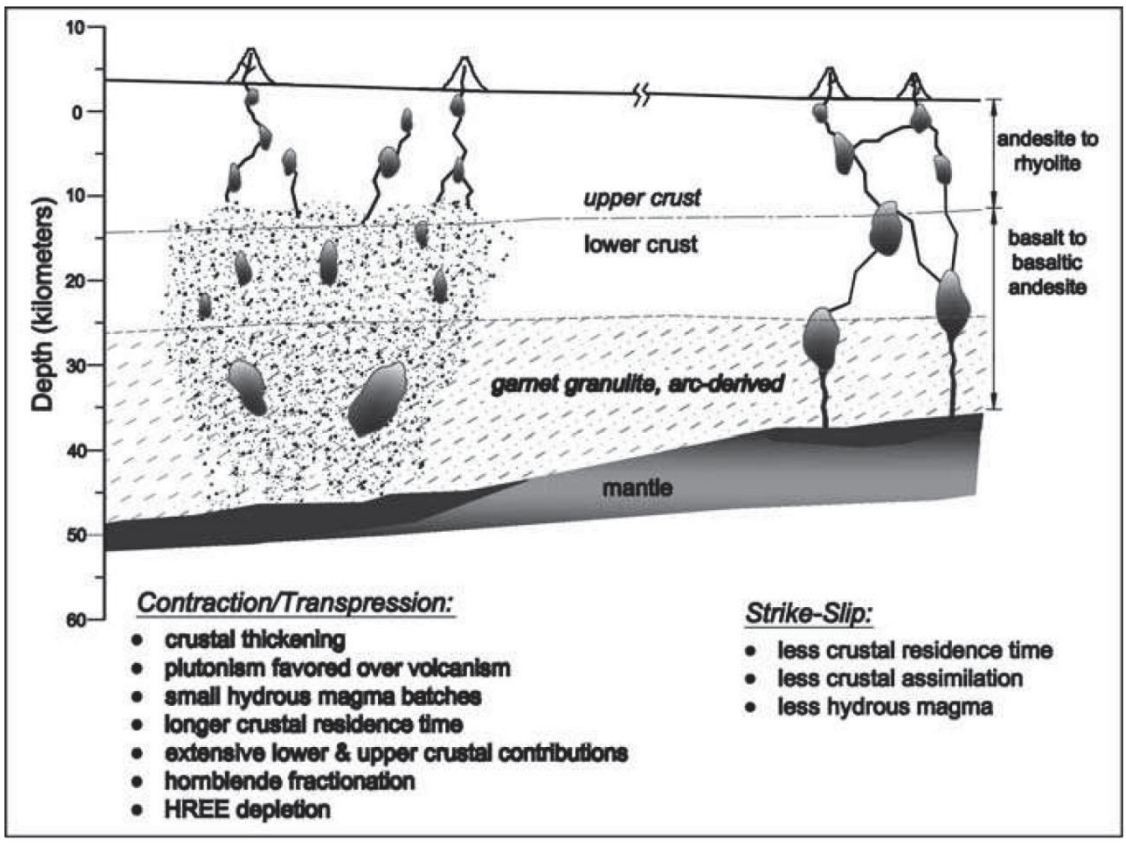

Figure 34 – Petrogenetic schematics of contractional-derived volcanism (left) and strike-slip-derived volcanism (right). Source: Tibaldi *et al.* (2009).

Considering all information presented so far, the evolution of intermediate and acid rocks can be interpreted accordingly to the following events, represented on the schematics bellow (Figure 35): (1) Contact between Curitiba and Luis Alves Terranes; (2) Rio-Pien Suit granites formation and placement as magmatic arc (Basei *et al.*, 1992; Machiavelli *et al.*, 1993; Siga Jr., 1995; Harara, 2001); (3) Basin formation provided by the activation of GMF

and GNSZ (Barão *et al.*, 2017); (4) Intermediate magma derivation from Luis Alves Terrane, whereas acid magma source is unknown; (5) Intermediate magma ascent through GMF, while acid magma ascent through magmatic conducts; (6) Fractional crystallization and spreading of intermediate magma at surface; (7) Fractional crystallization and eruption of acid magma, overlaying the intermediate one and producing magma mingling structure, simultaneously; (8) Later tectonic events, reshaping of basin's bounders, and Mesozoic volcanism placement.

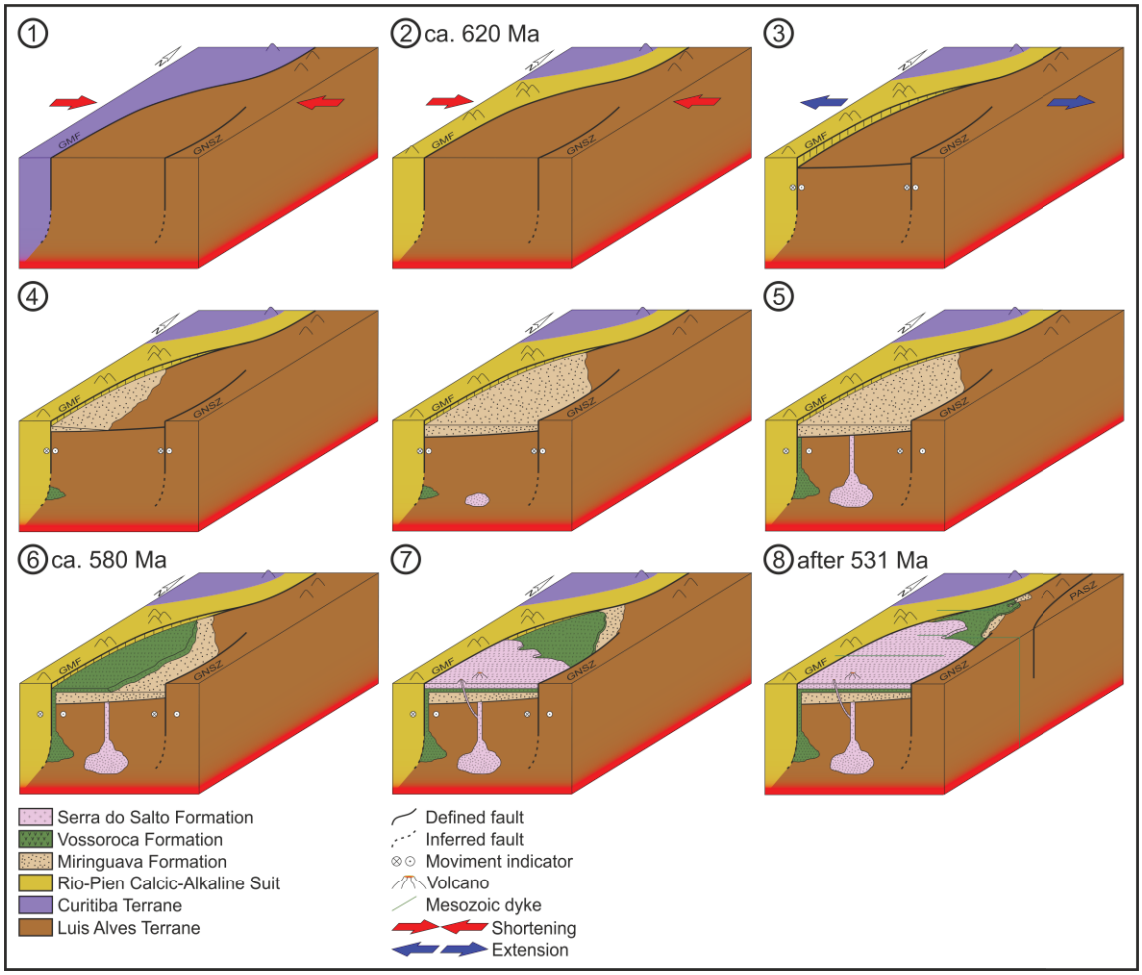

Figure 35 – Simplify schematics for volcanic rocks evolution in Guaratubinha basin.

8 CONCLUSION

The Guaratubinha Basin is mainly filled by volcanic rocks. In order to better understand their genesis it was performance a series of analyses to point out their geochemical characteristics. The studied rocks could be firstly classified as intermediates and acids, considering their SiO_2 content. The intermediates are geochemically named as phono-tephrite, trachy-basalt, basaltic andesite, basaltic trachy-andesite, trachy-andesite and andesite, whereas the acids are classified as rhyolite. They have a general subalkaline character, with the intermediates fitting into tholeiitic series and the acids into calc-alkaline series. Their evolutionary trends and geochemical signatures have many differences that seem to be given mainly by their differences in mineral assemblage, specially the type of feldspar. Their lithogeochemical differences discard the partial melting of a single source, as possible petrogenetic process, since they denoted that there was no common source for the studied rocks. Analyzing the isotopic data, it could be observed that the two studied rock sets originated at crustal depth but evolved independently from each other. Although both sets are related to paleoproterozoic parental rocks, the intermediate set evolves according to a simple-stage model while the acid set evolves as a double-stage model. Concerning geochronological data, the intermediate rocks bear three types of zircon crystals. First type is volcanic ones, which establish the main volcanism period between 580 and 593 Ma. The second and third are xenocrystals inherited from Guaratubinha basin bed rocks, the Rio-Pien Suite, from Neoproterozoic, and Luis Alves Domain, from Paleoproterozoic. It is reasonable to assume that, if there was a contamination process involved, it would reflect in variations not only on lithogeochemical aspects but on isotopic data as well. All in all, that the most suitable hypothesis is that the studied rocks originated from different sources and evolve through different paths.

REFERÊNCIAS

Alexander J.L., Bailey E.H., Pickering, K.T. 2000. Using rare earth elements as provenance indicators in mudrocks from a range of tectonic settings. Journal of Conference Abstracts v.5(2), p.134.

Almeida F.F.M., Brito Neves B.B., Fuck, R. 1981. Brazilian structural provinces: an introduction. Earth-Science Reviews v.17, p.1-29.

Anczkiewicz A.A., Anczkiewicz R. 2016. U–Pb zircon geochronology and anomalous Sr–Nd–Hf isotope systematics of late orogenic andesites: Pieniny Klippen Belt, Western Carpathians, South Poland. Chemical Geology, v.427, pp.1-16.

Barão L.M. 2016. Arcabouço Estratigráfico-Estrutural da Bacia do Guaratubinha e Deformações Associadas, Sudeste do Paraná. Dissertação de Mestrado. UniversidadeFederal do Paraná. 135p.

Barão L.M., Trzaskos B., Vesely F.F., Castro L.G., Ferreira F.J.F., Vasconcellos E.M.G., Barbosa T.C. 2017. The role of post-collisional strike-slip tectonics in the geological evolution of the late Neoproterozoic volcano-sedimentary Guaratubinha Basin, southern Brazil. Jornal of South America Earth Sciences. v.80, p.29-46.

Barbosa T.C. 2015. Litogeoquímica das associações vulcânica e vulcanoclástica da Bacia do Guaratubinha. Trabalho de Conclusão de Curso, Departamento de Geologia, Universidade Federal do Paraná, 60 p.

Basei M.A.S. 1985. O Cinturão Dom Feliciano em Santa Catarina. São Paulo, 190p. (Tese - Doutorado) - Instituto de Geociências, Universidade de São Paulo.

Basei M.A.S., Siga Junior O., Machiavelli, A., Mancini, F. 1992 Evolução Tectônica dos Terrenos entre os Cinturões Ribeira e Dom Feliciano (PR e SC). Rev Brás. Geoc., v.2, p.216-221.

Basei M.A.S., McReath I., Siga Jr. O. 1998a. The Santa Catarina Granulite Complex of Southern Brazil: a review. Gondwana Research, v.1(3-4), p.383-391.

Basei MAS, Citroni SB, Siga Jr O. 1998b. Stratigraphy and age of Fini-Proterozoic basins of Paraná and Santa Catarina States, southern Brazil. Boletim IG-USP, Série Científica, v.29, p.195-216.

Bowen N.L. 1928. The evolution of the igneous rocks. Princeton University Press.

Boynton W.V. 1984. Geochemistry of the rare earth elements: meteorite studies. In: Henderson P. (ed.), Rare earth element geochemistry. Elsevier, p.63-114.

Campos C.P., Perugini D., Ertel-Ingrisch W., Dingwell D.B., Poli G. 2011. Enhancement of magma mixing efficiency by chaotic dynamics: an experimental study. Contrib Mineral Petrol., v.161, p.863-881.

Castro N.A., Reis Neto J.M., Assine M.L. 1993. Rochas Vulcanogênicas da Formação Guaratubinha, PR. In: V Simpósio Sul Brasileiro de Geologia. Boletim de Resumos e Programa.

Citroni SB. 1998. Bacia de Campo Alegre – SC. Aspectos petrológicos, estratigráficos e caracterização geotectonica. São Paulo, 198p. (Doctorate Thesis. Instituto de Geociências da USP).

Cox, K.G., Bell, J. D., Pankhurst, R.J. 1979. The Interpretation of Igneous Rocks, George Allen & Unwin, London, United Kingdom 445 pp.

Daitx E.C., Carvalho M.A.S. (Coord.) 1980. Projeto geoquímico da área Guaratubinha-Piên. Curitiba, Ministério de Minas e Energia & Departamento Nacional da Produção Mineral – Convênio DNPM/CPRM. VI.

DePaolo D.J. 1988. Neodymium Isotope Geochemistry. An Introduction. Springer-Verlag. Mineral and Rocks v.20, p.181.

DePaolo D.J., Linn A.M., Chubbert G. 1991. The continental age distribution: method of determining mantle separation ages from Sm-Nd isotopic data and application to the southwestern United States. Journal of Geophisical Research, v.96, p.2071-2088.

Dostal J., Hamilton T.S., Shellnutt J.G. 2017. Generation of felsic rocks of bimodal volcanic suites from thinned and rifted continental margins: Geochemical and Nd, Sr, Pb-isotopic evidence from Haida Gwaii, British Columbia, Canada. Lithos, v.292-293, p.146-160.

Elhlou S., Belousova E., Griffin W.L., Pearson N.J., O'Reilly S.Y. 2006. Trace element and isotopic composition of GJ-red zircon standard by laser ablation. Geoch. Cosmoch. Acta, v70(18), p.A158.

Fisher R.V. 1966. Rocks composed of volcanic fragments and their classification. Earth Science Reviews v.1, p.287-298.

Fuck R.A., Marini O.J., Trein E. 1967. A Formação Guaratubinha. Boletim Paranaense de Geociências, v.23-25, p.237-256.

Geraldes M.C. 2010. Introdução a geocronologia. Sociedade Brasileira de Geologia, São Paulo, 146 p.

Gutmanis J.C. 1989. Wrench faults, pull-apart basins, and volcanism in central Oregon: a new tectonic model based on image interpretation. Geological Journal, v.24, p.183-192.

Harara O.M.M. 2001. Mapeamento e investigação petrológica e geocronológica dos litotipos da região do alto Rio Negro (PR-SC): Um exemplo de sucessivas e distintas atividades magmáticas durante o Neoproterozóico III. São Paulo, 240p. (Tese - Doutorado) - Instituto de Geociências, Universidade de São Paulo.

Harara O.M.M., Basei M.A.S., Siga Junior O. 2002. From subduction to late and post-collision settings: a record from neoproterozoic sucessive magmatic in the upper Rio Negro regions. In: XXXXI Congresso Brasileiro de Geologia, João Pessoa – PB, v.1, p.310.

Harara O.M.M., Basei M.A.S., Siga Junior O., Campos Neto M.C., Prazeres Filho H.J. 2003. Dating of high-grade metamorphism by U-Pb, Sm-Nd na K-Ar isotopic systems: Paleoproterozoic I-type granulites from the northern border of the Luis Alves gneiss-granulite terrain, southern Brazil. IV SSAGI, Salvador – BA, v.2, p.568-571.

He H., Li Y., Wang C., Zhou A., Qian X., Zhang J., Du L., Bi W. 2018. Late Cretaceous (ca. 95 Ma) magnesian andesites in the Biluoco area, southern Qiangtang subterrane, central Tibet: Petrogenetic and tectonic implications. Lithos, v.302-303, p.389-404.

Ibañes O.D., Sruoga P., Japas M.S., Urbina N.E. 2017. Neogene Tiporco Volcanic Complex, San Luis, Argentina: An explosive event in a regional transpressive - local transtensive setting in the pampean flat slab. Journal of South American Earth Sciences, v.76, p.306-319.

Irvine T.N. & Baragar W.R.A. 1971. A guide to the chemical classification of the common volcanic rocks. Can. 3. Earth Sci., v.8, p.523-48.

Jerram, D. & Petford, N. 2014. Descrição de Rochas Ígneas. Guia geológico de campo. 2 ed. Editora Bookman, Porto Alegre, RS.

Kaul P.F.T. 1997. O magmatismo na Serra do mar e Adjacências (Sul do Brasil) no final do Proterozoico e seus condicionantes tectônicos. São Paulo, 291p. (Tese - Doutorado) - Instituto de Geociências, Universidade de São Paulo.

Kaul P.F.T. & Cordani U. G. 2000. Geochemistry of Serra do Mar granitoid magmatism and tectonic implications Southern Brazil. Revista Brasileira de Geociências, v.30(1), p.115-119.

Le Maitre R.W., Bateman P., Dudek A., Keller J., Lameyer Le Bas M.J., Sabine P.A., Schmid R., Sorensen H., Streckeisen A., Wolley A.R., Zanettin B. 1989. A classification of igneous rocks and glossary of terms. Blackwell, Oxford.

Licht O.A.B. 1988. Levantamento geoquímico de semi-detalhe da Sequência vulcano-sedimentar Guaratubinha - PR. Curitiba, MINEROPAR. Relatório Interno.

Machiavelli A., Basei M.A.S., Siga Jr. O. 1993. Suíte Granítica Rio Píen: um arco magmático do Proterozoico Superior na Microplaca Curitiba. Geochimica Brasiliensis, v.7(2), p.113-129.

Ottino J.M. 1989. The mixing of fluids. Sci. Am., v.260, p.56-67.

Pearce J.A. 1982. Trace element characteristics of lavas from destructive plate boundaries. In: Thorpe R.S. (ed.), Andesites. Wiley, Chichester, p.525-548.

Pearce J.A., Harris N.B.W. and Tindle A.G. 1984. Trace element discrimination diagrams for the tectonic interpretation of granitic rocks. 3. Petrol., v.25, p.956-983.

Potts J.P. 1993. Laboratory Methods of Analysis. In: Riddle C. (eds.) Analysis of Geological Material. Marcel Dekker Inc, New York, p.123-220.

Reis Neto J.M., Pinheiro Jr. V., Rostirolla S.P., Soares, P.C. 1998. Integração e reavaliação de dados litológicos, estruturais e litoquímicos nas Folhas de Curitiba, Cerro Azul e Apiaí, PR. In: SBG, Congresso Brasileiro de Geologia, 40, Belo Horizonte, Anais, v.35.

Reis Neto J.M., Vasconcellos E.M.G., Bittencourt C. 2000. Guaratubinha Formation – PR: petrographic characterization of volcaniclastic rocks. Revista Brasileira de Geociências, v.30, p.371-374.

Rollinson H. 1993. Using geochemical data: evaluation, presentation, interpretation. New York: Longman Scientific &Technical, New York, 352 p.

Rutherford E. & Soddy F. 1903. Radioactive change. Phil. Mag., v.6, p.576-591.

Sato K. 1998. Evoluçãoo Crustal da Plataforma Sul Americana, com base na geoquímica isotópica Sm-Nd. PhD thesis, São Paulo University, Brazil, 300p.

Sato, K. & Siga Junior, O. 2001. Rapid grouth of continental crust between 2.2-1.8 Ga in the South American plataform. Integrated Australian, European, North American na SW USA crustal evolution study. Gondwana Research, v.5, p.165-173.

Sato K., Basei M.A.S., Sproesser W.M., Siga Jr. O. 2012. The application of U-Pb geochronology to zircon and titanite by laser ablation - icp-ms. In: The 8th International Conference on the Analysis of Geological and Environmental Materials, Geoanalysis 2012. Búzios, RJ. Abstract, p96.

Sato K., Tassinari C.C.G., Basei M.A.S., Siga Jr. O., Onoe A.T., Souza M.D. 2014. Sensitive High Resolution Ion Microprobe (SHRIMP IIe/MC) of the Institute of Geosciences of the University of São Paulo, Brazil: analytical method and first results. Geol. USP, Sér. cient., São Paulo, v.14(3), p.3-18.

Siégel C., Bryan S.E., Allen C.M., Gust D.A. 2018. Use and abuse of zircon-based thermometers: A critical review and a recommended approach to identify antecrystic zircons. Earth-Science Reviews, v.176, p.87-116.

Siga Jr. O. 1995. Domínios Tectônicos do Sudeste do Paraná e Nordeste de Santa Catarina: Geocronologia e Evolução Crustal. Tese de Doutorado, Instituto de Geociências, Universidade de São Paulo. 232 p.

Siga Jr. O., Basei M.A.S., Machiavelli A. 1993. Evolução geotectônica da porção nordeste de Santa Catarina e sudeste do Paraná com base em interpretações geocronológicas. Curitiba. Revista Brasileira de Geociências, v.23, p.215-223.

Siga Jr. O., Basei M.A.S., Reis Neto J.M., Machiavelli A., Harara O.M. 1995. O Complexo AIUba: um cinturão paleoproterozóico intensamente retrabalhado no Neoproterozóico. Bol. IG-USP. Sér.Cient., v.16, p.69-98.

Siga Jr. O., Basei M.A.S., Sato K., Citroni S., Reis Neto J. M., Weber W., Harara O.M., Sproesser W.M. 1999. Post-orogenic Magmatism and sedimentation in Neoproterozoic extensional regimes in the Brazilian Southern Region. In: II Simpósio Sul-Americano de Geologia Isotópica, Cordoba - Argentina. Extended Abstracts - II South American Symposium on Isotope Geology. (II SSAGI) - Corpo Editorial. v.1, p.367-370.

Siga Jr. O., Basei M.A.S., Cordani U.G., Citroni S.B., 2000. U-Pb and Sm-Nd isotopic studies of Campo Alegre and Guaratubinha volcanosedimentary basins, southern Brazil. 31° Int. Geol. Congr. Rio de Janeiro – Rj. Digital abstract (CD).

Silva P.C.S., Vasconcelos C.V.S., Yamato A.A. 1998. A cartografia do Complexo Atuba na Folha Curitiba (SG22-X-D-I). In: SBG, Congresso Brasileiro de Geologia, 40, Belo Horizonte, Anais, v.10.

Tatar O., Yurtmen S., Temiz H., Gursoy H., Koçbulut F., Mesci B.L., Guezou J.C. 2007. Intracontinental Quaternary Volcanism in the Niksar Pull-Apart Basin, North Anatolian Fault Zone, Turkey. Turkish Journal of Earth Sciences, v.16, p.417-440.

Teixeira, A.L., Gaucher, C., Paim, P.S.G., Fonseca, M.M., Parente, C.V., Silva Filho, W.F., Almeida, A.R. 2004. Bacias do estágio de transição da Plataforma Sul-Americana. In: Mantesso-Neto, V., Bartorelli, A., Carneiro, C.D.R., Brito-Neves, B.B.B. (Eds.), Geologia do Continente Sul-Americano. Evolução da Obra de Fernando Flávio Marques de Almeida. São Paulo, p.487-536.

Terentiev R.A., Savko K.A., Santosh M. 2016. Paleoproterozoic crustal evolution in the East Sarmatian Orogen: Petrology, geochemistry, Sr-Nd isotopes and zircon U-Pb geochronology of andesites from the Voronezh massif, Western Russia. LITHOS, v.246-247, pp.61-80.

Tibaldi A., Pasquarè F., Tormey D. 2009. Volcanism in Reverse and Strike-Slip Fault Settings. In: Cloetingh S., Negendank J. (eds) New Frontiers in Integrated Solid Earth Sciences. International Year of Planet Earth. Springer, Dordrecht.

Wan Y., Ho K., Liu D., Zhou H., Dong C., Ma M. 2012. Micro-scale heterogeneity of andesite from Chilungshan, northern Taiwan: Evidence from melt inclusions, geochronology and Hf–O isotopes of zircons. Chemical Geology, v.328, p.244-258.

Waichel B.L. 1998. Caracterização geoquímica das rochas vulcânicas da Bacia de Campo Alegre – SC. Dissertação de Mestrado. 134p. Universidade Federal do Rio Grande do Sul. Porto Alegre.

Waichel B.L., Lima E.F., Nardi L.V.S., Sommer C.A. 2000. The Alkaline Post-Collisional Volcanism of Campo Alegre Basin in Southern Brazil: Petrogenetic Aspects. Rev Bras Geoc 30: 393–396.

Wood D.A., Joron J.L., Treuil N.F., Norry M. and Tarney J., 1979, Elemental and Sr isotope variations in basic Lavas from Iceland and the surrounding ocean floor. Contrib. Mineral. Petrol., v.70, p.319-339.

Wood D.A., Tarney J., Weaver B.L., 1981, Trace element variations in Atlantic ocean basalts and Proterozoic dykes from Northwest Scotland: their bearing upon the nature and geochemical evolution of the upper mantle. Tectonophysics, v.75, p.91-112.